SANTA CATARINA STATE UNIVERSITY- UDESC
TECHNOLOGICAL SCIENCES CENTER - CCT
GRADUATE DEPARTMENT OF ELECTRICAL ENGINEERING – PPGEEL

THAYNA OENING

LITHIUM-ION BATTERY TESTS USING A DESIGNED BMS

JOINVILLE, SC
2022

THAYNA OENING

LITHIUM-ION BATTERY TESTS USING A DESIGNED BMS

Thesis submitted to the Graduate Department of Electrical Engineering at the Technological Sciences Center of the Santa Catarina State University, in partial fulfillment of the requirements of the Master's degree of Electrical Engineering.

Supervisor: Joselito Anastácio Heerdt, PhD

Joinville, SC
2022

Ficha catalográfica elaborada pelo programa de geração automática da

Biblioteca Setorial do CCT/UDESC,

com os dados fornecidos pelo(a) autor(a)

Oening, Thayna
Lithium-ion battery tests using a designed BMS / Thayna Oening. -- 2022.
125 p.

Orientador: Joselito Anastácio Heerdt
Dissertação (mestrado) -- Universidade do Estado de Santa Catarina, Centro de Ciências Tecnológicas, Programa de Pós-Graduação Profissional em Engenharia Elétrica, Joinville, 2022.

1. Battery management system. 2. Battery charge and discharge. 3. Lithium-ion battery. I. Heerdt, Joselito Anastácio. II. Universidade do Estado de Santa Catarina, Centro de Ciências Tecnológicas, Programa de Pós-Graduação Profissional em Engenharia Elétrica. III. Título.

THAYNA OENING

LITHIUM-ION BATTERY TESTS USING A DESIGNED BMS

Thesis submitted to the Graduate Department of Electrical Engineering at the Technological Sciences Center of the Santa Catarina State University, in partial fulfillment of the requirements of the Master's degree of Electrical Engineering.

Supervisor: Joselito Anastácio Heerdt, PhD

EXAMINING COMMITTEE:

Prof. Joselito Anastácio Heerdt, PhD
Santa Catarina State University (Board's president/Supervisor)

Members:

Prof. Gierri Waltrich, PhD
Santa Catarina Federal University

Maria de Fátima N. C. Rosolem, MSc
CPqD - Research and Development Center in Telecommunications

Joinville, SC, 10 February 2022.

This work is dedicated to my family.

ACKNOWLEDGMENTS

I would like to thank the following people, without whom I would not have been able to complete this research.

My biggest thanks to my parents for all the support they have shown me through my entire life. And to my friends for motivating and encouraging me throughout the execution of this work.

I would like to acknowledge and give my thanks to my supervisor Prof. Joselito Anastácio Heerdt, who made this work possible. His guidance and advice carried me through all the stages of this project.

I must express my sincere thanks to the committee members, Dr. Gierri Waltrich and M.Sc. Maria de Fátima N.C. Rosolem, for their time to evaluate this document and provide valuable comments and contributions.

I also would like to thank the members of nPEE lab at Udesc university. The professors, students and the staff were a great support to complete this study. I made friends there and I will keep fond memories of this time.

A debt of gratitude is also owed to WEG company and my coworkers who always shared their knowledge and experiences, making this work better and complete.

In addition, I would like to express my appreciation for Texas Instruments company, for supporting my research providing technical explanations and samples of the devices used in this study.

ABSTRACT

In this work, the implementation of a lithium-ion battery management system (BMS) is performed. Using the BMS, studies were carried out on the behavior of batteries under different conditions of charge, discharge and temperature. The battery pack is composed of 5 cells in series, using NCR18650B (NCA - LiNiCoAl) batteries from Panasonic manufacturer, with nominal voltage of 3.6 V and capacity of 3350 mAh. The BMS uses the dedicated integrated circuits bq7692000PWR and bq78350R1A from Texas Instruments. This system allows the monitoring of the main variables (voltage, current and temperature), the estimations of the state of charge (SoC) and state of heath (SoH) and provides a wide range of protections. Tests were carried out with different charge and discharge rates (0.25C, 0.5C and 1.0C) and with different room temperature conditions (10 °C, 25 °C and 40 °C), being possible to verify the degradation of the battery pack capacity as a result of these conditions.

Keywords: Battery management system; Battery charge and discharge; Lithium-ion battery.

RESUMO

Neste trabalho, é realizada a implementação de um sistema de gerenciamento de baterias (BMS - *Battery Management System*) para baterias de íons de lítio. Utilizando o BMS, foram realizados estudos do comportamento de baterias em diferentes condições de carga, descarga e temperatura. O banco de baterias é composto por 5 células em série, utilizando baterias NCR18650B (NCA - LiNiCoAl) da fabricante Panasonic, com tensão nominal de 3,6 V e capacidade de 3350 mAh. O BMS utiliza os circuitos integrados dedicados bq7692000PWR e bq78350R1A, da empresa Texas Instruments. Este sistema permite a monitoração das principais variáveis (tensão, corrente e temperatura), a estimação do estado de carga (SoC) e do estado de vida útil (SoH) e possui uma ampla variedade de proteções. Foram realizados testes com diferentes taxas de carga e descarga (0,25C, 0,5C e 1,0C) e com diferentes condições de temperatura ambiente (10 °C, 25 °C e 40 °C), sendo possível verificar a degradação da capacidade do banco de bateria em decorrência destas condições.

Palavras-chave: Baterias de íon de lítio; Carga e descarga de baterias; Sistemas de gerenciamento de baterias.

LIST OF FIGURES

LIST OF TABLES

LIST OF ABBREVIATIONS

AC	Alternating Current
ADC	Analog-to-Digital Converter
AFE	Analog Front-End
BMS	Battery Management System
CAN	Controller Area Network
CC-CV	Constant Current - Constant Voltage
CEDV	Compensated End-of-Discharge Voltage
DoD	Depth of Discharge
ECU	Electronic Control Unit
EIS	Electrochemical Impedance Spectroscopy
FET	Field Effect Transistor
FCC	Full Charge Capacity
GG	Gas Gauge
GPIO	General Purpose Input Output
HEV	Hybrid Electric Vehicles
IC	Integrated Circuit
I^2C	Inter-Integrated Circuit
LDO	Low Dropout
Li-air	Lithium-air
Li-ion	Lithium-ion
Li-S	Lithium-sulfur
LCO	Lithium Cobalt Oxide
LFP	Lithium Iron Phosphate

LMO	Lithium Manganese Oxide
LTO	Lithium Titanium Oxide
NCA	Nickel Cobalt Aluminum
NCH	N Channel
NCM	Nickel Cobalt Manganese
NiCd	Nickel-cadmium
NiMH	Nickel-metal hydride
NTC	Negative Temperature Coefficient
OCV	Open Circuit Voltage
OCD	Overcurrent in Discharge
OV	Overvoltage
PCB	Printed Circuit Board
PCH	P Channel
PTC	Positive Temperature Coefficient
RC	Remaining Capacity
SCD	Short-circuit in Discharge
SPI	Serial Peripheral Interface
SoC	State of Charge
SoH	State of Health
TI	Texas Instruments
UPS	Uninterruptible Power Supplies
UV	Undervoltage
VCU	Vehicle Control Unit
ZEBRA	Zeolite Battery Research Africa

CONTENTS

1 INTRODUCTION

Over the last decade, the use of portable electronic products has rapidly increased as much as renewable energy production and electric vehicles. Such things have in common the necessity for energy storage. Among energy storage devices, batteries are the most popular because of their good energy density.

Considering cost and environmental concerns, batteries used to power these devices should be rechargeable. The lithium-ion (Li-ion) battery is the most attractive type among them. The Li-ion batteries offer the advantage of a high average operation cell voltage of 3.6 V (mostly) and high energy density, resulting in lighter devices when compared to other battery types at the same capacity. Li-ion batteries also have considerably low self-discharge rates, do not suffer from the memory effect and have a long cycle life. The most common applications using lithium-ion batteries are presented in Figure 1. There are a large number of applications using batteries. In some cases with other storage systems, such as supercapacitors, as can be seen in (MORAES et al., 2021).

Figure 1 – Typical battery applications

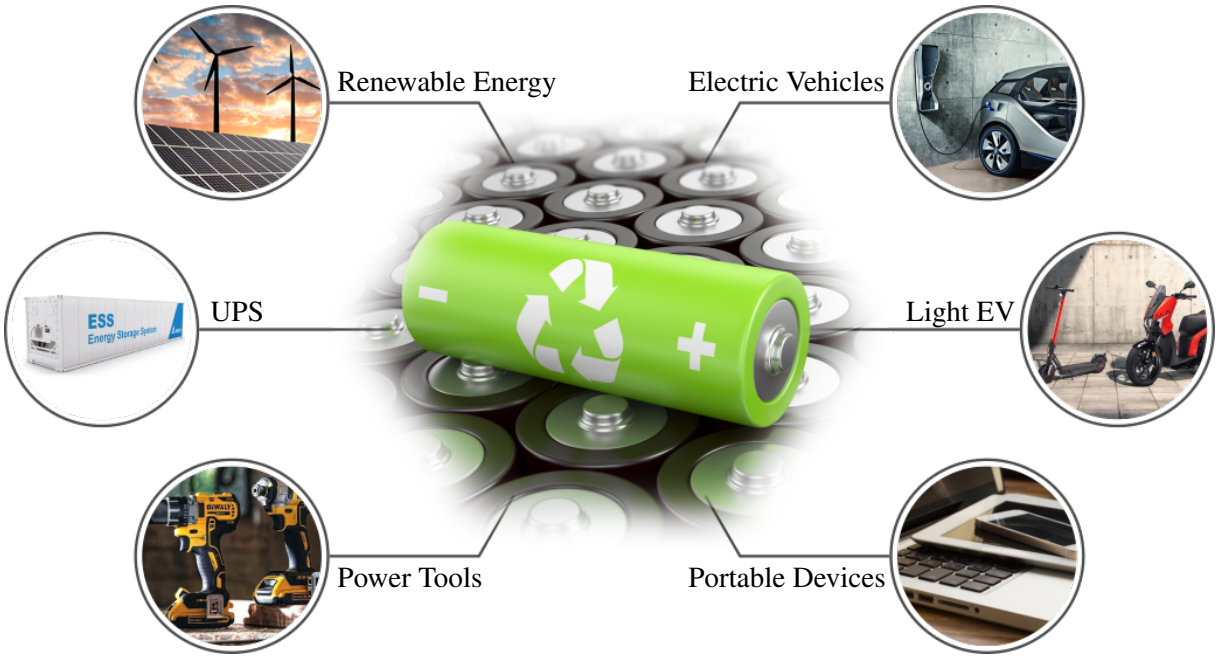

Source: the author

Lithium-ion batteries are widely used for all the mentioned positive characteristics, but they also have some disadvantages. Li-ion batteries are really sensitive to high and low temperatures, overcharge and overdischarge. First of all, this type of battery needs a special charging algorithm because overcharging leads to a decrease in cycle life. Without precautions, overcharging or fast-charges lead to dangerous situations and may even cause a fire or an explosion of the battery (HUANG et al., 2021). Therefore, strict control of the charge and discharge processes is essential for safety reasons and for retaining a long cycle life. Overdischarge may result in capacity degradation, decrease of cycle life and also internal short-circuit which can cause battery explosion (GUI et al., 2016).

Considering that lithium-ion batteries have serious safety issues, protection systems are extremely necessary to prevent accidents. These protection systems are implemented using

external electrical circuits and are known as battery management system (BMS). The BMS is responsible for monitoring, controlling and protecting batteries. Many functions can be implemented in a BMS, according to the complexity of the application. The main functions are related to measuring the voltage, current and temperature of each cell battery or the battery pack assembly. This information can be used by other functions, as cell balancing, estimation of state of charge (SoC) and state of health (SoH), and can also be used to protect the battery from overcharge and overdischarge.

Several different methods to perform each function are available in the current literature. Some methods use advanced technologies to provide accurate estimations and more reliable measurements and robustness, but they normally demand high computational power or they make the system too expensive for practical use. In commercial applications, the user safety is the main concern and a trade-off between accuracy and cost is generally necessary.

In this context, this work presents a study using a battery pack composed of 5 lithium-ion battery cells series connected, using NCR18650B NCA (LiNiCoAl) from Panasonic and dedicated integrated circuits from Texas Instruments for BMS applications. The bq769200PWR is an analog front end responsible for providing battery monitoring and protection and the bq78350-R1A is the battery management controller that provides more advanced functions for the BMS. Using the *bqStudio*® (from Texas Instruments), a user interface to monitor and control the battery and the BMS functions, several tests in different conditions are performed while cell voltage, current during charge or discharge, battery temperature, remaining capacity, state of charge, state of health and others parameters are monitored and analyzed.

1.1 GENERAL OBJECTIVE

The motivation for this work is the understanding of the lithium-ion battery behavior during charge and discharge under different operating conditions using a designed BMS.

1.2 SPECIFIC OBJECTIVES

To achieve the general objective, this study was divided in the following specific objectives:

1. Analysis of the state of the art of lithium-ion battery applications behavior;
2. Study of BMS functions and the different methods used to perform them;
3. Development of a complete experimental setup to test the batteries and the main functions of a commercial BMS;
4. Analysis of the charge and discharge behavior under different test conditions;
5. Comparison of the obtained results with the battery datasheet and the literature;
6. Understanding about the capacity fade due to different room temperatures.

1.3 TEXT STRUCTURE

This work is divided into the six chapters described as follows:

Chapter 1 (Introduction): presents a brief contextualization about the battery applications and the necessity for battery management systems. The motivation and the objectives of this work are also presented in this chapter;

Chapter 2 (Batteries): describes the definitions of main characteristics of batteries and the most popular battery types. Next, the lithium-ion battery is detailed and its electrical characteristics are compared with the other battery types;

Chapter 3 (Battery management system): contains the description of the main BMS functions and the different methods to perform them;

Chapter 4 (System development): explains in detail each component of the experimental setup developed in this work. The designed BMS, the battery pack and the complete prototype development are shown;

Chapter 5 (BMS functional tests): validates the main BMS functions. The BMS measurements, estimations, protections and algorithms are tested and the results are presented;

Chapter 6 (Charge and discharge tests): exposes the proposed tests under different charge and discharge conditions and the analysis of the obtained results;

Chapter 7 (Controlled room temperature tests): presents the tests under different room temperatures and the analysis of the results;

Chapter 8 (Conclusion): discusses the main conclusions and perspectives for future research.

2 BATTERIES

Batteries are devices that convert chemical energy into electrical energy. The electrical energy is created through an electrochemical oxidation-reduction reaction within the battery. This allows energy storage and a direct method of producing constant current. When connected to a load, batteries will produce electrical energy until the reactions are depleted (MORRIS; TOSUNOGLU, 2012).

Batteries consist of a positive electrode (cathode), a negative electrode (anode), an ionic conductor (electrolyte) and a separator. The electrolyte can be liquid, a gel or solid. The separator is placed between the cathode and the anode preventing short circuiting, but also allowing charged ions to flow.

There are two major classification for batteries: primary cells and secondary cells. Primary cells can be discharged only once and then, they need be discarded or recycled. They are typically used in toys and TV remote controls, for example. Secondary batteries can be easily recharged, which provide a longer service life. Common applications are laptop computers and cell phones. This study will focus on secondary cells.

There are several rechargeable battery technologies, characterized by their composition. The most commonly used are the lead-acid, nickel-cadmium (NiCd), nickel-metal hydride (NiMH), sodium-nickel chloride (ZEBRA) and lithium-ion (Li-ion). Over the next sections, these battery technologies are explored and the lithium-ion battery is presented in details, as it is the type used in this study.

2.1 COMMON TERMINOLOGY

In this section, the main electrical and application-related characteristics of the secondary batteries for the most commonly used technologies are presented. Some useful terms are defined as follows (BHATT; DARIEBY, 2018).

Energy density: the volumetric energy storage density of a battery, expressed in Watt-hours per liter (Wh/l);

Power density: the volumetric power density of a battery, expressed in Watts per liter (W/l);

Rated capacity: the capacity of a battery, expressed in Ampere-hour (Ah), which is the total charge that can be obtained from a fully charged battery under specified discharge conditions. These conditions are specified by the manufacturer;

Specific energy: the gravimetric energy storage density of a battery, expressed in Watt-hours per kilogram (Wh/kg);

Specific power: the gravimetric power storage density of a battery, expressed in Watts per kilogram (W/kg);

C-rate: the relationship between charge or discharge current and battery energy capacity. For example, the 1C discharge current of a battery with capacity of 2250 mAh is 2250 mA;

Cycle life: the number of cycles that a cell or battery can be charged and discharged under specific conditions, before the available capacity in [Ah] fails to meet a specific performance criterion, which usually is 80% of the rated capacity;

Self-discharge: the recoverable loss of capacity of a cell or battery. This is usually expressed in a percentage of the rated capacity lost per month at a certain temperature, because self-discharge rates of batteries are strongly temperature-dependent;

Memory effect: the decline in effective capacity with repeated partial charge/discharge cycles;

State of charge (SoC): the remaining battery capacity that is available for discharge as a percentage of the nominal battery capacity;

State of health (SoH): the maximum currently available capacity compared to the nominal capacity, indicated as percentage;

Depth of discharge (DoD): the discharge percentage of the battery. A DOD of 100% represents a fully discharged battery;

Calendar life: the time period before the battery becomes unusable;

Capacity fade: the amount of battery capacity reduction during battery life;

Power fade: the reduce of the power capability of the battery, mainly caused by the increment of battery resistance;

Energy efficiency: the percentage maximum rate of conversion of energy by the battery.

The power density, the energy density, the cycle life, the calendar life and the cost per kWh are the key parameters for comparison among batteries. Energy efficiency, discharge safety and the volume of battery pack are also considered for the selection (BHATT; DARIEBY, 2018).

2.2 LEAD-ACID

The lead-acid battery was developed in 1860 by Raymond Louis Gaston Planté and it is the oldest type of rechargeable battery. The main advantages of the lead-acid batteries is the low cost for the amount of power. They are used for electrically starting internal combustion engines in most vehicles and also in other applications as light electric vehicles (bikes, golf carts, etc.) and stationary power devices, such as emergency lighting and uninterruptible power supplies (UPS) (ROOT, 2010).

The nominal voltage of each lead-acid cell is 2 V and it has low specific energy (between 30 - 45 Wh/kg). Lead is a toxic metal, so there are strict regulations concerning the disposal of lead-acid batteries. Nowadays, almost all of the lead batteries are recycled. Also, this battery can be very heavy due to the lead and other components, thus adding weight to any application, and must operate in an environment considering temperature and physical damage.

2.3 NICKEL-CADMIUM (NiCd)

The nickel-cadmium (NiCd) cell was developed in the late nineteenth century by Waldemar Jungner from Sweden. The use of NiCd batteries for traction applications grew in the years before World War II. This battery is commonly known as robust. For many years, NiCd was the preferred choice for radios, emergency medical equipment, professional cameras and power tools. The characteristic of high power delivered made NiCd batteries very popular at this time (BERGVELD, 2001). These batteries are still used in a number of portable devices.

The main electrical characteristics of a nickel-cadmium are 1.2 or 1.3 V as nominal cell voltage and an energy density between 50 - 60 Wh/kg. However, under some conditions, some batteries may exhibit the memory effect. This occurs when a NiCd battery is repeatedly charged before the cell is completely discharged (OMAR et al., 2014). The memory effect is reversible, fortunately. The battery will recover its full capacity after a few discharge and charge conditioning cycles wherein the battery is completely discharged (ROOT, 2010).

Most of nickel-cadmium batteries are been replaced by nickel-metal hydride (NiMH) and lithium-ion batteries, both described later in this chapter. This occurs because of the cadmium toxicity and the higher energy density of the other batteries.

2.4 NICKEL-METAL HYDRIDE (NiMH)

The nickel-metal hydride battery is made up of multiple components and was created as a solution for the nickel-cadmium disadvantages. NiMH batteries offer the same average operating voltage as NiCd batteries (1.2 or 1.3 V), with the great advantage of a higher energy density between 50 - 110 Wh/kg (FETCENKO; KOCH; ZELINSKY, 2015). The memory effect is still present in this battery but it is reduced when compared with NiCd battery.

This battery is used in a large variety of applications, such as power tools, medical instruments and equipment, cameras and also in hybrid electric vehicles (HEV).

2.5 SODIUM-NICKEL CHLORIDE (ZEBRA)

The sodium-nickel chloride battery, also called ZEBRA (acronym for the Zeolite Battery Research Africa project) was patented in 1978 in South Africa. The main characteristic of this battery is the operation temperature of 270 to 350°C, since sodium is found in its molten state at these temperatures. For this, this battery is also referred as molten salt battery. Special pack design and thermal considerations are needed to maintain the high operating temperature (CHEMALI et al., 2016).

The specific energy in this battery is around 100 - 120 Wh/kg and the nominal voltage is 2.58 V. They were designed for electric vehicles but can be also applied in stationary electrical systems (DUSTMANN, 2004). The cells have a low resistance short-circuit state when cell damage occurs, that allows continuous operation during cell failures. This makes them operationally safe (CHEMALI et al., 2016). A disadvantage of this battery is the high self-discharging because of the thermal management.

2.6 LITHIUM-ION (Li-ion)

The first lithium-ion battery was commercialized by Sony in Japan in 1991, since then it has become popular and is widely used. Lithium is attractive because it is the lightest metal and thus produces lighter batteries. It provides the largest specific energy, between 90 and 220 Wh/kg and a common nominal voltage between 3.2 V and 3.7 V (BHATT; DARIEBY, 2018). Lithium-ion batteries are considered to have the highest power among the battery systems and there is still potential for development. Typical applications include laptop computers, cell phones, cameras and they are also used in space, military and electric vehicles applications (ROSOLEM; BECK, 2018). The demand for Li-ion batteries surpassed the combined demand for NiCd and NiMH batteries several years ago (ROOT, 2010).

Li-ion batteries have other advantages, as relatively low self-discharge rate, no memory effect, increased cycle life when reducing the depth of discharge, good charging and discharge

efficiency and long service life. But some disadvantages are also present: high cost if compared to the other battery types presented in this paper, decreased performance as temperature increases, safety issues operating in high temperature, loss of capacity and decrease of cycle life if overdischarged and overcharged and the flammability of the electrolyte (ROOT, 2010), (CHEMALI et al., 2016).

To avoid the overcharge condition, an appropriated charge method is necessary. The method known as Constant Current- Constant Voltage (CC-CV) is highly used to charge Li-ion batteries. This method consist of two steps, during the first step is applied a constant current and the charge voltage increases. In the second step, the charge voltage remains constant and the current decreases until the battery is fully charged. The maximum current and voltage are defined by the manufacture (GAO et al., 2019). Figure 2 presents the typical charging profile of a lithium-ion battery cell using the CC-CV method.

Figure 2 – Typical characteristics of the lithium-ion battery charging using CC-CV method

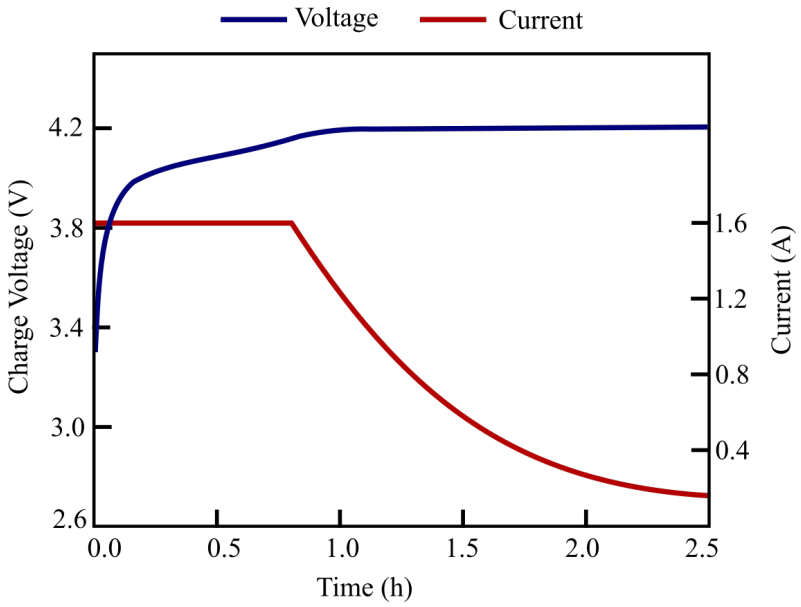

Source: the author

Another characteristic of Li-ion batteries is the non-linearity of the relationship between cell voltage and state of charge. Figure 3 presents a typical curve for the discharge under different current rates. In this case, each curve presents a different SoC value for the same cell voltage. The SoC also depends on temperature, cycle life and differs according the application conditions. For this reason, to obtain an accurate SoC value it is necessary to use estimation algorithms.

Table 1 presents a comparison of the typical characteristics of the batteries presented in this chapter. These values were compiled from literature survey and corroborate to the superior electric characteristics of the Li-ion battery. The Li-ion specifications present a wide range because of the different materials used in it. The most common used chemical materials are presented, but new types are being constantly developed and studied.

There are various materials used in the construction of Li-ion cell electrodes. Each material results in different energy characteristics, lifespan, safety, cycle life and cost. The main sources of the active lithium-ions in a battery are the positive electrode material. Some typical cathode materials include lithium manganese oxide (LMO, $LiMn_2O_4$), lithium cobalt oxide (LCO, $LiCoO_2$), lithium nickel cobalt manganese oxide (NCM, $LiNiMnCoO_2$), lithium

Figure 3 – Typical curves of lithium-ion battery discharging

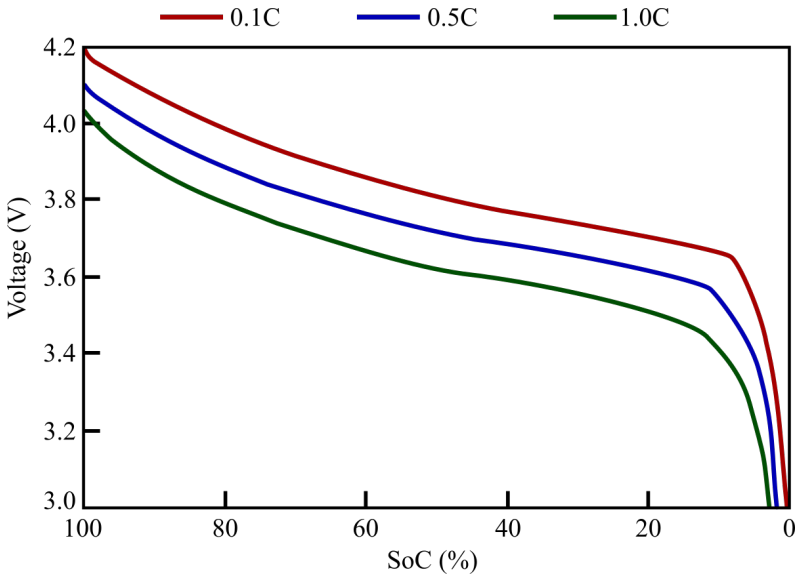

Source: the author

Table 1 – Typical characteristics of batteries

Specifications	Lead-acid	NiCd	NiMH	ZEBRA	Li-ion
Nominal cell voltage (V)	2.0	1.2 - 1.3	1.2 - 1.3	2.58	3.2 - 3.7
Specific energy (Wh/kg)	30 - 45	50 - 60	50 - 110	100 - 120	80 - 600
Energy density (Wh/l)	60 - 75	90 - 150	60 - 150	135 - 180	230 - 2600
Specific power (W/kg)	180	80 - 150	80 - 400	150 - 200	250 - 3000
Cycle life	500 - 800	300 - 700	1200 - 2000	>2500	80 - 5000
Temperature range (°C)	−20 to 60	−20 to 50	−20 to 60	270 to 350	−20 to 60
Cost ($/kWh)	100 - 150	?	150 - 250	100 - 200	300 - 600

Source: adapted from (MORRIS; TOSUNOGLU, 2012), (FETCENKO; KOCH; ZELINSKY, 2015), (BHATT; DARIEBY, 2018), (CHEMALI et al., 2016)

nickel cobalt aluminum oxide (NCA, $LiNiCoAlO_2$) lithium iron phosphate (LFP, $LiFePO_4$) and lithium titanium oxide (LTO, $Li_4Ti_5O_12$) (NITTA et al., 2015).

The LCO presents high specific energy and energy density, low self-discharge and good cycling performance (charge capacity retention and recovery). Its major disadvantages are the low thermal stability and fast capacity fade at high current rates (NITTA et al., 2015). LMO battery delivers a high power density and the thermal stability and safety are higher than the LCO battery. However, it presents a limited lifespan and higher loss of capacity while charging (HANNAN et al., 2018). The LFP is know for its thermal stability and its stability in over-charged condition, which provide a high security score. Other positive characteristic is the high cycle life number, which results in wide usage in storage systems. However, this battery has a average density energy. NMC battery presents a high specific energy and high energy density, its materials presents a good overall performance and is widely used in the battery market, but it presents instability if overcharged. The NCA battery type presents high specific energy and density and a long lifespan, its disadvantages are the higher cost and the lower safety because of thermal instability and overcharged sensibility. Finally, the LTO battery has a good energy density, a superior thermal stability, a long lifespan and high performance despite the low cell voltage (2.4 V), the high cost and lower capacity (NITTA et al., 2015).

Figure 4 compares the specific energy, specific power, energy density, power density, cost, safety issues, overall performance and cycles life of various lithium battery types.

In Table 2 are presented the main advantages, disadvantages and the common applications of each Li-ion battery type mentioned in this chapter.

Figure 4 – Comparison among lithium-ion battery types indexed values

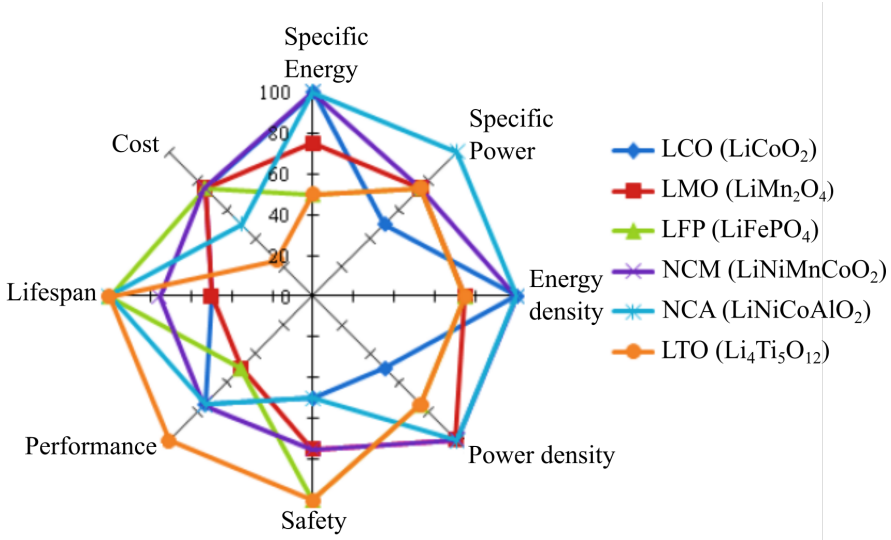

Source: adapted from (HANNAN et al., 2018)

Table 2 – Performance comparison and applications among lithium-ion battery types

Li-ion types	Advantage	Disadvantage	Application
LCO	High specific energy and power	Short life span, limited specific power and safety	Cell phones, laptops and digital cameras
LMO	Good specific power and high safety	Moderate in overall performance	EVs, HEVs and medical equipment
LFP	Good thermal stability, high current rating, excellent safety and long life spam	Moderate specific energy, small cell voltage (3.2 V), sensitive to low temperature	EVs, power tools and portable devices
NCM	High specific energy and good overall performance	Moderate safety	Power tools, EVs and energy storage
NCA	High specific energy and power, good life spam	High cost and marginal safety	EVs and power trains
LTO	High performance, safety and life spam	Lower cell voltage (2.4 V), low energy density and difficult to manufacture	Advanced nano-technology applications

Source: adapted from (HANNAN et al., 2018)

Nowadays, Li-ion batteries are still being extensively researched and developed to significantly increase energy and power capabilities as well as operating voltage. Two new compositions have been gaining a great deal of interest from research community: lithium-air (Li-Air, Li_2O_2) and lithium-sulfur (Li-S). The primary reason is due to their high theoretical specific energy of 3582 Wh/kg and 2567 Wh/kg, respectively. Another reason is the abundance of the

materials such as O_2 and elemental sulfur (CHEMALI et al., 2016). A key and important factor inhibiting commercialization of these Li_2O_2 cells is electrolyte degradation giving rise to poor lithium cycling efficiencies and capacity fading. Currently, research on Li-Air cells show as much as 50% capacity fade after only 20 discharge cycles. Similarly, Li-S cells suffer from poor sulfur cycling efficiency which leads to fast capacity fading, prototype cells experience a 50% capacity fade after 50 discharge cycles (CHEMALI et al., 2016).

The fragile nature of lithium-ion battery is caused by the electrolyte. The liquid electrolytes usually consist of lithium salt and a mixture of non-aqueous organic alkylcarbonate solvents, which are highly flammable compounds (WEN; YU; CHEN, 2012). The electrolyte is stable only over a restricted range of voltage and temperature. If operating conditions go beyond this range, the battery can be damaged and may even explode.

Considering the need to ensure a safe operation for lithium-ion batteries, the battery management system (BMS) becomes necessary (SENDER et al., 2018). The BMS delivers the control and the management of the features regarding the energy storage and transfer, such as charging and discharging control, battery cell voltage monitoring and balancing, battery charge equalization, input/output current and voltage monitoring, temperature control, battery protection, fault diagnosis and assessment and so on (HANNAN et al., 2018). In the follow chapter is described the operation of a BMS.

3 BATTERY MANAGEMENT SYSTEMS

The battery management systems is a key element to make the utilization of batteries safe, reliable and efficient. As already mentioned, Li-ion batteries are vulnerable to temperature, overcharging and overdischarging.

In addition to providing the necessary protections for the safe use of the Li-ion batteries, the BMS also provides a optimal performance and estimates important variables, such as state of charge (SoC), state of health (SoH) and remaining capacity (HANNAN et al., 2018). BMSs are also a interface between the batteries and the user, providing status information.

The complexity of a BMS is totally dependent on the application. Single cell batteries, as the ones used in mobile phones, e-book readers could provide just measured voltage, temperature and current and use simple methods to estimate the battery's current SoC. In more complex devices, like electric vehicles, the BMS has to perform more sophisticated functions, for example measure each cell voltage, perform cell balancing, provide charging control, protections and estimate SoH and available energy (LELIE et al., 2018). Figure 5 shows the BMS for electric vehicle application.

Figure 5 – BMS for electric vehicle key functions

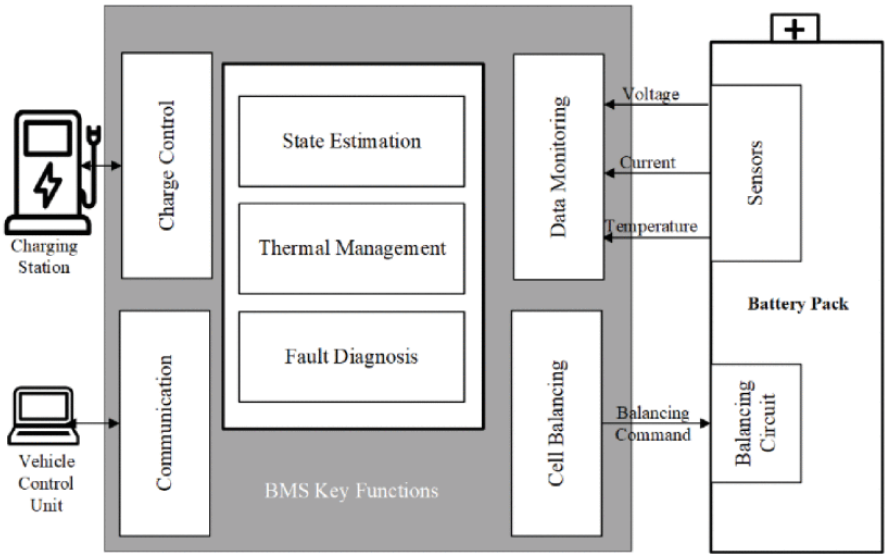

Source: (NAGUIB; KOLLMEYER; EMADI, 2021)

The main functions of a BMS are divided in seven classes, as illustrated in Figure 6. Each of these classes is described in the next sections. After presenting the BMS functions, the communication with other devices is also elucidated.

Figure 6 – Typical functions in a BMS divided in seven main classes

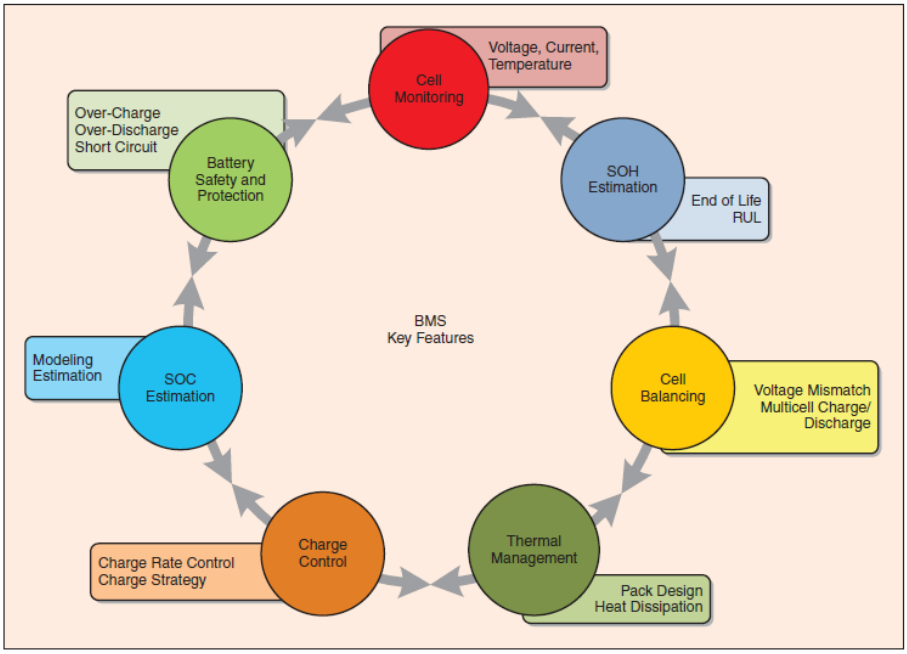

Source: (RAHIMI-EICHI et al., 2013)

3.1 CELL MONITORING - MEASUREMENTS

The first and the more important BMS function is the measurement. The main variables to be measured are voltage, current and temperature. These measurements need to provide an accurate value, as other functions use these values to enable protections and estimate other parameters as the states of charge and health.

3.1.1 Voltage

As most applications use series connected battery cells, the BMS may offer voltage measurement from each cell or just from the pack. Cell voltages are just a few Volts (operation range are normally between 2.5 V to 4.2 V, for lithium-ion batteries), but the pack voltage can reach hundreds of Volts. Therefore, measurement circuits must consider the voltage range of these two quantities. Usually, the chips have an absolute accuracy of 1 mV and a full range scale of 12 to 16 bits, which leads to a resolution of about 380 μV (LELIE et al., 2018).

The voltage measurement is used to ensure the cell operation only inside an allowed voltage range. These over and undervoltage can be defined using resistors arrays or programming a register and are compared with the measured voltage.

The biggest concern regarding voltage measurement accuracy is the estimation of the state of charge, as many methods are based on open circuit voltage (OCV) to determine the SoC during stand-still periods. Some battery types have a very small voltage response regarding SoC and it can provide a high inaccuracy.

3.1.2 Current

Current of discharge (flowing out of the battery) and of charge (flowing into the battery) must also be carried out with high accuracy. This value is used to provide protections of short-circuit and overcurrent during charging or discharging. The current is also used to estimate the

SoC during the operation, as in Coulomb Counting algorithm (RAHIMI-EICHI et al., 2013).

The current sensor needs to have a high bandwidth in most of applications, being able to measure currents starting of miliampere up to 1000 Ampere range, for example (LELIE et al., 2018). The shunt resistor current sensor is widely used. In this measurement method, a low-resistance high-precision resistor in combination with a high precision voltage measurement system is used to determine the current. The current flows through the shunt and the voltage drop is measured. To keep the power losses as small as possible, a low resistance value is needed but the value also needs to be high enough to generate a suitable voltage drop. The power loss also leads to a temperature rise of the shunt resistor, so thermal drift is an important characteristic of the resistor. Advantages of this method are simplicity and linearity of the measurement system, the possibility to achieve high bandwidths and the low cost.

Other commonly used method is the contactless current sensor. These sensors use the magnetic field that the current produces. Hall sensor is a popular sensor that uses the Hall effect to indicate a current. In this case, when a current flows through the sensor, it generates a voltage that is proportional to the product of magnetic flux density and current (LELIE et al., 2018). This sensor does not add any resistance to the current path, which means that no additional conductive losses occur. It also provides a galvanic isolation, so no further optocoupler or digital insulators are required. The main disadvantage is the limited bandwidth, and when compared to the shunt resistor, the Hall sensors are more expensive and have a larger volume. It has also a variable off-set, that needs to be compensated.

3.1.3 Temperature

The most common temperature sensors for the measurement of temperatures in the region that is relevant for battery management applications are the Negative Temperature Coefficient (NTC) or the Positive Temperature Coefficient (PTC) types (LELIE et al., 2018). These sensors change their resistance as function of the temperature. NTC decreases the resistance as the temperature increases and PTC does the opposite. A constant current flows through the resistor and the voltage drop is measured. Most of the BMS provides one or more ADC channels for temperature measurement and the NTC are commonly used.

These sensors provide enough temperature region, from -50 °C to 150 °C, are relatively cheap, easily applicable and are linear in a certain range (nonlinear in very low and very high temperatures).

3.2 PROTECTIONS

The other main function of the BMS is to ensure the safety of the battery and protect it from operating at conditions that are harmful to both battery and user (RAHIMI-EICHI et al., 2013). The BMS sets safety limits to protect the battery from working beyond the safe range of voltage, current in charge and discharge and temperature, for example.

The operational voltage range for lithium-ion cell batteries is commonly between 2.5 V and 4.2 V. The current limitation is defined by the battery manufacturer and the common recommended temperature operating range is between 20 °C and 40 °C.

The overcharge, overdischarge or short-circuit result battery reactions as formation of dendritic lithium on the anode, dissolution of current collector, exothermic decomposition of electrolytes, which will result in gas and heat generation, thermal runaway and ultimately to fire or explosion of the batteries (WEN; YU; CHEN, 2012).

The BMS avoids these situations by interrupting the charge if the cell voltage reaches the maximum value and by stopping the discharge process when the voltage reaches the mini-

mum value. It needs to be able to protect the batteries from overcurrent during the charge and discharge processes. Short-circuit protection during discharge is also required. The temperature needs to be constantly monitored and if the value reaches a critical level, protections must be activated.

3.3 CELL BALANCING

Most of the applications consist of a large number of battery cells connected in series. As individual cells exhibit mismatches in characteristics such as capacity and internal resistance, the cell voltage may also vary during the same operational state. When a mismatch between voltage or capacity occurs, the entire battery pack can not operate in optimal condition (RAHIMI-EICHI et al., 2013). During a discharge, for example, the protection is enabled as soon as the first cell reaches the cutoff voltage. The remaining charge in the rest of the cells can not be utilized. To avoid this situation, some methods to equalize the cell voltages are applied.

The methods available to promote the cell balancing are classified as energy dissipative and non-dissipative, according to whether the electric energy is wasted in the form of heat or transferred to other cells during the equalization procedure.

In dissipative methods, the excess energy from the higher voltage cell is removed, normally connecting a resistor in parallel. These methods are considered the most cost-effective and are most frequently used in lithium-ion battery packs (MOORE; SCHNEIDER, 2001). In this methods, the heat dissipation needs to be considered to not increase the difficulty of thermal management.

In non-dissipative equalization methods, the excess energy is exploited by the other cells of the battery pack. Different techniques are available in the literature, using inductor, capacitor or power converters to transfer the equalization energy between the cells, as presented in (LORENCETTI; HEERDT, 2017) and (RUTHES, 2020), or to diffuse it in the whole battery pack according to the need of each cell. These methods are more efficient compared with the dissipative, but they are also more expensive and complex to implement, requiring an additional hardware in the system (KOSEOGLOU et al., 2020).

3.4 THERMAL MANAGEMENT

Li-ion batteries need to be operated at a certain temperature range. Otherwise, damage could occur to the cells and to the application. High temperature may result from excessive current or high ambient temperature and can decrease the battery capacity or even result in an explosion. Low temperature operation may lead to lithium deposition, which may cause battery rapid degradation and even lead to safety issues (HAN et al., 2019).

For this reason, the battery temperature should be controlled carefully to promote mainly safety. Generally, the temperature is controlled between 20 °C and 40 °C to ensure the better performance and cycle life (LI; ZHU, 2014). The BMS is able to access the temperature measurement and protect the batteries from over and under temperature as well as activating cooling, heating or ventilation functions.

3.5 CHARGE AND DISCHARGE CONTROL

The discharge rate of the battery is defined by the application and the BMS needs to provide protection if this rate is exceeded because the battery pack may be damaged. Also, to control the charge process is a desired function in a BMS. The charging rate depends on the

user's requirement and the battery specifications. For most of the applications, the user wishes a fast charge, an example is the electric vehicles, but battery limitations must be considered to keep the performance and the cycle life (RAHIMI-EICHI et al., 2013). Lithium-ion battery packs are normally charged using the CC-CV (Constant current - Constant voltage) method.

Lithium-ion battery charging, especially in electric vehicle applications, is the subject of extensive research. The topology, the assembly of the charger (off or on-board), the increase in its efficiency and the control techniques are points of interest, as shown by (MENGATTO, 2019) and (REMES et al., 2020).

The charging station is responsible for the charging process, however, the BMS on the battery pack also needs to have this built-in feature to manage, optimize, and protect the charging regime when the specific charger is not available.

3.6 SOC ESTIMATION

In general, the state of charge of a battery is defined as the ratio of its current capacity ($Q(t)$) to the nominal capacity (Q_n). The nominal capacity is specified by the manufacturer and represents the maximum amount of charge that can be stored in the battery (CHANG, 2013). The Equation (3.1) is used to define the state of charge.

$$SoC(t) = Q(t)/Q_n \tag{3.1}$$

As the capacity can not be directly measured, there are various mathematical methods for estimating the state of charge. There are a lot of new proposed techniques in the literature and this subject is widely studied nowadays. These methods can be divided into four categories: direct measurement, book-keeping estimation, adaptive systems and hybrid methods (CHANG, 2013).

3.6.1 Direct measurement

In direct measurement methods, the physical battery properties such as the terminal voltage and impedance are directly related to the state of charge. The most popular methods are: open circuit voltage, terminal voltage and impedance method.

The open circuit voltage (OCV) method is based on the voltage measured when the batteries are disconnected from the load for a period longer than two hours (CHANG, 2013). The relationship between the SoC and the OCV is linear for Lead-acid batteries but is not for lithium-ion cells. The relationship OCV-SoC differs even among batteries of the same type under different environmental temperatures and cycle life (ZHANG et al., 2018). This method is limited by the working conditions, as the OCV cannot be directly measured if there is no sufficient rest time.

The terminal voltage method is based on the terminal voltage drops because of the internal impedance when the battery is discharging. The terminal voltage of the battery is approximately linearly proportional to the SoC. This method has been employed at different discharge currents and temperatures, but at the end of the discharge, the estimation error is large, as the terminal voltage of the battery suddenly drops (CHANG, 2013).

Measuring the battery impedance is also a way to estimate SoC. But it is very difficult to measure online electrical impedance because sinusoidal alternating current (AC) may be required (ZHANG et al., 2018). For this reason, this method is not popular in applications as electrical vehicles.

3.6.2 Book-keeping

Booking-keeping estimation method uses battery discharge current data as input. The most popular method is known as Coulomb Counting and consists of measuring the charging or discharging current and integrating it over time in order to estimate SoC (CHANG, 2013). In Coulomb Counting, the $SoC(t)$ is estimated from the current $I(t)$ and the previously estimated SoC value $SoC(t-1)$, as calculated in Equation (3.2), where Q_n is the nominal capacity.

$$SoC(t) = SoC(t-1) + I(t)/Q_n \cdot \Delta t \tag{3.2}$$

This method is simple to implement and requires low computational capacity and for this reason it is widely used. However, there are several factors that affect the accuracy of the estimation: temperature, current rate and battery remaining capacity. Also, the unknown initial SoC, capacity fading, self-discharge rate and current sensor errors are some of the error sources for the Coulomb Counting method (ZHANG et al., 2018).

3.6.3 Adaptive systems

Adaptive systems use artificial intelligence to estimate the SoC. Methods include back propagation or radial basis function neural network, fuzzy logic and Kalman filter, for example. With the development of artificial intelligence, various new adaptive systems for SoC estimation have been developed and are available in the literature (ZHANG et al., 2018).

In general, a neural network contains an input layer, and output layer and a hidden layer. The input layer uses some battery data, as voltage, current and temperature. Output layer provides the current SoC. The hidden layer perform nonlinear transformations of the inputs. Different weights can be defined to the inputs (CHANG, 2013). Figure 7 presents a basic network architecture of neural network used to estimate SoC. These methods require at least two phases: a training phase to set the weights at those that result a best compromise and an evaluation phase to test the accuracy of the results. Neural network methods provide a good accuracy of the SoC (errors lower than 3%) and no accurate battery model is necessary, but requires a high computational effort, resulting in expensive implementation (POP et al., 2008).

Fuzzy logic is another useful algorithm used to present a nonlinear complex model with the help of the appropriate training dataset (ZHANG et al., 2018). In Fuzzy logic a large amount of experimental data, test curves and reliable expert knowledge is used for online identification of the battery state of charge. An original battery model is developed at the initial stage of the measurement process, then the calculated result with data from Fuzzy logic system is compared with the actual measurement, from which the feedback from the error is used to adjust the Fuzzy system and determine the system parameters (ZHOU; LI, 2015). After several continuous corrections, a relatively ideal battery model can be obtained with high precision on battery SoC estimation. However, it requires complex computations and large storage memory units, which results in high cost.

Another popular adaptive method is the Kalman filter. This technique is an optimum state estimator. The most attractive feature of the Kalman filter is that it has a self-correcting nature when the system is running, which helps to tolerate high variations (ZHANG et al., 2018) (REMES, 2016). The disadvantage is that it requires high performance model and high calculation capability of the BMS (ZHOU; LI, 2015). Variations of the Kalman filter are also popular: extended Kalman filter and unscented Kalman filter can be applied in nonlinear system, more detail about both methods can be seen in (HUANG et al., 2018).

Figure 7 – Architecture of neural network SoC estimation method

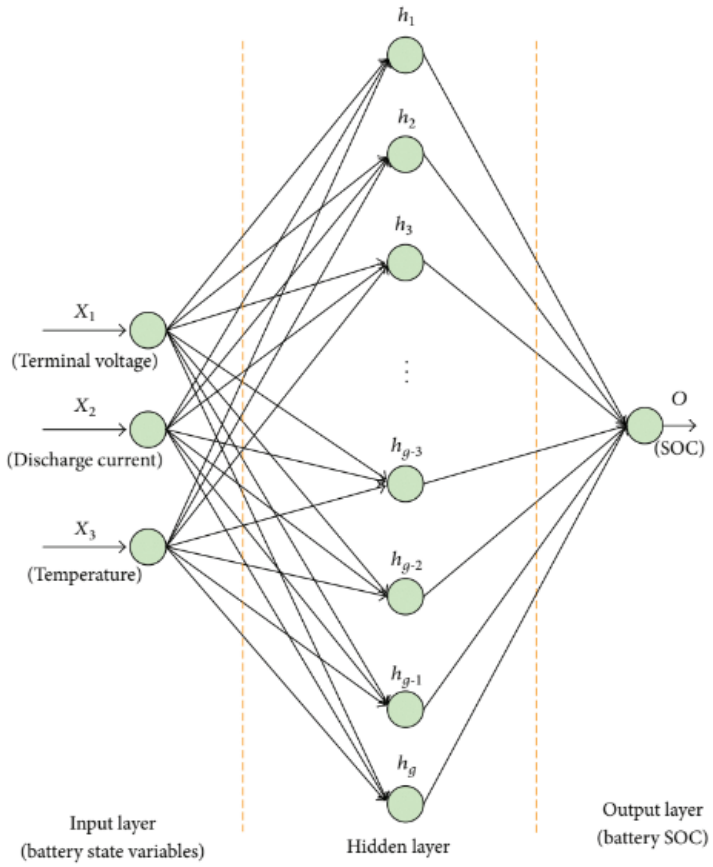

Source: (CHANG, 2013)

3.6.4 Hybrid methods

A hybrids algorithm method is composed of two or more algorithms. In this way, it can improve the efficiency and accuracy of the battery model and avoid the shortcomings of a single algorithm (ZHANG et al., 2018). The information used in an individual method is limited, thus a hybrid method can maximize the available information, integrate individual model information and make the best use of the advantages of multiple estimation methods. The literature show that hybrid methods generally produce good SoC estimation results compared to individual methods.

Coulomb counting and terminal voltage method compose a new SoC estimation method. Direct measurement method with the terminal voltage measurement during the equilibrium state and book-keeping estimation using Coulomb counting method during the discharge state has been applied in real-time estimation system. Coulomb counting and Kalman Filter combination also provides a new method to estimate SoC. In this case, Kalman filter method corrects the initial values using in Coulomb counting method (ZHANG et al., 2018). There are also several other method combinations available in literature.

3.7 SOH ESTIMATION

The state of health (SoH) is a indicator of the battery degradation. Most studies consider the Equation (3.3) to define the SoH of the battery, where Q_n is the nominal capacity and Q_c is the current capacity that is degraded due to charge and discharge cycles and calendar life of the

battery (YAO et al., 2021).

$$SoH(\%) = Q_c/Q_n \cdot 100 \tag{3.3}$$

A wrong SoH estimation can lead to misjudgment of the operating state, affect accurate identification of the battery fault state and increase the risk of battery system's hidden safety hazard. As a consequence, the accurate estimation and prediction of SoH is very important in vehicle operation. There are few reviewed methods and the classification of the existing relevant ones is relative rough. The SoH estimation face some problems: it can not be directly measured, it has a strong time variability and a high non-linearity (YAO et al., 2021). A possible classification for the prediction methods is: model-based methods, data-driven methods and hybrid methods (TIAN et al., 2020). As this function is not the main point at this study, the methods will not be presented in details.

The model-based method is based on the degradation and the failure mechanism of the lithium-ion batteries. This method is relatively mature, including several forms, such as the electrochemical impedance spectroscopy (EIS) model, the thermoelectric coupling model, the Thevenin model and the shunt of the multi-stage resistor-circuit model. The accuracy of model-based methods depends on the complexity of the model and the accuracy of parameter identification (TIAN et al., 2020). Data-driven methods do not need to consider the complex electrochemical changes and the fluctuations of related active substances inside the battery. This method uses the characteristic value of parameters measured directly or indirectly and combine with data mining algorithm, so the relationship between the parameters and the state of health is established from the data's overall level. Different data-driven methods are available and are divided into four categories: statistical filtering, neural network, vector machine and statistical data method (TIAN et al., 2020).

Hybrid methods, as in SoC estimation, combine the advantages of different methods and the decrease the shortcomings. The model-based methods are considered simple and easy to operate, but the reliability is sensitive to the accuracy of model construction and parameters identification, while the data-driven method has strong robustness and strong anti-interference resistance to parameter fluctuation, but requires experimental data.

3.8 COMMUNICATION

The BMS usually has to communicate to the complete system, for example a vehicle control unit (VCU), to provide status information and receive instructions and parameters. Different communication protocols are available and to select one, some specifications need to be considered: required speed, robustness and reliability. Apart from system level, between BMS components, communication is also needed. For modular system, it is necessary to define if there is a master module and how it talks to slave modules (LELIE et al., 2018).

Nowadays, the Controller Area Network (CAN) bus is one of the most prominent buses used in vehicles environments because it is very flexible regarding the number of bus members and it offers a good noise resistance. Other communication methods are SPI (Serial Peripheral Interface), I^2C (Inter-Integrated Circuit) and Onewire bus.

In applications with high power, the battery pack consists of several cells and in these cases, the BMS consists of some analog front-end (AFE) integrated circuits daisy-chained and one central module or electronic control unit (ECU). The AFE devices are used for basic functions like signal acquisition, and they are often referred to as BMS-slaves. The advanced functions are implemented in ECU, also known as BMS-master. The communication between master and slave can use I^2C, SPI and CAN (LELIE et al., 2018).

4 SYSTEM DEVELOPMENT

The implementation of the complete experimental setup used to perform the tests and evaluate the BMS features and batteries behavior is presented in this chapter. This setup is composed of the designed BMS evaluation module, that consists of the bq7692000PWR and the bq78350R1A dedicated integrated circuits (ICs), the battery pack with 5 series cell of NCR18650B Li-ion batteries, the DC power supply used as charger and an electronic load used to discharge the battery with constant current. The interface board (EV2400) provides communication with the BMS from the laptop and the *bqStudio*® software is used to program the BMS and record the data log. Figure 8 presents am illustration of the experimental setup with all components.

Figure 8 – Experimental setup developed to perform tests

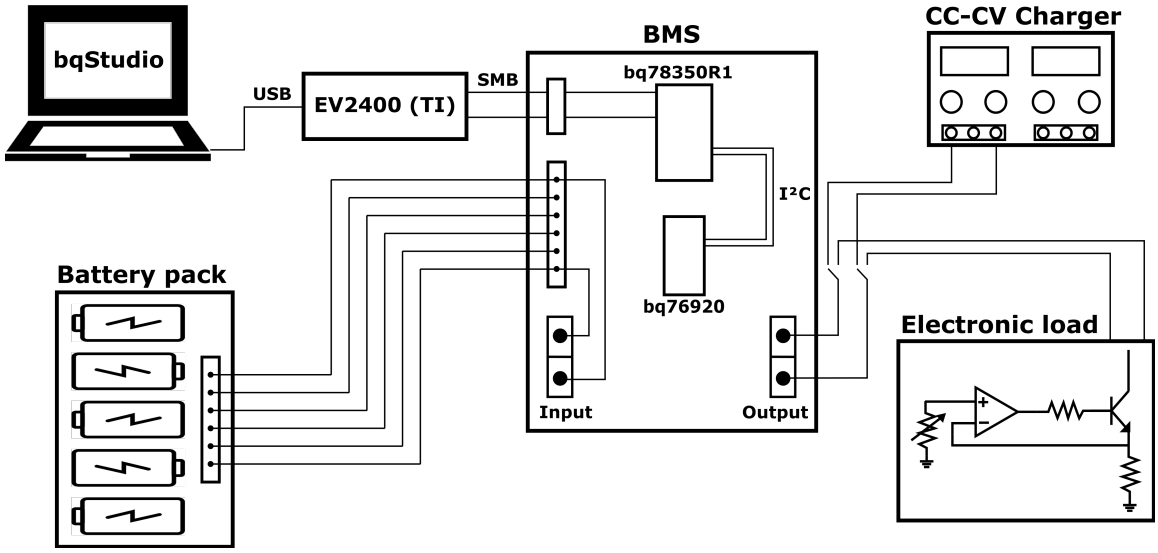

Source: the author

4.1 BMS EVALUATION MODULE

Considering the functions mentioned in Chapter 3 and the analysis of the main commercial BMS, available in Appendix A, a set of dedicated integrated circuits from Texas Instrument was selected. This BMS uses two ICs, the bq7692000PWR (also referred as bq76920 in this document) and the bq78350R1A.

The bq76920 is an analog front-end (AFE) circuit, responsible for measuring voltage, current and temperature and also provide a hardware protection based on these measures. This device needs a host-controller to define the thresholds and enable the other functions.

In this study, the host-controller is the bq78350R1A, designed to control the bq769x0 AFE family. It is a gas gauge (GG) circuit and provides the more advanced functions for the system, as cell balancing, state of charge and state of health estimation and protection features. According to the manufacturer, the combination of these circuits provides a solution to different applications, as light electric vehicles, power tools, uninterruptible power supply and others.

Figure 9 presents a simplified schematic with both circuits. The bq76920 provides the battery cells connection, the current and temperature sensors, the hardware protection and it is

able to power on the bq78350R1A. These ICs communicate with each other using the Inter-Integrated Circuit (I^2C) communication protocol. The bq78350R1A provides a SoC indication using until five LEDs and commands the AFE based on the information received and its functions.

Figure 9 – Simplified schematic of the BMS evaluation module circuit

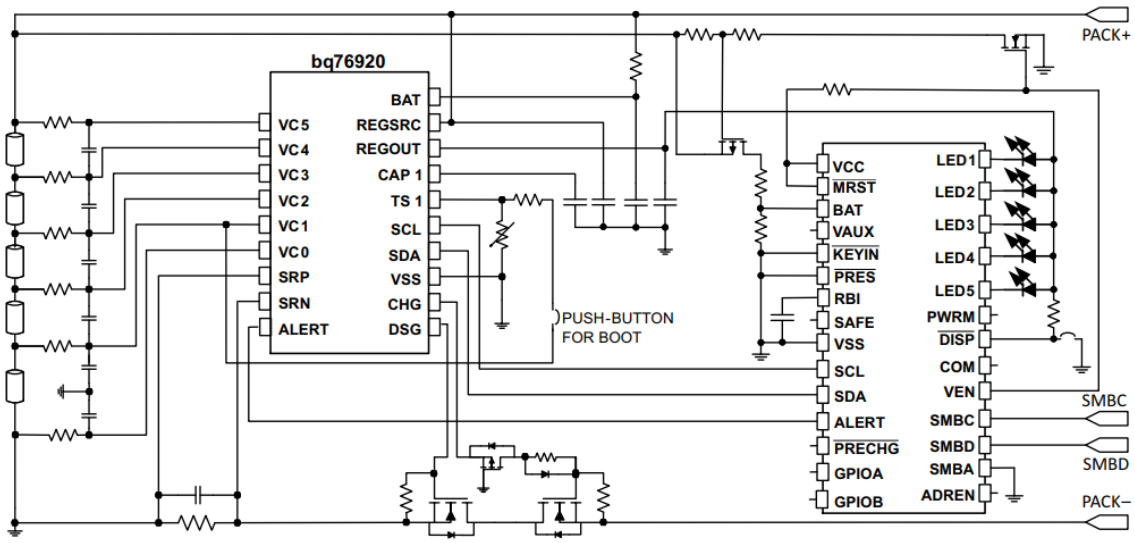

Source: (TEXAS INSTRUMENTS, 2019b)

4.1.1 bq7692000PWR - Analog front-end circuit

The bq7692000PWR is part of the bq769x0 family of analog front-end devices. This device provides a complete battery pack monitoring and protection solution. The bq76920 supports up to 5 series cells or typical 18V packs of a variety of battery types, as lithium-ion and lithium-iron-phosphate. Through the I^2C communication, the host-controller (in this case, the bq78350R1A) can use the bq76920 to implement many battery pack management functions. The AFE offers the basic functions, such as monitoring each cell voltage, pack current, temperature, protection functions controlling the charge and discharge field effect transistors (FET) and also internal drivers to cell balancing. The host is required to set the protection thresholds and to recover the FET control outputs. If the AFE operates unsupervised, a fault condition would leave the battery system disabled with no recovery attempt.

4.1.1.1 Pin description

The pin diagram of bq76920 is illustrated in Figure 10(a). The integrated circuit has 20 pins in a 20-TSSOP package (Figure 10(b)). The description of the pins follows.

DSG and CHG: responsible for enabling the discharge and charge FET, respectively;

VSS: chip ground;

SDA and SCL: data and clock lines, respectively, I^2C communication wires;

TS1: thermistor positive connection;

CAP1: output voltage around 3.6V;

Figure 10 – Pin diagram of bq7692000PWR integrated circuit

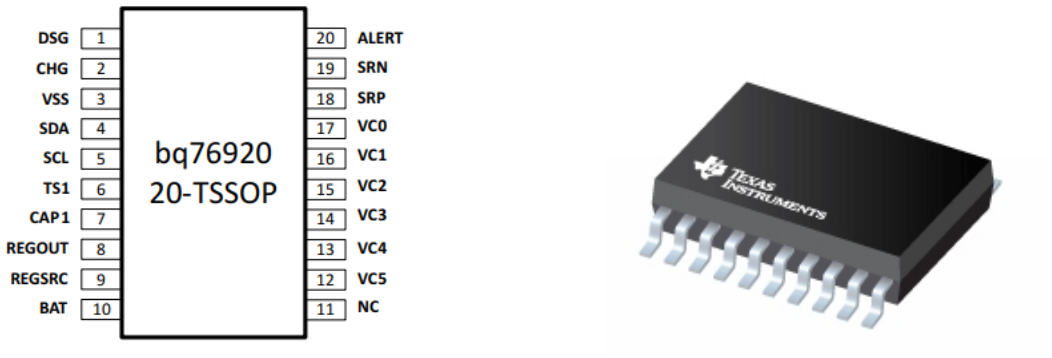

(a) Pin diagram (b) 3D model

Source: (TEXAS INSTRUMENTS, 2019a)

REGOUT: regulated output voltage (Low Dropout - LDO) used to supply the host-controller;

REGSRC: input source for LDO, DSG and CHG pins. It is connected to the battery pack positive terminal;

BAT: battery pack (top cell positive connection);

NC: not connected;

VC0: sense voltage pin to the first cell, negative terminal;

VC1 to VC5: sense voltage pin to the i-th cell positive terminal, $i \in \{1,\ldots,5\}$;

SRP and SRN: positive and negative pins, respectively, for current measurement;

ALERT: I/O pin used to interrupt the charge or discharge process.

The bq76920 consists of three major subsystems: measurement, protection and control. These subsystems work together to ensure that the fundamental battery pack parameters (voltage, current and temperature) are accurately captured and easily available to the host-controller. At the same time, it ensures a baseline or secondary level of hardware protection in which case the host-controller is unavailable to manage the fault conditions (TEXAS INSTRUMENTS, 2019a). These subsystems are presented in details next.

4.1.1.2 Measurement

The measurement subsystem is responsible for measuring the main variables of a battery pack, in this case, cell voltages, pack current and temperature and provides this data for other functions. Using analog-to-digital converters (ADC), the variable is measured using specific circuits and stored in registers, so the host-controller can read it and perform a function. Cell voltage and temperature use a 14-bit ADC while the pack voltage and current use a 16-bit ADC.

This 14-bit ADC measures all differential cell voltages and thermistor temperature with an unsigned full scale range of 0 to 6.275 V and a least significant bit (LSB) of 382 μV. Each cell is measured over a 50 ms decimation window and a complete update is available every 250 ms. If the cell balancing function is enabled, this time is reduced to 12.5 ms.

Each device is factory-trimmed for gain and offset and requires no additional calibration or correction factor application. The Equation (4.1) shows how to convert the 14-bit ADC reading into an analog voltage.

$$V_{cell} = GAIN \cdot ADC_{cell} + OFFSET \tag{4.1}$$

The temperature is measured using a 10 kΩ NTC 103AT thermistor. This is measured by applying a factory-trimmed internal 10 kΩ pull-up resistance to an internal regulator value of nominally 3.3 V. This thermistor can be placed in any area in the battery pack or in the BMS, to measure for example, a cell temperature or the FET heating. Temperature measurement is taken every 2 seconds. The Equation (4.2) presents how to use the 14-bit ADC reading to determine the resistance of the external 103AT thermistor. To convert the thermistor resistance into temperature, the user needs to refer the component manufacturer's datasheet.

$$R_{TS1} = (10{,}000 \cdot V_{TS1})/(3.3 - V_{TS1}), \tag{4.2}$$

where $V_{TS1} = ADC_{TS1} \cdot 382\mu V$.

The 16-bit integrating ADC is responsible for measuring the current. It provides measurements of accumulated charge across the current sense resistor in a integration period of 250 ms. The full scale range of this ADC is ±270 mV, with a maximum recommended input range of ±200 mV, thus yielding an LSB of approximately 8.44 μV. The Equation (4.3) presents how to use the 16-bit ADC reading to determine the voltage drop at the current sense resistor.

$$V_{CC} = ADC_{CC} \cdot 8.44\mu V \tag{4.3}$$

where ADC_{CC} is the result of a 2's complement of the 16-bit ADC.

The pack voltage is also measured by a 16-bit ADC. Once converted to digital form, each cell voltage is added up and the summation result is stored in specifics registers. This 16-bit value has a nominal LSB of 1.532 mV. Equation (4.4) presents how to convert the pack voltage ADC reading into an analog voltage.

$$V_{bat} = 4.GAIN.ADC_{cell} + (N_{cell}.OFFSET) \tag{4.4}$$

where N_{cell} is the number of connected cells.

4.1.1.3 Hardware Protection

The bq769x0 family provides a hardware protection for the battery pack, that is an extra degree of safety and is intended to complement the standard protection feature set that would be incorporated into the host-controller. In bq769x0 device, is possible to set threshold and delay to protect the batteries against overvoltage (OV), undervoltage (UV), overcurrent in discharge (OCD) and short-circuit in discharge (SCD). The voltage protections consider the voltage in each cell and current protections consider the pack current. All protection thresholds and delays should be loaded into the AFE by the host-controller during the system startup, but the AFE is predefined with default values in case the host is unable to program the protection. Figure 11 presents the circuit used to interrupt the batteries charge or discharge. The bq76920 provides two low-side FET drivers (DSG pin for discharge and CHG pin for charge protections), which control N channels (NCH) power FETs or may be used as a signal to enable other circuits such as a high-side N channel FET. The CHG and DSG outputs are powered from a 12 V supply regulated from the REGSRC supply pin.

During the discharge, if the undervoltage threshold, the overcurrent or the short-circuit current threshold is reached, the DSG pin is set to 0 V and the FET interrupts the discharge current path. In the same way, during a charge, if the overvoltage or the overcurrent threshold is exceeded, the CHG pin is set to 0 V and the charge current path is blocked. In this way, other protections conditions can be implemented by the host-controller.

The AFE device is not able to automatically restart a charge or discharge process after a protection. The host-controller must initiate all protection recoveries. If the protection condition persists, the fault may immediately retoggle.

Figure 11 – Hardware protection circuit of bq76920 using low-side FETs

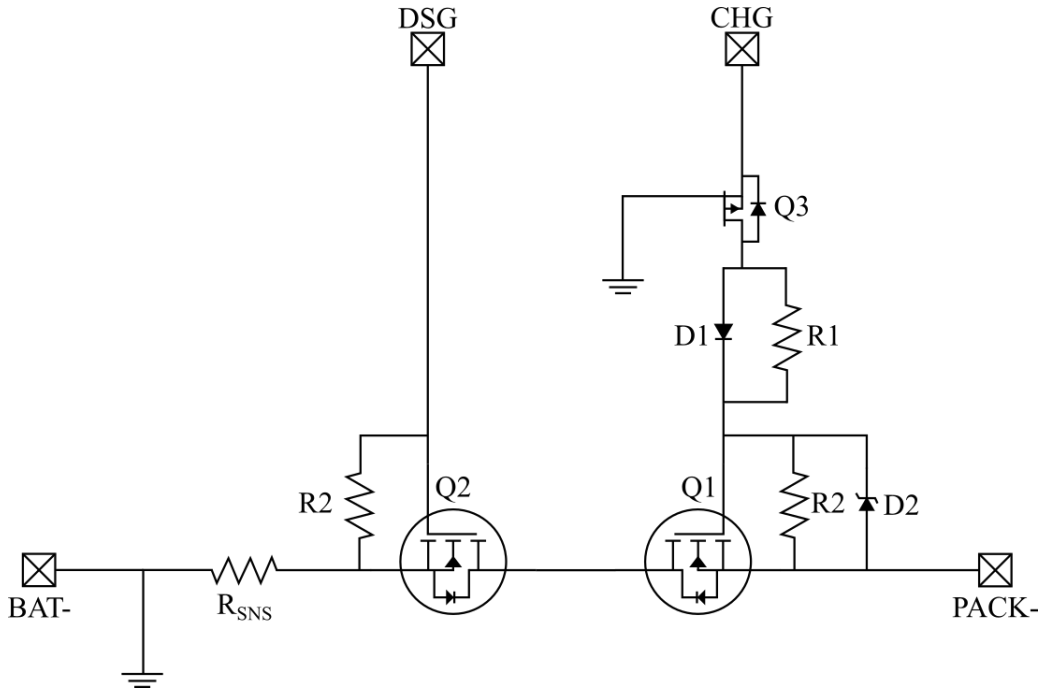

Source: adapted from (TEXAS INSTRUMENTS, 2019a)

4.1.1.4 Control

The control subsystem in the bq769x0 family implements a suite of useful pack features, including direct low-side NCH FET drivers, cell balancing drivers, the ALERT digital output, an external low-dropout (LDO) regulator and a load detection.

As already described in Section 4.1.1.3, the AFE device provides two low-side FET drivers (CHG and DSG pins), to control NCH power FETs or may be used as a signal to enable other circuits, such as high-side NCH circuit. Both DSG and CHG drives have a fast pull-up to nominally 12 V when enabled. DSG uses a fast pull-down to VSS when disabled and CHG uses a high impedance pull-down path when disabled. To enable the charge FET (CHG), the CHG_ON register bit needs be set to 1, to disable it, the register needs be set to 0. The discharge FET (DSG) is controlled through the DSG_ON register bit similarly.

The bq76920 device, used in this project, can provide internal and external passive cell balancing options. The algorithm to determine the conditions to enable the balancing must be implemented by the host-controller while the AFE provides the cell voltage measurement and the balancing drivers. When using the internal balancing drivers, the current is limited up to 50 mA per cell. This is the option considered in this project. To activate a particular cell balancing channel, the corresponding bit for that cell needs to be set. Multiple cells can be

simultaneously balanced but not adjacent cells. When using the internal balancing, care should be taken to avoid exceeding package power dissipation ratings.

The ALERT pin can be used as an active high digital interrupt signal. This pin can be connected to a GPIO (General Purpose Input Output) port of the host-controller. The ALERT pin is enabled if any bit of the SYS_STAT register is set. The pin can also be driven by an external source, and when it is forced high externally while low, the device will recognize this signal as a fault condition and set the OVRD_ALERT bit. This event automatically disables both CHG ans DSG FET drivers.

An LDO voltage regulator is available as a simple way to provide power to additional components in the BMS circuit. The LDO is set by the manufacturer and can deliver 2.5 V or 3.3 V through the REGOUT pin. In this project, the 2.5 V option is used to supply the host-controller bq78350R1A.

A load detection circuit is available on the CHG pin and is activated whenever the CHG FET is disabled. This circuit detects if the CHG pin is externally pulled high when the high impedance pull-down path should actually be holding the CHG pin to VSS. It is useful for determining if the PACK– pin (outside of the AFE) is being held at a high voltage, for example, if the load is present while the power FETs are off. The state of the load detection circuit is read from the LOAD_PRESENT bit and the host-controller can monitor it.

4.1.2 bq78350R1A - Gas gauge circuit

The bq78350R1A is a battery management controller for lithium-ion (Li-ion) batteries. It is provided as a companion to the bq769x0 family of AFE devices. It receives the measurement information from the AFE and thus can perform its functions. The main functions will be described in this section.

4.1.2.1 Pin Description of the bq78350R1A

Figure 12 presents the pins diagram. The bq78350R1A has 30 pins and is a TSSOP package type. The description of the pins is presented as follows.

Figure 12 – Pin diagram of the bq78350R1A integrated circuit

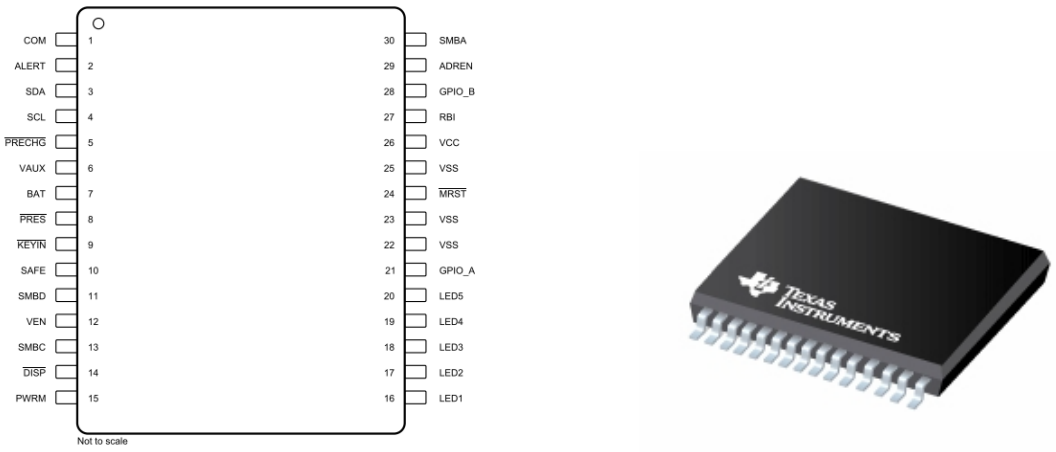

(a) Pin diagram (b) 3D model

Source: (TEXAS INSTRUMENTS, 2019b)

COM: LCD display common connection, it is not used in this work;

ALERT: input from the bq76920 AFE;

SDA and SCL: data and clock lines, connected with the bq76920;

PRECHG: optional pre-charge FET driver, used in this work to perform pre-charge;

VAUX: auxiliary voltage input. It is not used in this work, so it is connected to VSS;

BAT: translated battery pack voltage;

PRES: input pin used to sense a battery pack reinsertion to recover current-based protection. It is not used in this work and is tied to VSS;

KEYIN: input pin used as a hardware command to enable or disable the DSG FET, in case safety conditions allow. Not used in this work, thus it is connected to VSS;

SAFE: output voltage to enforce an additional protection level, used to blow a fuse, for example. It is not used and is tied to VSS;

SBBD: SMBus data line;

VEN: output signal used to switch the input voltage circuit to reduce power consumption of the BAT translation divider network;

SMBC: SMBus clock line;

DISP: display control for the LEDs;

PWRM: power mode state indicator output. Not used in this work.

LED1 to LED5: LED or LCD drivers used to indicate the SoC;

GPIO A and B: configurable input or output, not used in this work;

VSS: chip ground;

MRST: master reset input that forces the device into reset when held low. This pin is held high for normal operation;

VCC: positive supply voltage, 2.5V from the REGOUT pin of bq76920;

RBI: RAM backup input. Connected to a capacitor to protect loss of RAM data in case of short-circuit condition;

ADREN: optional digital signal that enables address detection. Not used;

SMBA: optional SMBus address detection input. Not used in this work, it remains tied to VSS.

The bq78350R1A has features related to manufacture production, as device security, data flash access and format, manufacturing configuration and testing. There are also some advanced usage features, as life time data collection and different power modes. These features are not evaluated in this work, since the main objective is to verify the main functions of the BMS related to the battery pack. These functions are described in the next sections.

4.1.2.2 Basic Measurement System

As already mentioned in Section 4.1.1, the bq76920 is responsible for the measurements of voltage (each cell and the complete pack), charge and discharge currents and also the temperature. The bq78350R1A reads these values and uses them to perform the protection functions, for example.

4.1.2.3 Protections

The bq78350R1A device supports a wide range of battery and system protection features that can be configured. These protections can be separated into two levels: primary and secondary levels. The primary safety features include the following protections:

- Cell overvoltage and undervoltage;
- Charge and discharge overcurrent;
- Short-circuit;
- Charge and discharge overtemperature.

The secondary level can be used to indicate more serious faults via the SAFE pin. This pin can be used to blow an in-line fuse to permanently disable the battery pack from charging or discharging. The secondary safety protection features include:

- Safety overvoltage;
- Safety undervoltage;
- Safety overcurrent in charge and discharge;
- Safety overtemperature in charge and discharge;
- Charge FET and precharge FET fault;
- Discharge FET fault;
- Voltage imbalance detection;
- Open thermistor detection;
- AFE communication fault.

The protections can be adjusted as desired. It is possible to enable or disable each protection (except for the hardware protection in the bq76920), set the threshold value and the delay time to activate the protection and also a threshold value to recover the operational state.

4.1.2.4 Cell Balancing Algorithm

Cell balancing is accomplished by connecting a parallel bypass load to each cell depending on its individual voltage. The GG algorithm only provides cell balancing during the battery pack charge. If a battery cell has a higher voltage than the others during charging, the bypass load is connected to that cell by closing the integrated low power control FETs in the AFE IC. With that, a fraction of the charging current bypasses that cell and prevents it to reach a high voltage (TEXAS INSTRUMENTS, 2004). Using the internal FETs and load, the balancing current is limited up to 50 mA.

The bq78350R1A is responsible for defining the cell and the moment to enabled the function based on the user configuration. The cell balancing is enabled if two conditions are satisfied: the cell voltage is higher than the cell balance threshold and the largest voltage difference between the cells is above the cell balance minimum value. These conditions are verified at fixed intervals, which may be defined by the user. To keep the function operational until the end of the charge, a window value is defined. As soon as any cell voltage exceeds the threshold value plus the window value, the threshold is updated by the result of the sum of these two values (TEXAS INSTRUMENTS, 2004). The parameters and their default values are presented in Figure 13. The described behavior can be seen in Figure 14.

Figure 13 – Cell balancing configuration of bq78350R1A

Cell Balancing Config		
Cell Balance Threshold	3900	mV
Cell Balance Window	100	mV
Cell Balance Min	40	mV
Cell Balance Interval	20	s

Source: the author

The cells to be balanced are prioritized by highest cell voltage but the bq78350R1A will not try to balance adjacent cells. If adjacent cells need to be balanced, the GG will alternate between the highest and next-highest adjacent cells until they are balanced.

Figure 14 – Cell balancing behavior

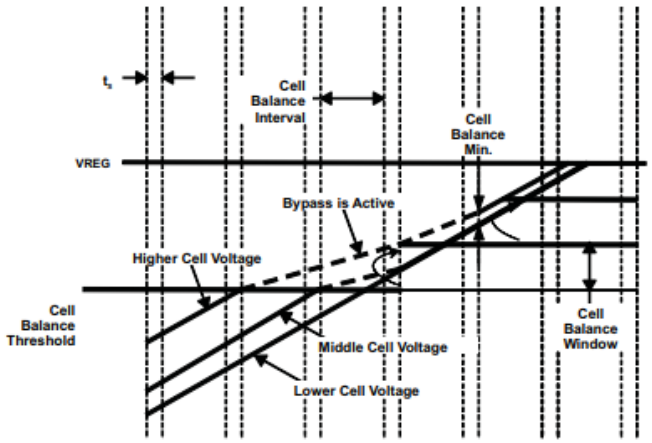

Source: (TEXAS INSTRUMENTS, 2020)

4.1.2.5 Charge Control Algorithm

The device is able to provide a range of options to configure the charging algorithm and its actions based on the application requirements. Based on the battery type, appropriate charging current and charging voltage are predefined, considering a CC-CV charging method.

There are two charging stages available: pre-charge and fast-charge, and the user can set the values to current and cell voltage for each mode. Pre-charge is enabled if any cell voltage is lower than the Start Voltage. It is a cell battery recommendation, to provide limited charging current when voltage cell is too low. During the pre-charge, if the cell voltage reaches the Recovery Voltage, the fast-charge is enabled and the current is limited by a higher value (3500 mA, in this case).

There are temperature-based protections that control the charge process. The BMS is able to prevent the charge to start if the battery temperature is out of the security range, the user can define this range through the charge inhibit low and high temperature parameters. During the charge, if the temperature reaches some of the limits defined in charge suspend low or high temperature parameters, the charge process is interrupted.

When the battery pack is fully charged, the BMS should stop the charging current. The termination condition is defined by the user and is composed of the minimum charge current desired (taper current) and the voltage termination, which is added to the maximum cell voltage during the charge and the result must be higher than the cell charge voltage.

All these parameters and their values can be seen in Figure 15.

Figure 15 – Charge algorithm configuration values

Name	Value	Unit
◢ Temperature Ranges		
Charge Inhibit/Suspend Low Temp	0	degC
Precharge Temp	0	degC
Charge Inhibit High Temp	43	degC
Charge Suspsend High Temp	45	degC
Hysteresis Temp	3	degC
◢ Fast Charging		
Voltage	4200	mV
Current	3500	mA
◢ Pre-Charging		
Current	100	mA
Start Voltage	2500	mV
Recovery Voltage	2900	mV
◢ Termination Config		
Charge Term Taper Current	250	mA
Charge Term Voltage	75	mV

Source: the author

The charging process can be disabled under some situations: the valid charge termination conditions were reached, battery cell overvoltage, overcurrent during the charging or cell temperature out the range. The CHG FET is disabled until a recovery condition is achieved.

4.1.2.6 Compensated End-of-Discharge Voltage Gas Gauging Algorithm

The gas gauge function in bq78350R1A uses the Compensated End-of-Discharge Voltage (CEDV) gauging algorithm to estimate important data about the charge state of the battery pack. The remaining capacity and the state of charge are the most important outputs. The user can determine the capacity units by choosing between mAh or mWh. In this work the mAh unity is used.

Using the battery nominal capacity as the maximum capacity, the BMS accumulates the measured quantities of charge and discharge to indicate the remaining capacity (RC) of the battery pack. This information is counted up during charge to a maximum value of full capacity and down during discharge and self-discharge to a minimum of 0 mAh. The BMS compensates the charge current measurement for temperature and state-of-charge of the battery pack. The bq78350R1A also adjusts the self-discharge estimation based on temperature.

Besides charge and self-discharge compensation, the BMS calibrates the RC at three low battery cell voltage thresholds. These thresholds are three fixed setpoints (EDV2, EDV1 and EDV0) wich are compared with the lowest cell voltage during the discharge. When the lower cell voltage reaches the EDV2 setpoint, the SoC indication is corrected to a predefined SoC percentage, the same happens for the other setpoints. In this work, after some experimental tests, the values are defined as EDV2= 2.65 V at SoC= 7%, EDV1= 2.55 V at SoC= 3%, EDV0= 2.525 V at SoC= 0%, considering the minimum cell voltage of 2.5 V. This provides a voltage-based calibration to the RC counter (TEXAS INSTRUMENTS, 2020). The user can access the available capacity at any time through the register.

The full charge capacity (FCC) data represents the initial or last measured full discharge of the battery pack. It is used as the battery full charge reference for relative capacity indication. The BMS updates FCC after the battery pack undergoes a qualified discharge from nearly full to a low battery level. In this way, the bq78350R1A learns the true discharge capacity of the battery under system-user conditions.

The SoC is indicated through two different parameters: ASOC (absolute state of charge) and RSOC (relative state of charge). The value presented in ASOC relates remaining capacity and the nominal capacity, while the RSOC relates the remaining capacity and the full charged capacity.

The SoH is also provided by the gas gauge algorithm. The value is calculated as the percentage ratio of the full charge capacity and the nominal capacity, it is a read-only data.

The BMS also provides a predicted remaining time, in minutes, to fully charge the battery pack or to discharge it. This estimation relates the current and the remaining capacity.

Summarizing, the BMS gas gauging algorithm estimates the remaining capacity during charge and discharge and the other indications are related to this value.

4.1.3 Prototype development

Using the bq76920 and the bq78350R1A, the evaluation board circuit was developed considering the recommendations available in (TEXAS INSTRUMENTS, 2018). The development process starts with the circuit schematic, which was made using the *Proteus*® software. The schematic is available in Appendix B. After that, it was possible to start the components placement and routing the connections. The final 3D version of the prototype is presented in Figure 16(a) and the Figure 16(b) shows the final assembly of the prototype.

The AFE peripheral circuitry is composed of a RC filter to measure the battery cell voltages; a battery cell simulator, using resistors, that can be used by connecting shunts on the J11 header and connecting a DC power supply in the input connector; a shunt resistor used to measure the current during charge or discharge; the SDA and SCL wires to provide communication with the GG IC and the power FETs circuit used to control the current path during a protection state. There is also an NTC input to measure the battery cell temperature and switch S1 is used to boot the circuit, sending a cell voltage for the TS1 pin.

The GG peripheral circuits are composed of a supply circuit using the battery pack voltage to power on the IC; a circuit to provide the communication between the ICs, via I^2C and with the external adapter via SMBus. There is a circuit to perform the pre-charge; also a

Figure 16 – Prototype 3D view and the final prototype

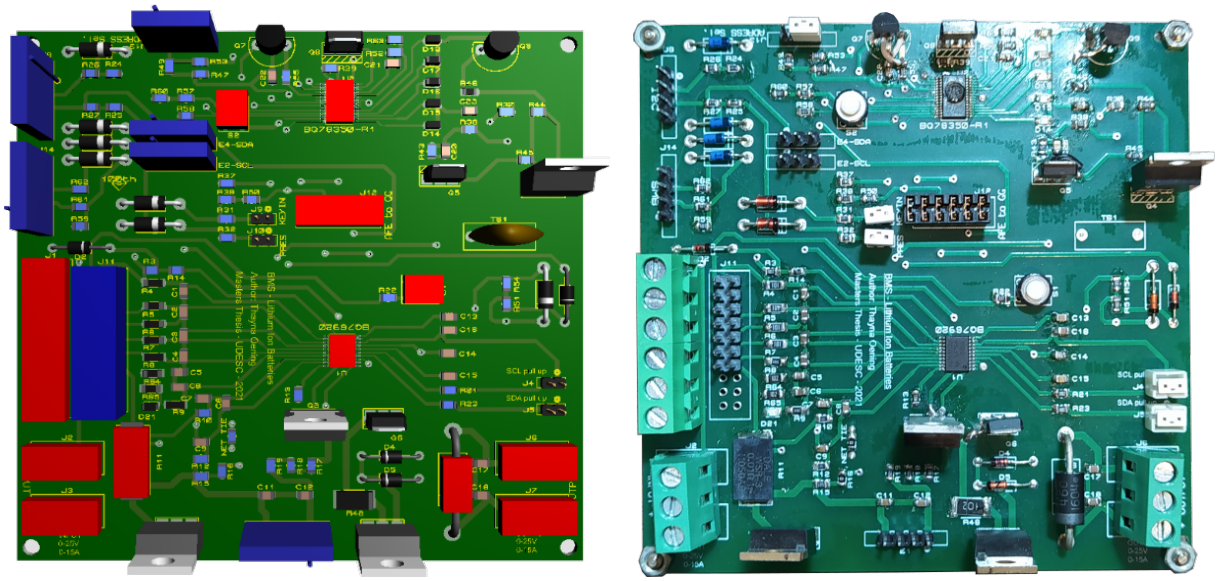

(a) 3D prototype view (b) Final prototype

Source: the author

circuit using LEDs to indicate the battery pack SoC, it is activated through S2 switch. The ICs are connected to each other using the J12 header.

4.2 NCR18650B - PANASONIC BATTERY

A NCR18650B lithium-ion battery was selected to perform the tests in this work. It is a cylindrical cell, unprotected, with nominal voltage of 3.6 V and typical capacity of 3350 mAh from Panasonic manufacturer. Its material is composed of lithium nickel cobalt aluminum oxide (NCA - $LiNiCoAlO_2$).

A battery pack composed of 5 series cells are used to provide a nominal voltage of 18 V. Figure 17(a) provides an image of the batteries used in this work and Figure 17(b) shows the battery pack assembly used during the tests. This assembly was used because it allows for an easy change of cell position or the use of a new cell.

The NCA battery was selected because it delivers a high energy density and it is also used by the EV manufacturers. It provides high specific energy, a good specific power and a long cycle life. However, it is not as safe as the other lithium ion batteries and it is more costly to manufacture (see Figure 4 and Table 2). The main electrical and operational specifications are shown in Table 3.

The manufacturer provides some operational behaviors, as presented in Figures 18 and 19. The recommended charge mode is the CC-CV method (Figure 18(a)), already described in this work. The ideal charge current, during the constant current charge, is 1650 mA (equivalent of 0.5C), and the maximum charge voltage is 4.2 V per cell. There is also the information about the capacity fade under charge and discharge cycles (Figure 18 (b)), which indicates a capacity reduction of 20% in 200 cycles. The battery capacity is reduced to around 2250 mAh after 500 cycles, close to 67% of the typical capacity.

Figure 17 – NCR18650B lithium-ion battery

(a) NCR18650B Li-ion

(b) Battery pack with 5 series cell

Source: the author

Table 3 – NCR18650B battery cell specifications

Specifications	Value
Rated capacity (at 20 °C)	3200 mAh
Minimum capacity (at 25 °C)	3250 mAh
Typical capacity (at 25 °C)	3350 mAh
Nominal voltage	3.6 V
Charging	CC-CV, 1625 mA, 4.20 V, 4 h
Temperature charge	10 to 45 °C
Temperature discharge	-20 to 60 °C
Temperature storage	-20 to 50 °C
Energy density	676 Wh/l
Specific energy	243 Wh/kg

Source: adapted from (PANASONIC, 2012)

Figure 18 – NCR18650B charge and cycle life characteristics

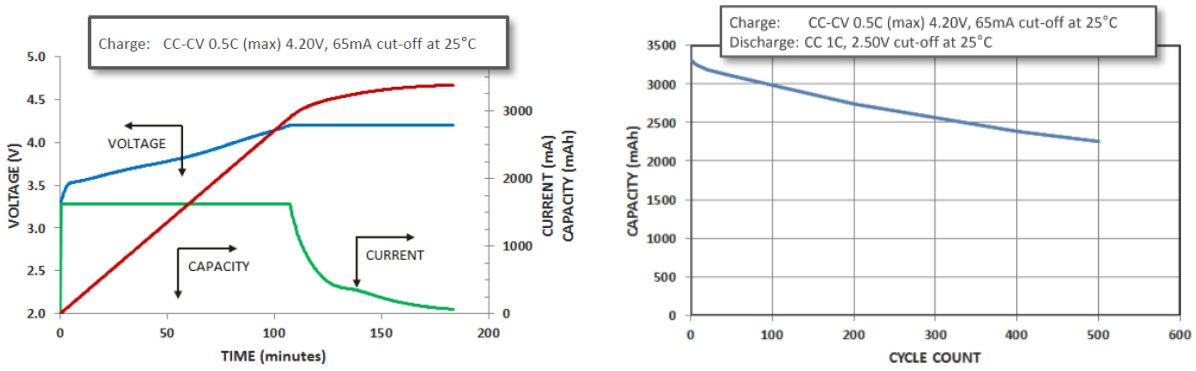

(a) Charge characteristics

(b) Cycle life characteristics

Source: (PANASONIC, 2012)

Figure 19(a) presents the discharge behavior under different rates of discharge. The cell is discharged from 4.2 to 2.5 V with different discharge current rates of 0.2, 0.5, 1.0 and 2.0C. The discharge capacity is indicated for each case and it is notable that the capacity is increased when the discharge rate is lower (0.2C) but very similar in 0.5, 1.0 and 2.0C. The manufacturer presents, in addition, the discharge behavior under different temperatures (Figure 19(b)). For negative temperatures and even 0 °C a high capacity reduction is indicated. The highest capacity value is presented at 40 °C. During the tests in this work, some of these information will be validated.

Figure 19 – NCR18650B discharge characteristics under different rates and temperatures

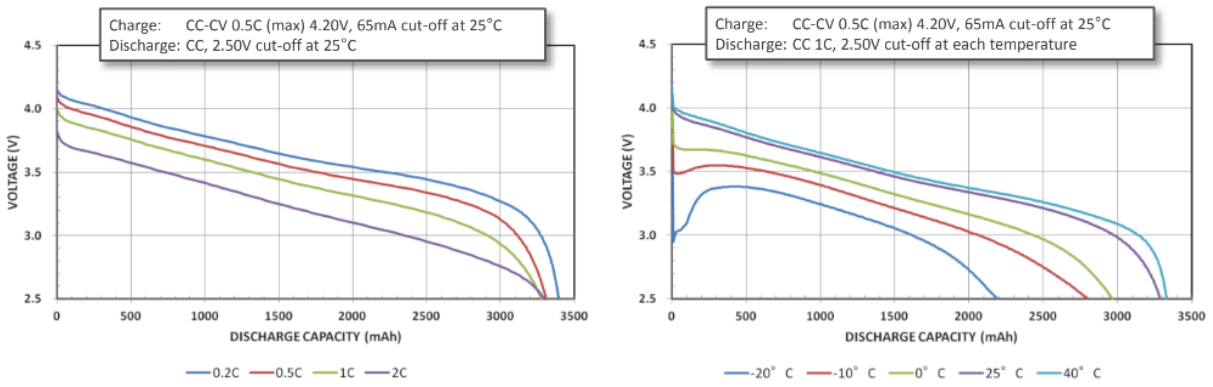

(a) Discharge characteristics by rate of discharge

(b) Discharge characteristics by temperature

Source: (PANASONIC, 2012)

4.3 *BQSTUDIO*® - USER'S INTERFACE SOFTWARE

The *bqStudio*® is an user's interface software from Texas Instruments. This software offers a full suite of tools to assist the user with the process of evaluating, designing, configuring and testing the BMS. The software requires the EV2400 communication interface adapter to communicate with the bq78350R1.

This software includes features that provide full access to registers and data memory, including support for real-time watching, graphing and logging. There is also a friendly interface to send commands, to configure the BMS functions, to calibrate the measurements, to perform a learning cycle and others.

In this work, the *bqStudio*® is used to configure and evaluate the BMS functions. During the tests, the measurements are monitored, as well as the main registers. For each test performed in this study, a log file containing the measurements, estimations and the full registers values is provided. With this log, it is possible to evaluate the batteries behavior and demonstrate it using graphics. The log records the value of the variables and the status of the registers every 2000 ms.

Figure 20 presents the main screen of the *bqStudio*® during the communication with the BMS. This screen is composed of the dashboard on left panel (1), which displays values for pack voltage, temperature and charge or discharge current. The dashboard only provide these information if the communication with the BMS is running. The default registers window (2) is shown in the middle of screen and reports the data of the measurements and estimations. The bit register tab (3) shows each bit status in real time. The commands window on the right side of the screen (4) is used to send commands to the BMS or to obtain information from it. The logging function is also available in this main screen (5).

Figure 20 – *bqStudio*® - Main window

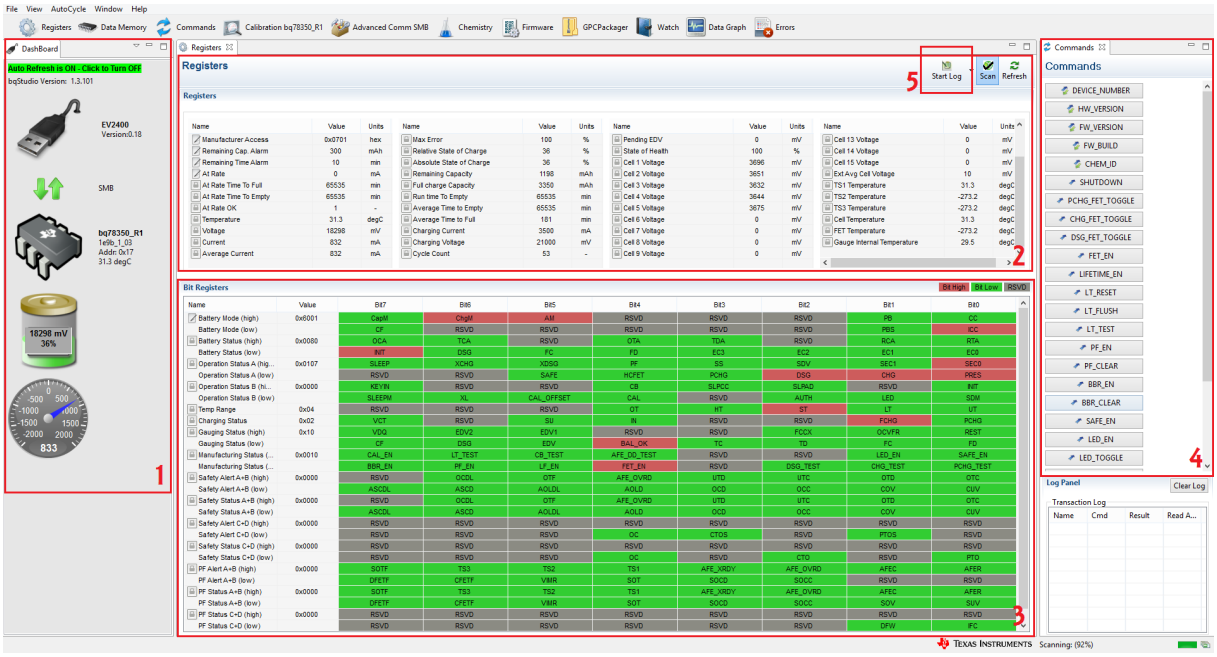

Source: the author

Another important part of the *bqStudio*® is the data memory window, illustrated in Figure 21. The data memory enables the user to configure the BMS functions parameters. The commands to read the values from the device or to write them are presented in this window, making the user to easily configure the device as desired.

Figure 21 – *bqStudio*® - Data memory window

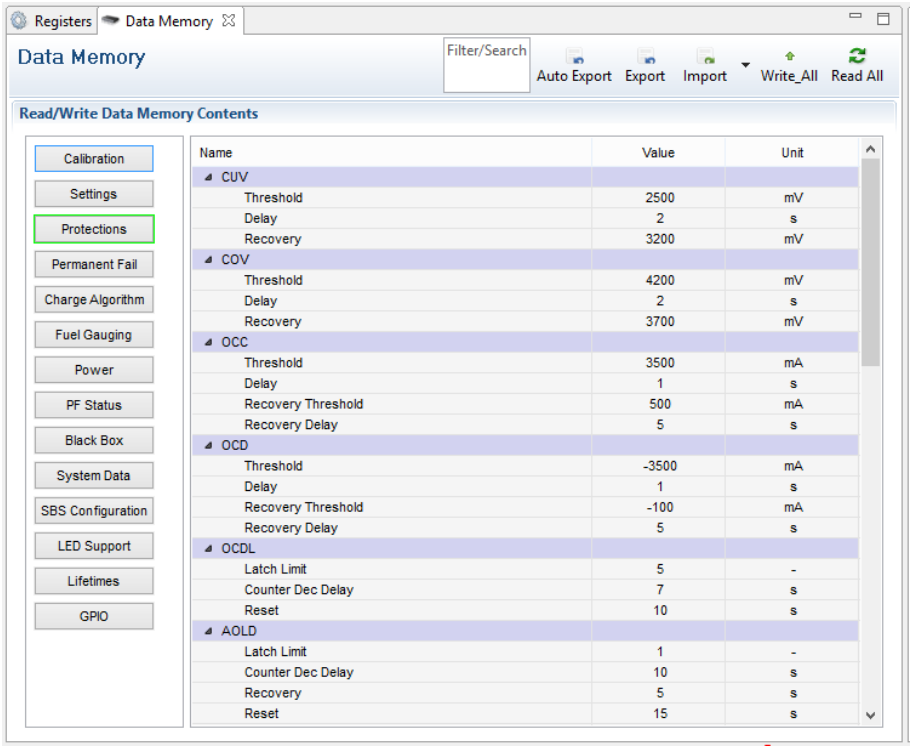

Source: the author

In *bqStudio*®, it is also necessary to select the battery chemistry ID. Chemistry ID refers to a set of tables containing information about the cell's characteristics and behaviors and could impact in some algorithm performance.

4.4 CONSTANT CURRENT DISCHARGE CIRCUIT

An electronic load prototype was developed to perform the discharge tests with constant current. The objective of this circuit is to vary the current setpoint and drain it from the battery pack. This circuit is widely used in this kind of application and is quite simple to implement. The circuit is adapted from (INSTRUCTABLES CIRCUITS, 2021).

The Figure 22 present the electric schematic of the circuit, which is mainly composed of an operational amplifier, a transistor and a sense resistor. A potentiometer connected in the op-amp non-inverting input (R_R) is used to adjust the desired current. The output current is measured in the sense resistor (R_S) as a voltage drop and compared with the desired value. The op-amp output controls the linear transistor to enable this current to be drained from the battery pack. Table 4 presents the description of the components.

Figure 22 – Prototype of the electronic load

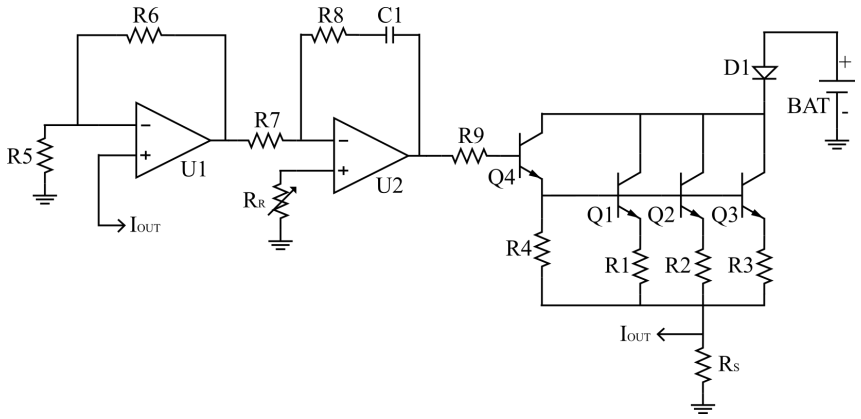

Source: the author

Table 4 – Components description used in the electronic load

Component	Description
C1	220nF - 50V
D1	42CTQ030 - 40A/30V (TO-220)
Q1,Q2,Q3	TIP35C - Transistor NPN, 100V/25A (TO-247)
Q4	BD139 - Transistor NPN, 80V/1.5A (TO-126)
R1,R2,R3	0R47 - 10W
R4	10kR - 1/4W
R5, R7, R9	1kR - 1/4W
R6	100kR - 1/4W
R8	470R - 1/4W
R_R	Trimpot 10kR - 103/25 cycles
R_S	0.01R 3W
U1,U2	LM358 IC (DIP-8)

Source: the author

5 BMS FUNCTIONAL TESTS

For the purpose of evaluating the functionality and usability of the designed BMS, some initial tests were carried out. These first tests are performed to validate the main functions, as the measurements and indications of the important battery pack parameters, the protections, the estimations available on the BMS and the cell balancing algorithm.

These features were verified and some of the main results are presented in this section. First, it is necessary to validate the measurement and indications presented by the BMS. As the measurement is calibrated and offers an accurate value, the protections can be tested. The parameters estimation is validate and finally the cell balancing function behavior is also evaluated.

5.1 EVALUATION OF BMS MEASUREMENTS

To validate the voltage measurement, was compared the BMS indications with a measurement using an oscilloscope. The BMS provides each cell and the battery pack voltages and all these parameters were verified. The equipment used is from the Rohde & Schwarz manufacturer, model RTH1004, with four isolated channels, bandwidth up to 500MHz and sample rate up to 5G sample per second. Figure 23 illustrates the comparison between the BMS measurement and the oscilloscope measurement of the cell 1 voltage. The BMS log offers the voltage for each 2 seconds while the oscilloscope provides 13 samples per second. Note the figure detail, where is highlighted the oscilloscope measurement oscillation and the BMS samples. The maximum error in a cell voltage was 20 mV, which represents 0.55% of the nominal voltage and is considered a low error.

Figure 23 – Cell 1 voltage comparison between BMS and oscilloscope measurements

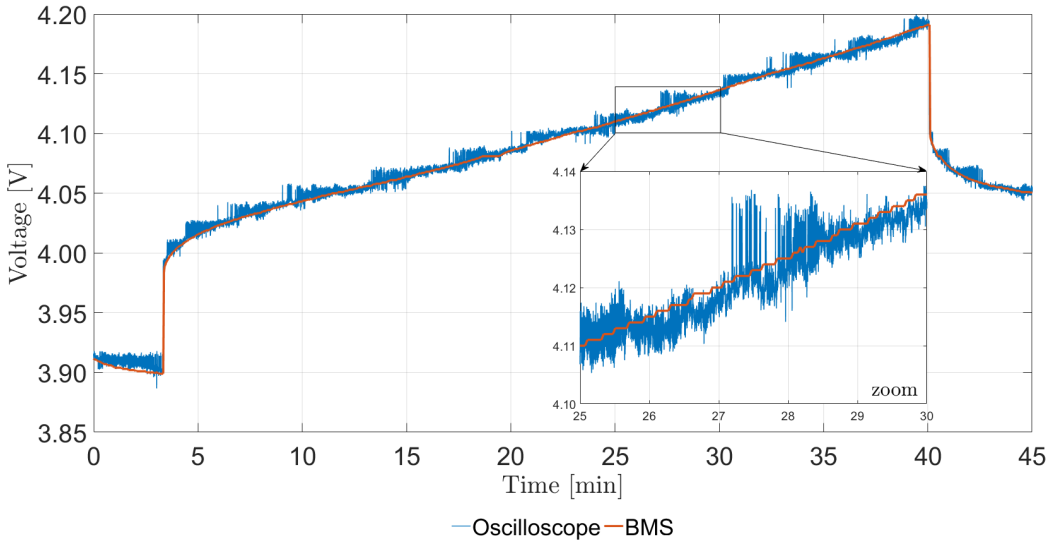

Source: the author

With the same oscilloscope, now using a current probe from Tektronix manufacturer, model A622, was validated the current measurement of the BMS. The current measurement needs be calibrated using the *bqStudio*® software. The process was followed for different current levels and then some tests were carried out. Both signals, the BMS and the oscilloscope measurements, are presented in Figure 24 during a battery pack charge. For different current

levels tested (up to 3.5 A), the maximum error presented was around 4% of the measured current.

Figure 24 – Current measurement test

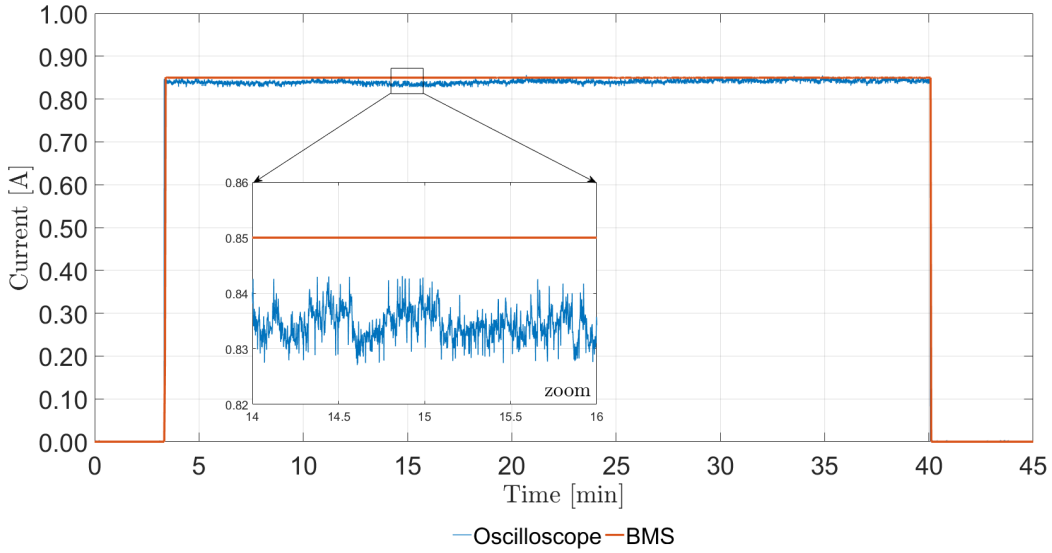

Source: the author

To calibrate the temperature measurement, the temperature register from the Yokogawa manufacture was used to compare the BMS measurement. The register temperature sensor is attached to the same battery cell of the BMS temperature sensor (NTC). At the beginning of the test, the BMS temperature measurement is calibrated to same value presented in the Yokogawa equipment. A discharge test is performed and both measurements were recorded. Figure 25(a) presents the both measurements during the battery pack discharge, the cell temperature increases during the test and when the discharge is complete, the temperature decreases. The error between the measures can be observed in Figure 25(b), where the value is presented in °C and the maximum error was 2.9 °C.

Figure 25 – Temperature measurement test

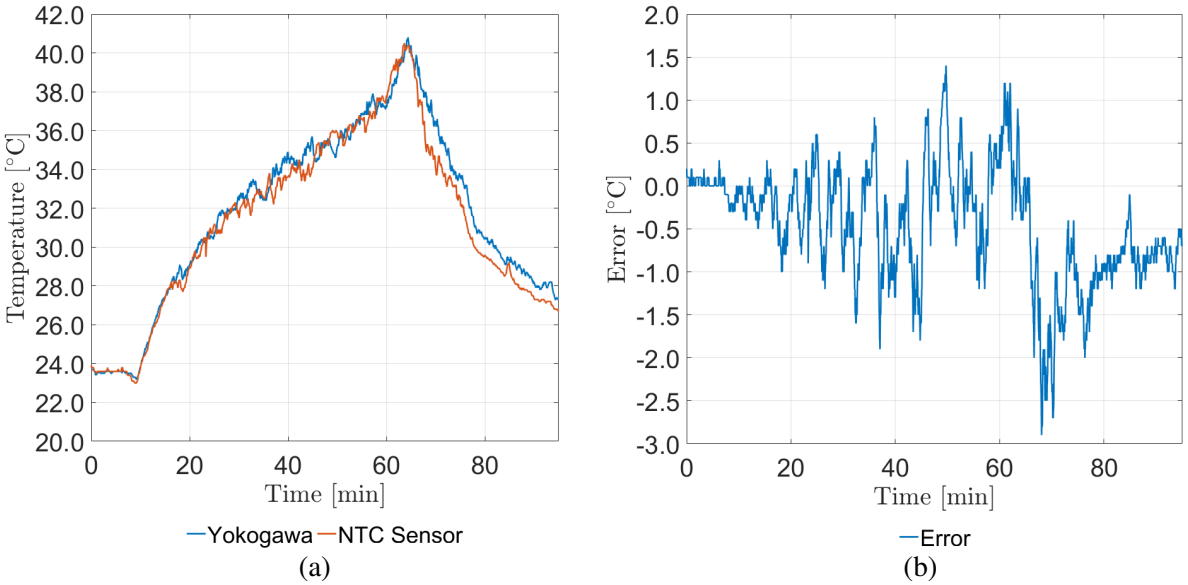

Source: the author

5.2 EVALUATION OF BMS PROTECTIONS

As already mentioned, the BMS provides a wide range of protections. There are protections related to voltage, current and temperature. It is possible to set a desired threshold and activation delay for all the protections. As part of the BMS features evaluation, these protection are verified and some of them are presented in this section.

The undervoltage protection was tested using the DC power supply to simulate the battery cell voltage. The threshold and the delay were set as 2.5 V and 2 s, respectively. A resistor of 10Ω and 150W is connected in the output terminal and used as load. Figure 26 presents the protection performance. The discharge current (yellow signal, channel 1) and the cell voltage (blue signal, channel 2) are measured using a oscilloscope (Tektronix, model TBS1072B) and a current probe (Tektronix, model A622). The cell voltage is decreased using the DC power supply until it reaches the protection threshold. After a 2 s delay, the protection is enabled and the discharge current drops to zero. The test was repeated with different threshold and delay values and the protection presented the correct behavior.

Figure 26 – Undervoltage protection test

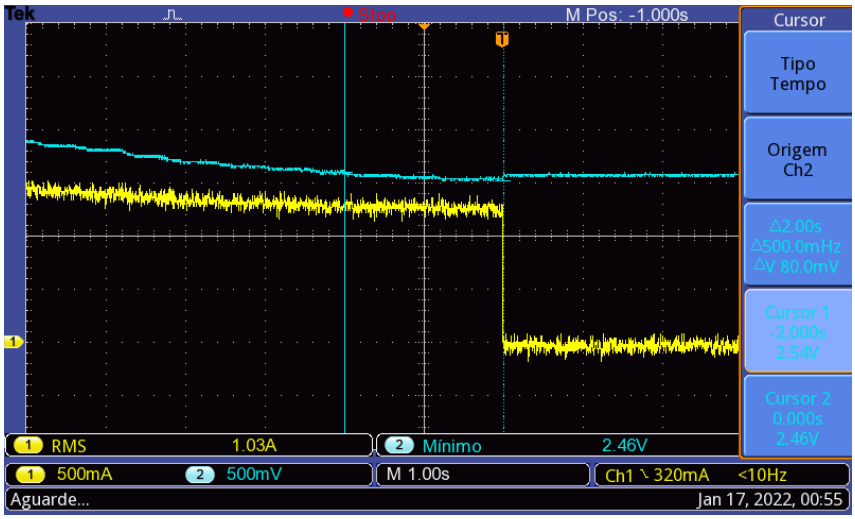

Source: the author

In the same way, the overcurrent protection was tested. The protection threshold and delay were set as 2.0 A and 1 s, respectively. As a resistive load is used, it is possible to increase the discharge current by increasing the DC power supply voltage. It was increased until the current reached the protection level. Figure 27 presents the discharge current signal during the test. This measurement presents some noise, but the protection behavior could be validated. Note that the protection configuration has been respected. Different values were used in the threshold and delay and other tests were carried out. All the results presented a good performance of the protection.

Figure 27 – Overcurrent protection during discharge test

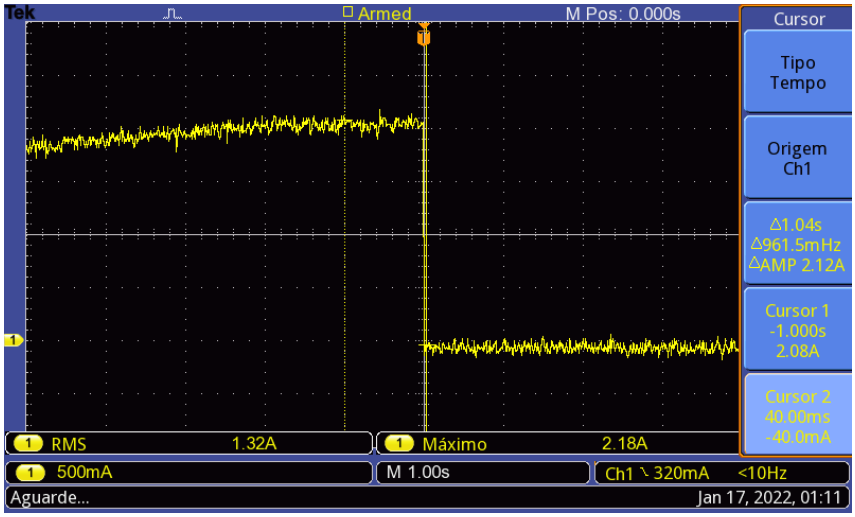

Source: the author

5.3 EVALUATION OF BMS ESTIMATIONS

The BMS also provides the estimation of some important parameters, as the SoC and the SoH of the battery pack. The method used in this BMS to deliver these estimations is presented in Section 4.1.2.6 with more details.

The indication of the SoC is carried out by estimating the remaining capacity of the battery pack. The remaining capacity is the result of the CEDV algorithm developed by Texas Instruments and available in this BMS. To evaluate this indication, this value is compared with the calculated capacity. The Equation (5.1) is used to calculate the capacity at a given instant t (Q_t) during the battery pack charge (accumulated capacity) or discharge (drained capacity), where Δt is the time between two measures and I_t is the current at the instant t, which is a positive value during charge and negative during discharge. The data log is used to calculate the capacity, which causes the current measurement error to be also present in the calculated value.

$$Q_t = \Delta t \cdot |I_t| + Q_{(t-1)} \tag{5.1}$$

Figure 28 presents the comparison between the remaining capacity, estimated by the BMS and the calculated value. During the charging process, the error between the values is very low, but at the end of the charge, the BMS jumps the remaining capacity value to match the full capacity previously estimated. This behavior only happens if the charge is complete according the charge termination conditions. For this reason, from this moment forward, the estimated value and the calculated one present an error around 190 mAh, which represents 5.6 % of the nominal capacity.

Figure 28 – Remaining capacity estimation compared with calculated capacity during charge

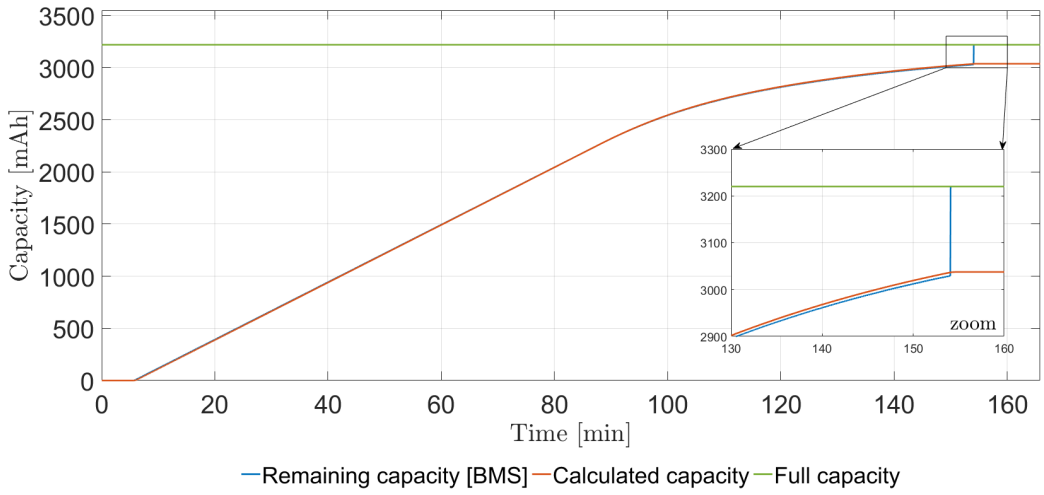

Source: the author

During the battery pack discharge, the remaining capacity value starts as the same of the full capacity estimation and decrease until the end of the discharge, as seen in Figure 29. Note that at the end of the discharge, the remaining capacity value drops abruptly to zero to correct the indication error. At this moment, the full capacity estimation is also changed to a different value. The error between the estimated value and the calculated one is around 200 mAh and is constant during the entire discharge.

Figure 29 – Remaining capacity estimation compared with calculated capacity during discharge

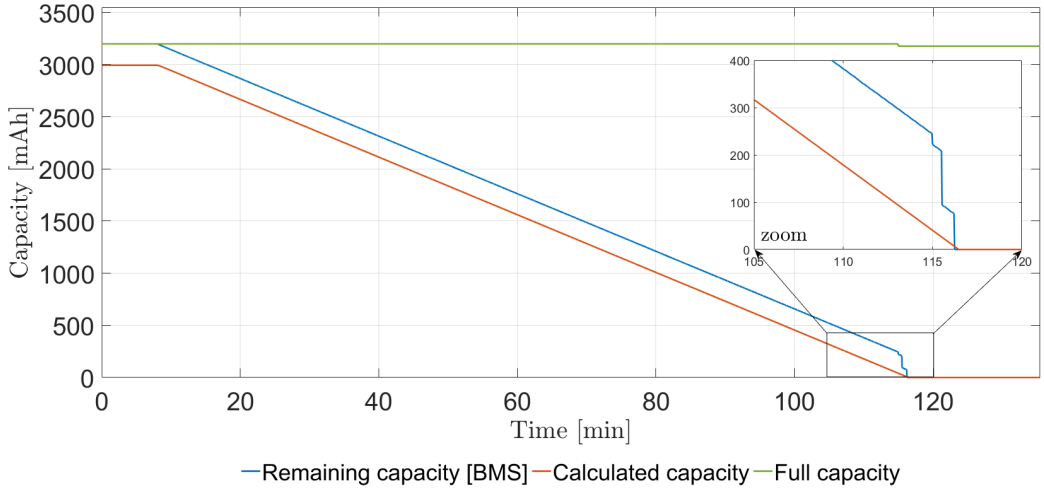

Source: the author

After evaluating the remaining capacity estimation, it is possible to compare the SoC estimation with the calculated value. Two SoC indications are available: the absolute state of charge (ASOC), which relates the remaining capacity to the battery nominal capacity, and the relative state of charge (RSOC), which relates the remaining capacity to the total capacity of the battery when fully charged. The calculated SoC is the relation between the capacity at the time and the maximum capacity presented in this test. For this reason, the same behavior observed in the capacity indication is expected for the SoC. Figure 30 provides the RSOC and ASOC, as

well as the calculated SoC during the battery pack charge. The ASOC is lower than the RSOC during the charge and both values are shifted as the charge is complete. RSOC jumps to 100% and the ASOC to the relation between the full capacity estimation and the nominal capacity.

Figure 30 – SoC estimation compared with calculated SoC during charge

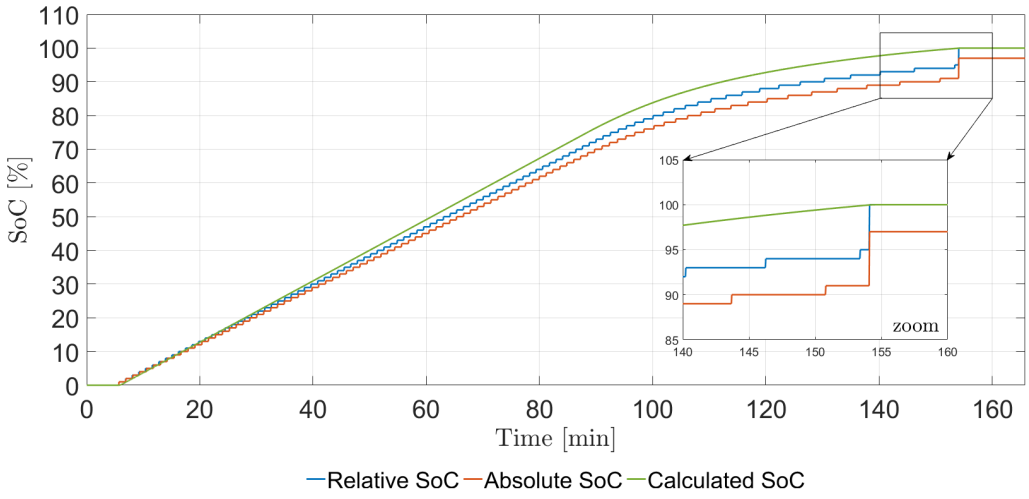

Source: the author

During the battery pack discharge, the RSOC starts from 100% and decreases until the end of the discharge. The ASOC has a similar behavior, however with different initial value. Figure 31 indicates the three curves: the calculated SoC, ASOC and RSOC. At the end of the discharge, ASOC and RSOC dropped to zero to correct the indication error. The maximum error presented in this test is 6%.

Figure 31 – SoC estimation compared with calculated SoC during discharge

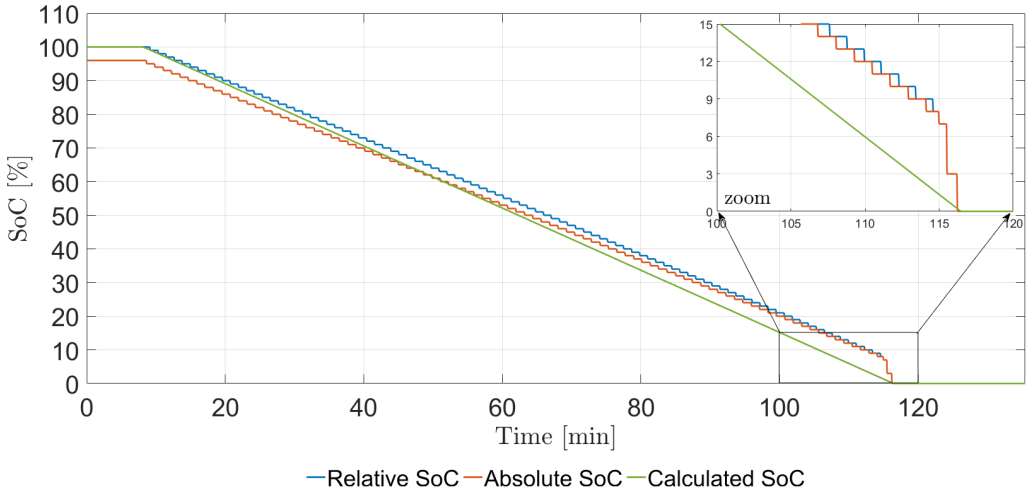

Source: the author

Another estimation available in this BMS is the SoH. This parameter indication is also related with the remaining capacity. The BMS offers the SoH in percentage, and it is purely calculated as the relation between the full capacity and the nominal capacity. During the tests performed in this work, the SoH value fluctuates due to different charging and discharging conditions, as well as changing the batteries used in the tests. To evaluate this indication, the

tests should keep, at least, the battery pack always the same. However, it is expected that the same errors presented in the capacity estimation will be observed in this parameter.

The BMS also provides the estimation of the time, in minutes, for the battery pack to reach the complete charge or discharge. This estimation uses the current measurement and the estimated full capacity. For the charge, the time decreases linearly during the constant current charge step, and so the current value is changed, the estimated time does not present good results, as seen in Figure 32. At the time the charging process is completed, in this test, the indicated time is 49 minutes.

Figure 32 – Average time to fully charged estimation compared with real time

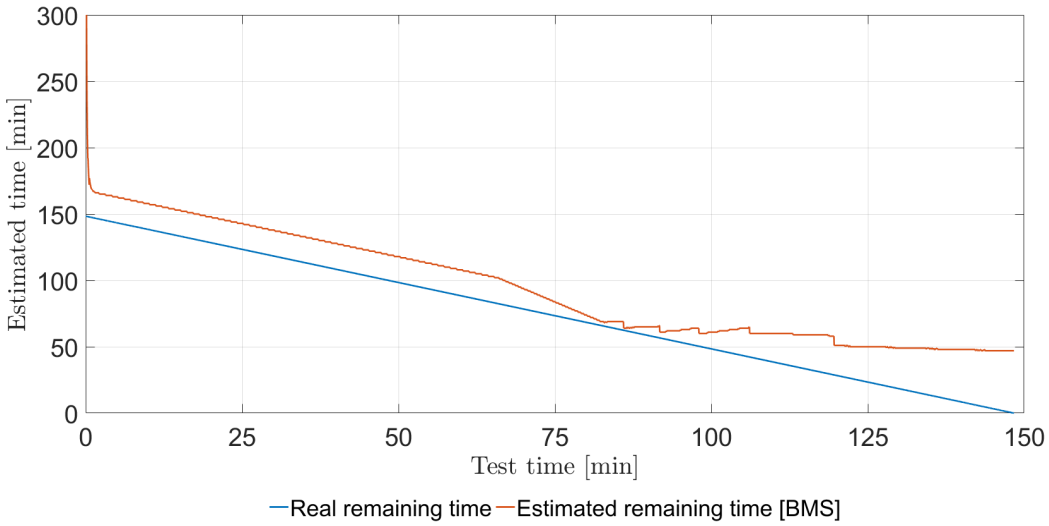

Source: the author

Figure 33 presents the comparison between the estimated time and the real remaining time during the battery pack discharge. In this case, the indication presents a better result, with a constant error around 8 minutes. This improvement is due to the discharge test being performed with constant current.

Figure 33 – Average time to fully discharged estimation compared with real time

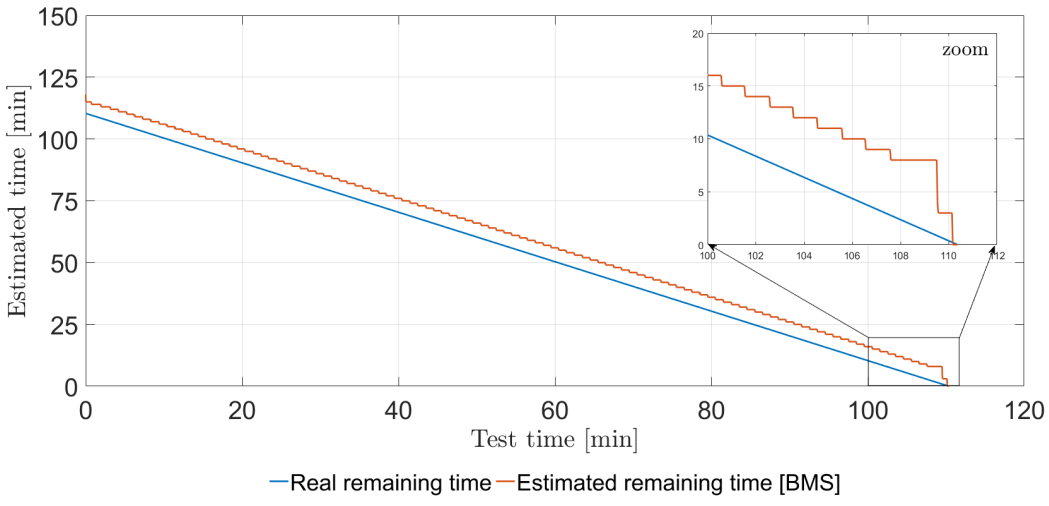

Source: the author

The tests presented in this section indicate the good functioning of the developed BMS. The errors presented do not affect the safety of using the BMS and the battery pack and are considered as system limitations. At this moment, this work is not intended to change any functionality of the BMS. In the next sections, charging and discharging tests of the battery pack are carried out and these limitations are used to analyze the results.

5.4 EVALUATION OF CELL BALANCING FUNCTION

The cell balancing algorithm was already described in Section 4.1.2.4. During the tests performed in this work, the cell balancing function has been kept enabled. For each charging process, when the required condition are met, the BMS starts balancing the cell with the higher voltage. The function configuration was also kept at the default values (see Figure 13).

Figure 34 presents the battery cell voltages and the CB bit status, which indicates that the balancing is taking place when it is set to 1.

Note that the algorithm presents a correct behavior. The cell balancing threshold is 3.9 V and as soon as the cell with the highest voltage reaches this value and the maximum difference in cell voltages exceeds 40 mV, the balancing is activated and the CB bit is set to 1. During this test, the cell 5 is the one with the highest voltage and the maximum voltage difference is 53 mV between cell 4 and 5.

The function remains active until the cell with the lowest voltage reaches the initial threshold, which occurs when cell 4 reaches 3.9 V. At this time, a new threshold is calculated by adding the value defined as cell balancing window (100 mV) to the previously threshold. It is observed that the charging behavior of cell 5 has not changed and the voltage difference between cell 4 and 5 is still around 53 mV.

Figure 34 – Cell balancing during charge

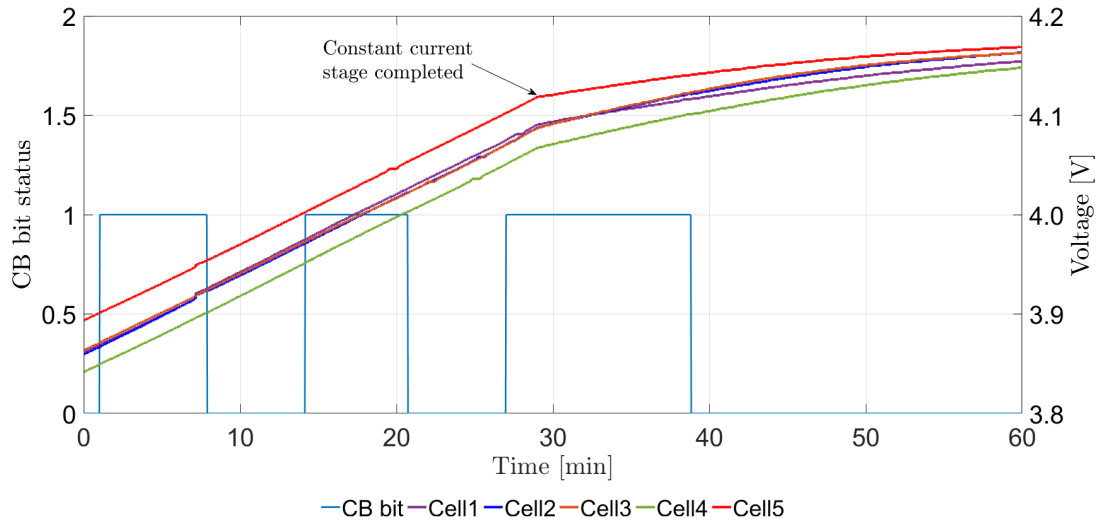

Source: the author

The new threshold is 4.0 V and the cell balancing is activated as soon as the cell with the maximum voltages reaches this value and the maximum difference voltage is higher than 40 mV. Again, the cell 5 achieves the threshold and the difference between the cell 4 and cell 5 voltages is 50 mV, then the balancing is activated. The function remains active until the cell 4 reaches 4.0 V and once more, the charging behavior of cell 5 has not changed during the balancing.

The balancing is activated again when cell 5 reaches 4.1 V. While balancing is active, the charging current decreases because the charging process initiates the constant voltage and variable current stage. For this reason, and not due to balancing, the difference in cell voltages decreases. Note that even after the balancing is disabled, cell voltages continue to converge.

The cell balancing algorithm presents the described behavior but the method was not effective to bypass the charging current of the highest voltage cell and decrease the difference between the cell voltages. The manufacturer presents a test demonstration in (TEXAS INSTRUMENTS, 2004), in which the cell balancing was achieved only after 18 test cycles. In this work, this evaluation is not performed.

6 CHARGE AND DISCHARGE TESTS

After verifying the main features of the BMS, the battery cells behavior was evaluated under different conditions of charge and discharge. In this chapter, these tests are presented in detail. The main objective is to evaluate the use conditions where the battery pack has the best performance and safety.

A rest time of at least 20 minutes is used between each charge and discharge test. With this time, the battery cell temperature is able to stabilize. For future work, an standard recommend rest time should be considered. The IEC-62620 international standard recommends the rest time between 1 and 4 hours.

The hole system is tested and a log data is recorded for each test. The log file provides all the registers status and the measures saved every 2 seconds. From this log file, it is possible to perform data analysis, build graphs and compare results.

Figure 35 presents a photography of the setup used to perform tests without controlled room temperature. It is an example of charging test. The laptop is used with the *bqStudio*® software to register the test data. The DC power supply is charging the battery pack (during the discharge test, the electronic load is used), and the BMS is monitoring and controlling the battery pack charging.

Figure 35 – Experimental setup photography

Source: the author

6.1 CHARGE TESTS

The battery pack charging tests were performed using the DC power supply to emulate a CC-CV charger. The charging method was presented in Section 2.6 and can be seen in Figure 2. The DC power supply provides voltage-controlled and current-limited charging.

In these tests, the 5 cell batteries remain connected in series. The DC power supply voltage is set at 21 V and the current is limited to 0 A. After connecting the battery pack to the DC power supply, through the BMS, the current limitation is changed up to the selected value (0.25C, 0.5C or 1.0C). During the charge, the power supply voltage reaches the battery pack voltage. The voltage raises to around 21 V and the current declines until the pack battery

is fully charged. The BMS reads the parameters and disables the charge FET as soon as the charge termination condition is achieved or some protection is activated, e.g. a cell overvoltage protection. When the charge is complete, the charge path is open and no more charge current can be applied until the battery is partially discharged. If the charge is interrupted by a protection, the recovery condition needs be reached to enable the charge again.

The charge termination condition can be achieved when the charge current is less or equal of the termination value (250 mA in these tests) for a fixed time (80 s, not able to change) and the cell voltage is near the nominal charge voltage. Some protection can also suspend the charge: if one of the battery cells reaches the maximum voltage (4.2 V), or if the charge current goes higher than the maximum value (3.5 A) or even the battery temperature reaches the high temperature protection (45 °C).

The manufacturer specification for the charge is to use a 0.5C rate maximum current. According to the manual, battery safety and good performance are achieved with this value. The charge tests, in this study, were performed with three different current rates: 0.25C, 0.5C and 1.0C. As the rate of 1.0C is higher than the recommended value, some precautions were taken: the cell temperature was monitored during all the tests and a physical barrier was used in case of explosion. The purpose is to compare the battery cells behavior under these conditions. Variables as pack and cell voltages, cell temperature and stored capacity are the main focus in these tests. The cell temperature is measured only in cell 3 because the BMS is able to measure only one temperature signal. All the cell temperature measurement present in this work is the cell 3 temperature.

Also temperature controlled tests were performed and are available in Chapter 7. In this case, a thermal chamber was used with the room temperature set at 10 °C, 25 °C and 40 °C. Tests where controlled temperature is not mentioned were carried out without the thermal chamber.

6.1.1 Charge tests results with current rate of 0.25C

The first test was performed applying a charge rate of 0.25C. With this charge rate, the battery pack was fully charged after around 4 hours. The initial pack voltage was 15.5 V and after the charge it was 20.86 V. The relative SoC, estimated by the BMS, starts in 0% and goes to 100% when the charge is complete. The cell temperature increased by 2.1 °C and the calculated capacity accumulated during the charge was 3106 mAh. All these data are summarized in Table 5.

Figure 36 shows the pack voltage and current during charge. Once the current is applied, the pack voltage starts to increase up to near the nominal charge voltage and then, the current drops until to the minimum value. The charge, in this test, has been suspended by the BMS after the charge termination condition is achieved.

Table 5 – Main parameters of charge test with current rate of 0.25C

Information	Value
Test	Charge
Current	837 mA
Duration	4h06min
Controlled temperature	No
Initial cell temperature	24.4 °C
Maximum cell temperature	26.5 °C
Cell temperature variation	2.1 °C
Initial pack voltage	15.491 V
Final pack voltage	20.867 V
Pack voltage variation	5.376 V
Initial RSOC	0%
Final RSOC	100%
Calculated capacity	3106 mAh

Source: the author

Figure 36 – Pack voltage and current during charge with current rate of 0.25C

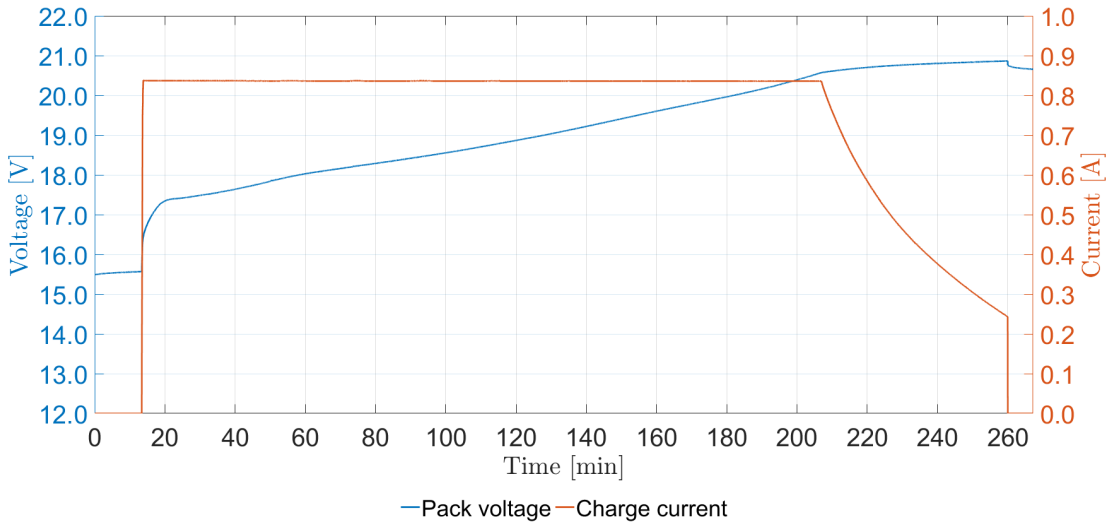

Source: the author

The cell voltages are shown in Figure 37. The cell voltages are different during the relaxation mode (OCV), but after the charge current is applied, they increase until close to the end of the charge.

The Table 6 presents the measured values for each cell during the test. For each measurement, the highest value is presented with bold numbers and the lowest value with bold and italics. The initial open circuit voltage is the first measurement cell voltage available in the log data. There is no current applied in the pack at this time. After 10 minutes in the charge process, the cell voltages are also presented. At this point, the cell voltages do not present high variation. With the complete charge, the last measurement before the charge current path is blocked, the cell voltage measurements are also presented. Finally, the last cell voltages measurement without current applied, are also available in the table. Note that at the end of charging, the cell voltages are balanced, unlike at the beginning of the test. The cell voltage behavior is nonlinear

and depends on the cell internal resistance.

Table 6 – Cell voltages measurements during charge with current rate of 0.25C

Description	Cell 1	Cell 2	Cell 3	Cell 4	Cell 5
Initial open circuit cell voltage [V]	3.077	3.129	3.140	**3.166**	***2.978***
Cell voltage after 10 minutes in charge [V]	3.487	3.485	3.485	***3.466***	**3.494**
Final charge cell voltage [V]	***4.165***	4.179	4.171	**4.182**	4.170
Final open circuit cell voltage [V]	***4.122***	4.135	4.134	**4.145**	***4.122***

Source: the author

Figure 37 – Cell voltages during charge with current rate of 0.25C

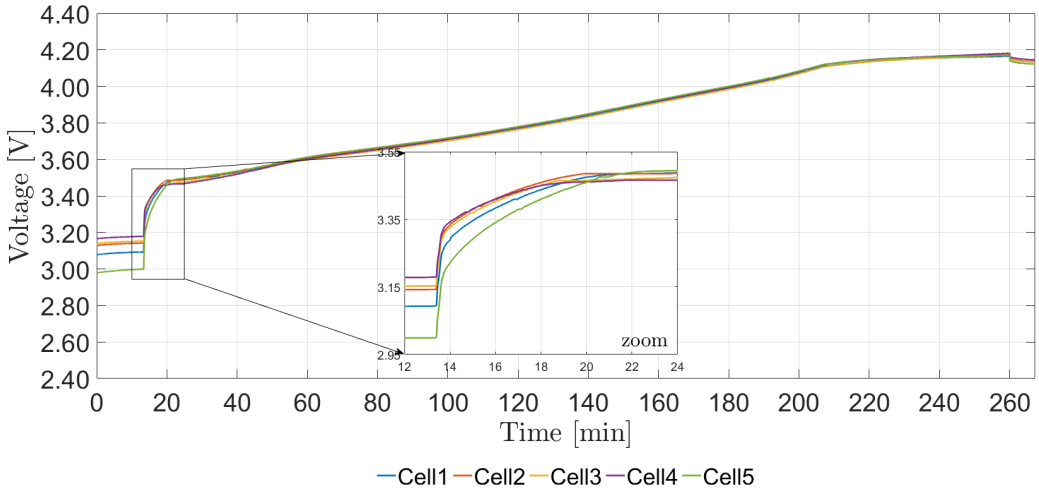

Source: the author

The relative SoC and the remaining capacity are estimated during the charge by the BMS and are illustrated in Figure 38. While the battery is being charged, its stored capacity and SoC increase. The BMS is set to jump the SoC to 100% and the remaining capacity to the full capacity value if the charge termination condition is achieved.

The battery cell temperature during the test can be seen in Figure 39. The battery cell temperature is measured in the packaging of the third battery and it presents a low variation (2.1°C). This behavior is expected, since the charging current is low.

Figure 38 – Remaining capacity and relative SoC during charge with current rate of 0.25C

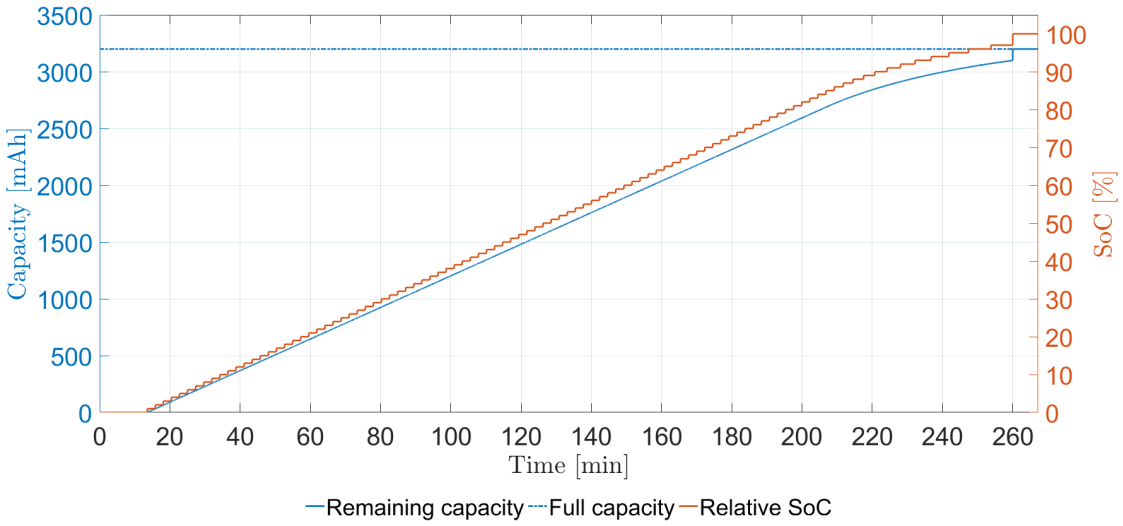

Source: the author

Figure 39 – Battery cell temperature during charge with current rate of 0.25C

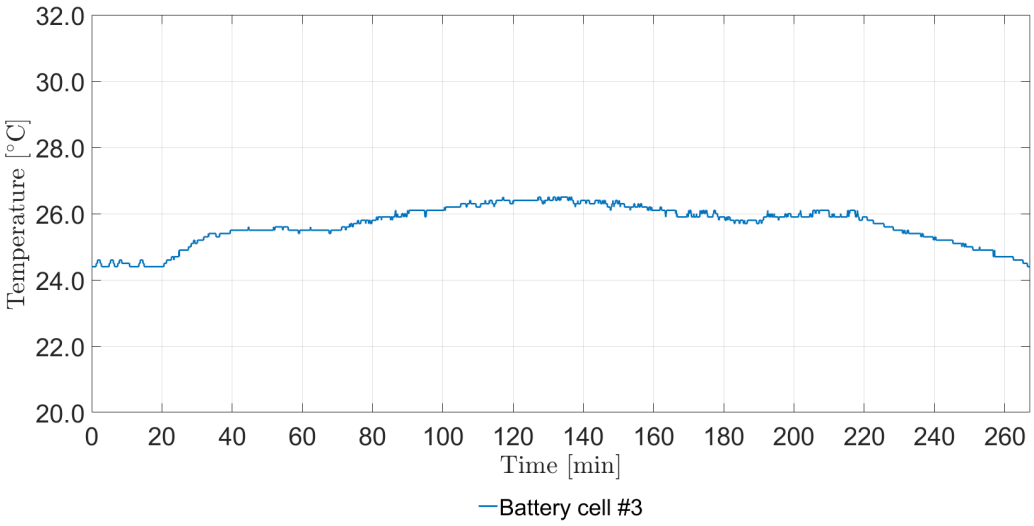

Source: the author

6.1.2 Charge tests results with current rate of 0.5C

A new charge test was performed changing the rate to 0.5C. In this test, the complete charge was achieved after 2h30min. Table 7 summarizes the information about the test. The battery cell presents a temperature increase of 5.2 °C. The test was finished by a charge termination condition and the battery pack stored a capacity of 3018 mAh.

The battery pack voltage and the current during the charge are illustrated in Figure 40. In this case, the constant current stage is shorter and the initial voltage increase is higher than in the test with 0.25C.

Table 7 – Main parameters of charge test with current rate of 0.5C

Information	Value
Test	Charge
Current	1649 mA
Duration	2h30min
Controlled temperature	No
Initial cell temperature	25.1 °C
Maximum cell temperature	30.3 °C
Cell temperature variation	5.2 °C
Initial pack voltage	16.450 V
Final pack voltage	20.885 V
Pack voltage variation	4.435 V
Initial RSOC	0%
Final RSOC	100%
Calculated capacity	3018 mAh

Source: the author

Figure 40 – Pack voltage and current during charge with current rate of 0.5C

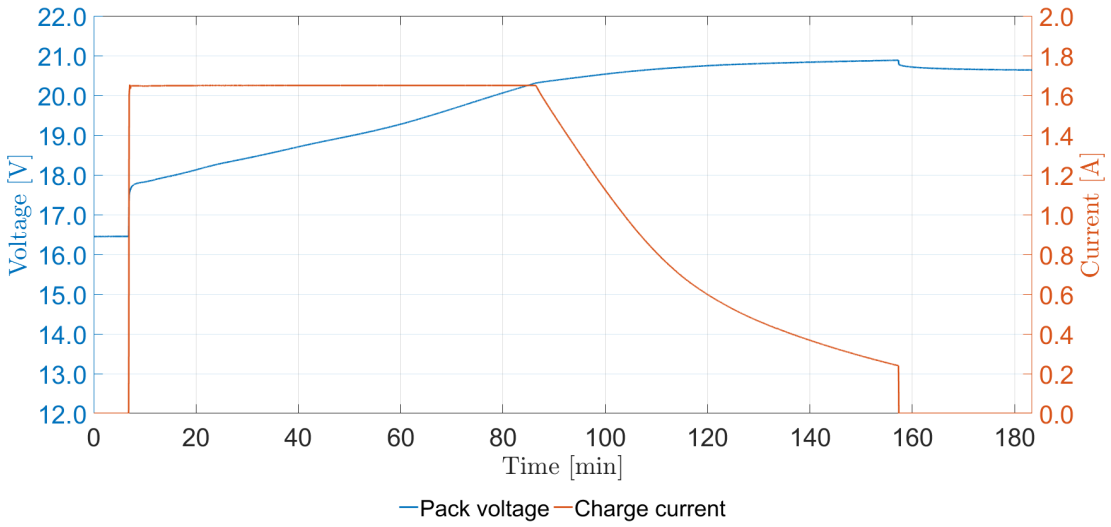

Source: the author

In Table 8, the cell voltages measurements are presented at different times during the charge and in Figure 41 the curves for all the cell voltages throughout the test are shown. The cell voltage behavior is similar to the first test, but as the current is applied, the instantaneous increase in voltage is greater. The difference in voltage of each cell is also greater during the charging period where the current is constant.

Table 8 – Cell voltages measurements during charge with current rate of 0.5C

Description	Cell 1	Cell 2	Cell 3	Cell 4	Cell 5
Initial open circuit cell voltage [V]	3.292	3.298	3.301	**3.308**	***3.251***
Cell voltage after 10 minutes in charge [V]	3.619	3.602	3.589	***3.583***	**3.632**
Final charge cell voltage [V]	***4.147***	4.163	4.158	**4.169**	4.148
Final open circuit cell voltage [V]	***4.117***	4.131	4.131	**4.141**	***4.117***

Source: the author

Figure 41 – Cell voltages during charge with current rate of 0.5C

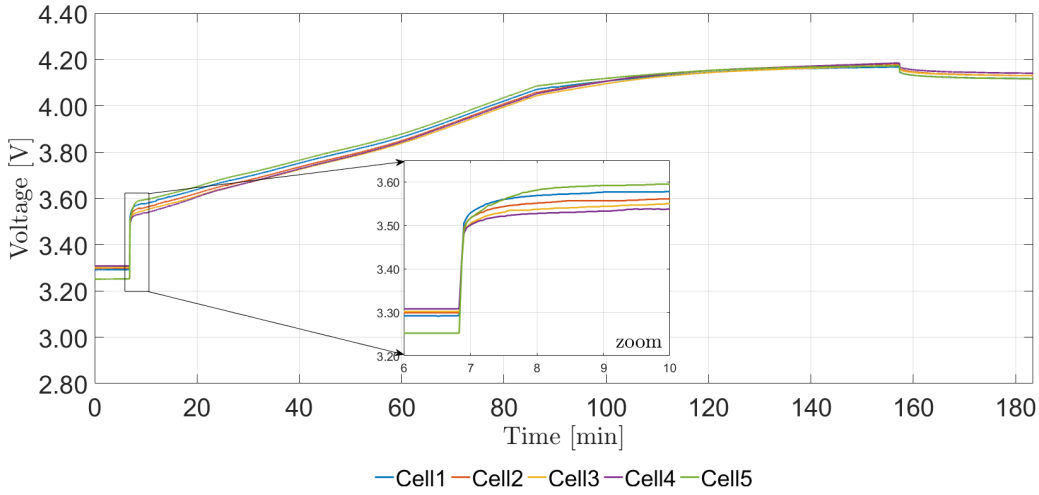

Source: the author

Figure 42 presents the relative SoC and the remaining capacity curves during the charge. Both values start from 0 and increase to the maximum. The full capacity, estimated by the BMS is also presented.

Figure 42 – Remaining capacity and relative SoC during charge with current rate of 0.5C

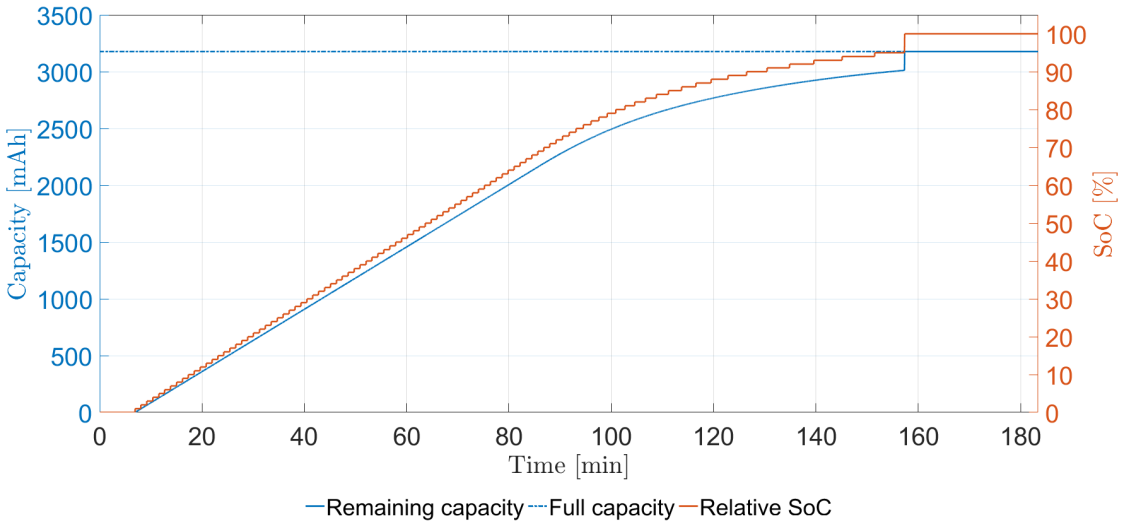

Source: the author

The battery cell temperature during the charge is illustrated in Figure 43. As the current

applied during this charge is higher than the previous test, the temperature variation in the cell is also higher (5.2 °C).

Figure 43 – Battery cell temperature during charge with current rate of 0.5C

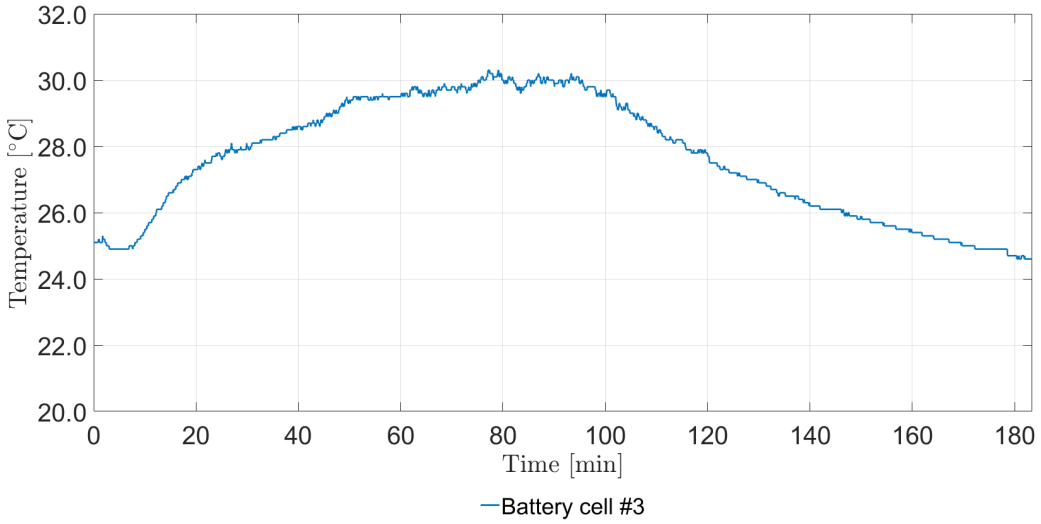

Source: the author

6.1.3 Charge tests results with current rate of 1.0C

The last charge test was made with a rate of 1.0C and the complete charge was achieved after 1h52min. The stored capacity in the battery pack was 3131 mAh, the higher capacity among the charge tests. Table 9 shows the main parameters for this test. The cell temperature variation is also the highest, 14.8 °C, as expected.

Table 9 – Main parameters of charge test with current rate of 1.0C

Information	Value
Test	Charge
Current	3345 mA
Duration	1h52min
Controlled temperature	No
Initial cell temperature	25.6 °C
Maximum cell temperature	40.4 °C
Cell temperature variation	14.8 °C
Initial pack voltage	15.709 V
Final pack voltage	20.910 V
Pack voltage variation	5.201 V
Initial RSOC	0%
Final RSOC	100%
Calculated capacity	3131 mAh

Source: the author

Figure 44 presents the pack voltage and the current during the batteries charge. In this test, the constant current charge stage is complete in around 30 minutes and the constant voltage stage takes most of the time.

Figure 44 – Pack voltage and current during charge with current rate of 1.0C

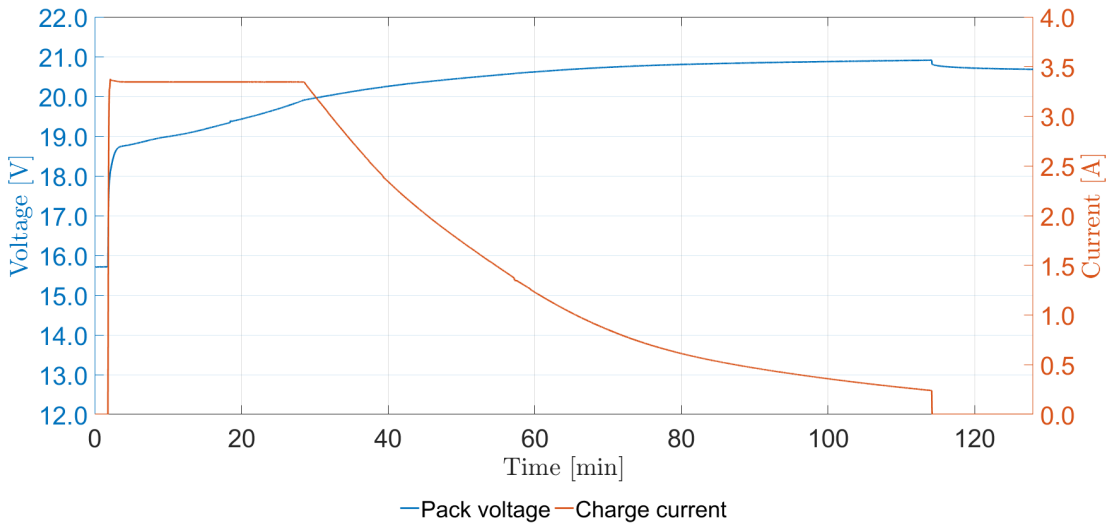

Source: the author

The cell voltages at different times of the charge can be seen in Table 10. Figure 45 illustrates the curve for the cell voltages during the charge. Note the instantaneous voltage increases as the current is applied. Also the cell voltages present different values during the constant current stage. This difference decreases during the rest of the charging and at the end of the test, the cell voltages are balanced.

Table 10 – Cell voltages measurements during charge with current rate of 1.0C

Description	Cell 1	Cell 2	Cell 3	Cell 4	Cell 5
Initial open circuit cell voltage	3.119	3.170	**3.206**	***3.046***	3.168
Cell voltage after 10 minutes in charge	3.824	3.792	3.784	***3.768***	**3.878**
Final charge cell voltage	***4.152***	4.169	**4.175**	4.155	4.158
Final open circuit cell voltage	***4.126***	4.141	**4.150**	4.128	4.135

Source: the author

Figure 45 – Cell voltages during charge with current rate of 1.0C

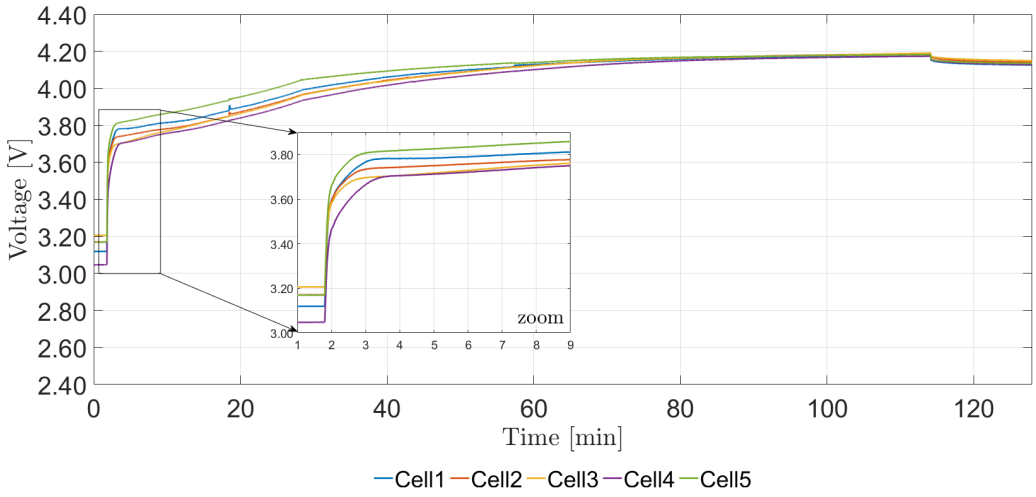

Source: the author

Figure 46 presents the relative SoC and remaining capacity curves during the charge, as well as the full capacity. The remaining capacity and the relative SoC starts from 0 mAh and 0%, respectively, and increased during the charge up to the maximum values.

Figure 46 – Remaining capacity and relative SoC during charge with current rate of 1.0C

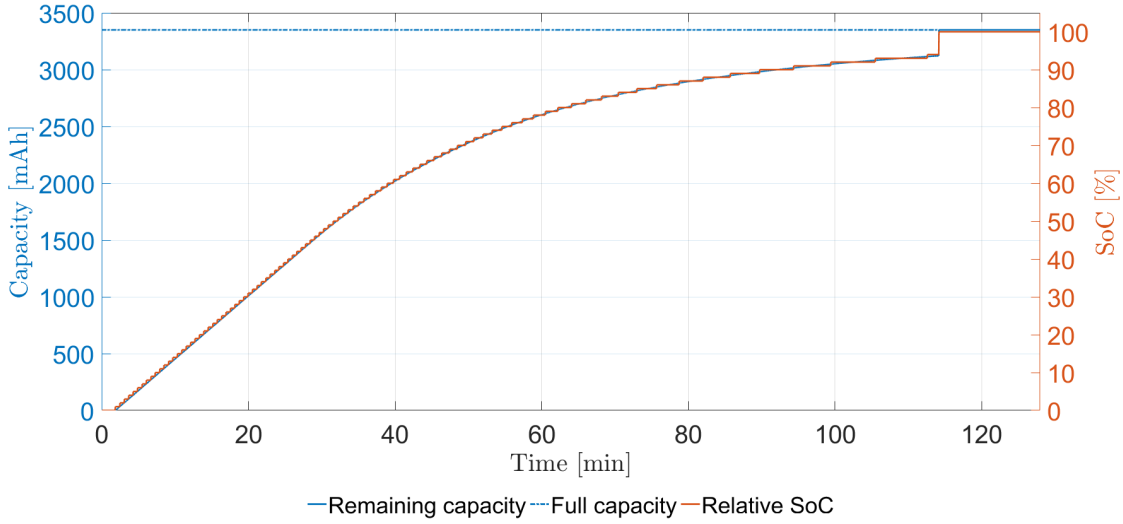

Source: the author

In this test, the higher cell temperature rise takes place, the battery cell variation is 14.8 °C, as shown in Figure 47. This temperature increase is caused by the level of the current applied to the battery pack, so this is an expected behavior.

Figure 47 – Battery cell temperature during charge with current rate of 1.0C

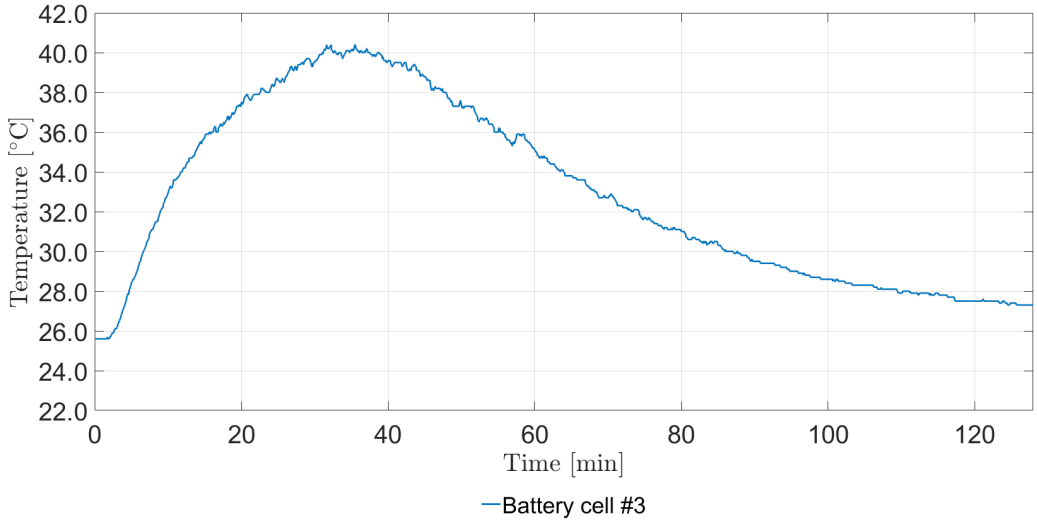

Source: the author

6.1.4 Comparison between the charge tests under different current rates

In this section, a comparison between the charge tests under different charge current rates is presented. These tests results are the same presented in Sections 6.1.1, 6.1.2 and 6.1.3 and they are here summarized and compared. Table 11 shows the main parameters for each test. All the tests presented in this section had the process finished because of the charge termination condition was met.

Table 11 – Comparison of the main parameters of charge tests with current rates of 0.25C, 0.5C and 1.0C

Description	0.25C	0.5C	1.0C
Current	837 mA	1649 mA	3345 mA
Duration	4h06min	2h30min	1h52min
Initial cell temperature	24.4 °C	25.1 °C	25.6 °C
Maximum cell temperature	26.5 °C	30.3 °C	40.4 °C
Cell temperature variation	2.1 °C	5.2 °C	14.8 °C
Initial pack voltage	15.491 V	16.450 V	15.709 V
Final pack voltage	20.867 V	20.885 V	20.910 V
Pack voltage variation	5.376 V	4.435 V	5.201 V
Initial RSOC	0%	0%	0%
Final RSOC	100%	100%	100%
Calculated capacity	3106 mAh	3018 mAh	3131 mAh

Source: the author

Note that applying a low charge current, the charging process duration may take a long time. It could be undesirable in many applications, but this charge rate provides a low temperature rise in battery cells and achieves a good capacity storage. On the other hand, charging the battery with a high current rate (1.0C) takes less time but provides a high temperature rise, which may damage the battery or reduce the life time. A good trade-off between charging time and battery safety is charging the battery with an average charge current, i.e. 0.5C, as the manufacturer's recommendation. In this case, the duration is not so long as in 0.25C charge rate but

also the temperature increase is not so high as in 1.0C. In this test, the charge with 0.5C provides the smallest stored capacity, but the value is not too low that may compromise the battery pack application.

Figure 48 presents the current curves during each charge test. The constant current stage during the charge is lower as the current is higher.

Figure 48 – Comparison of charging current in charge tests with current rates of 0.25C, 0.5C and 1.0C

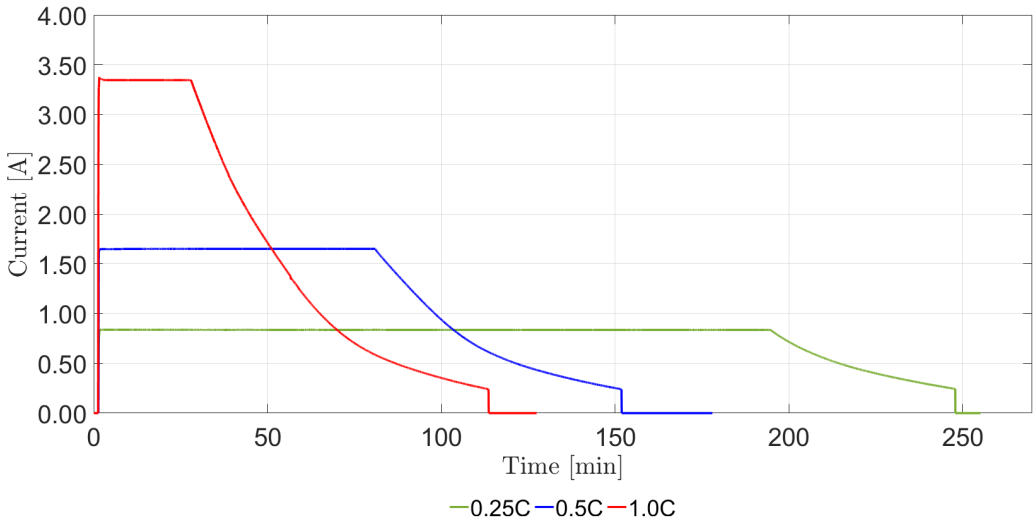

Source: the author

The pack voltage also presents a different behavior for each charge current, as shown in Figure 49. Note that the pack voltage increases as charge current is applied. The voltage increase is proportional to the level of the applied current. Also, during the charge with 0.25C rate, the voltage pack is more linear than at the other rates. This linear increase in pack voltage happens during the constant current stage.

Figure 49 – Comparison of pack voltage in charge tests with current rates of 0.25C, 0.5C and 1.0C

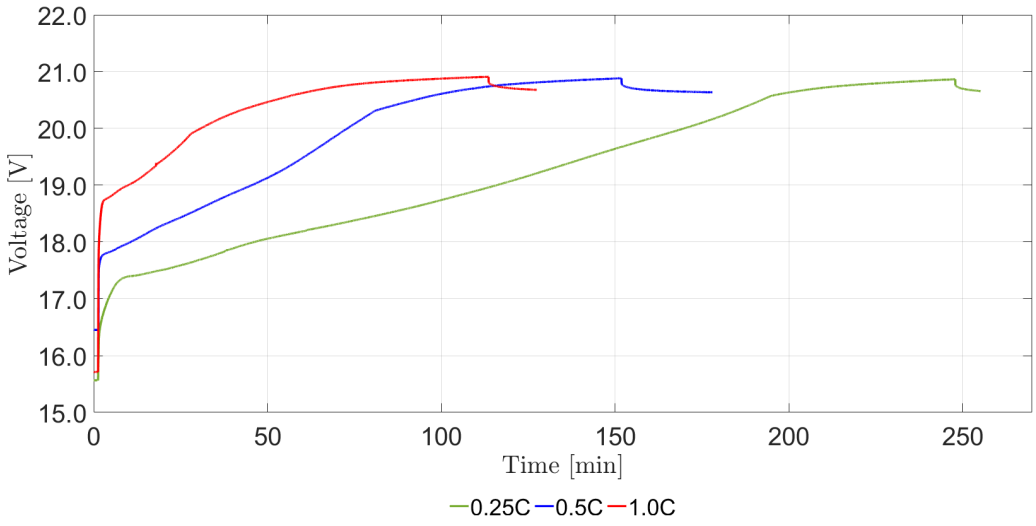

Source: the author

The calculated stored capacity in each test can be seen in Figure 50. The capacity value during the charge period is shown in Figure 50(a) and the final value comparison is illustrated

in Figure 50(b). The highest value was achieved with the 1.0C rate charge. A slightly smaller capacity has been reached in the 0.25C rate and with the 0.5C rate the lowest value was obtained.

Figure 50 – Comparison of stored capacity in charge tests with current rates of 0.25C, 0.5C and 1.0C

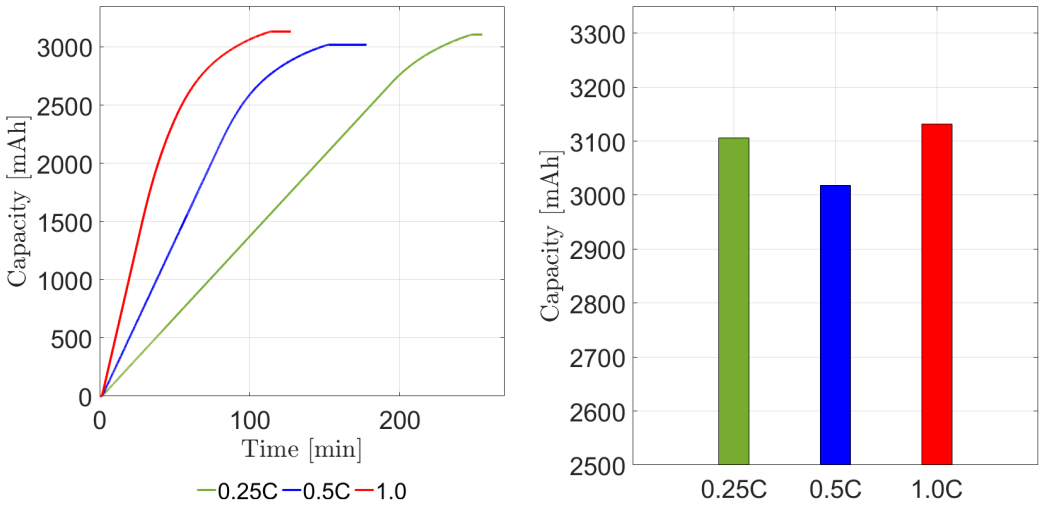

Source: the author

As already mentioned, in the charge test with rate of 1.0C, the battery cell temperature rise is higher than desired. This temperature increase can damage the battery pack and shorten the service life. The tests with 0.5C and 0.25C present low temperature rise. The curves for the cell temperature behavior are presented in Figure 51.

Figure 51 – Comparison of cell temperature in charge tests with current rates of 0.25C, 0.5C and 1.0C

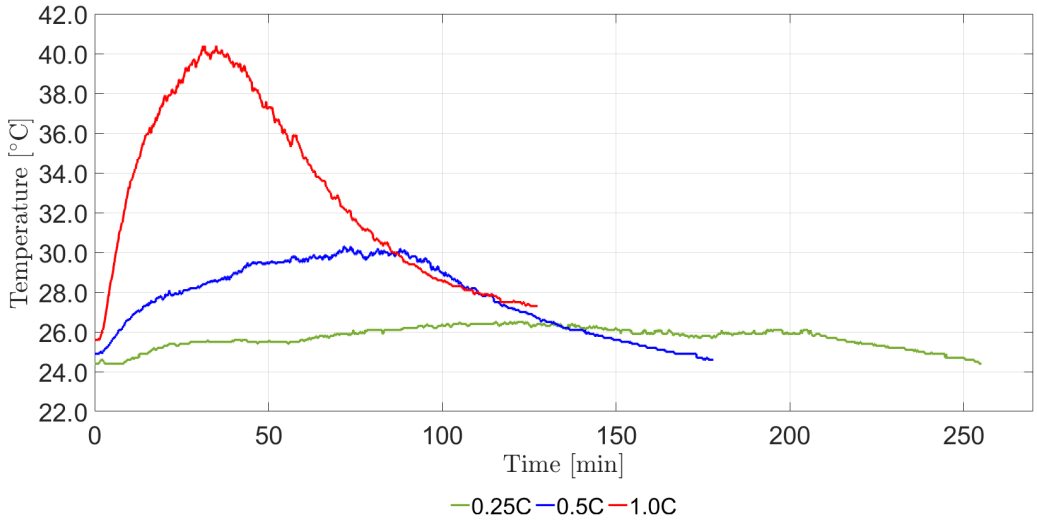

Source: the author

6.2 DISCHARGE TESTS

The battery discharge tests were performed using an electronic load to control the discharge current level, with the circuit presented in Section 4.4. The discharge current can be

varied with different values through a potentiometer and the current value remains constant during all the test.

The discharge path can be blocked by the BMS sending 0 V to DSG pin. Different conditions may suspend the battery pack discharge. If a cell voltage reaches the undervoltage protection value (2.5 V), for example, the discharge is interrupted. There are also protections for overcurrent and short-circuit during the discharge, as well as, for overtemperature (60.0 °C).

The tests performed in this work are made under controlled current levels and within the temperature range. For this reason, the battery pack discharging is suspended during these tests only when a cell voltage reaches the undervoltage level. In case of another condition being responsible for interrupting the discharge, it will be properly mentioned.

If a qualified discharge occurs, i.e. the battery pack is discharged from nearly full to a low battery voltage level, the BMS estimates a new full charge capacity. Thereby, the BMS learns the true discharge capacity of the battery under system-use conditions. Therefore, in some tests, the full capacity value is updated in the end of the discharge.

The tests presented in this section are separated by the charge current rate, to provide a fair comparison. The discharge tests with different current rates are compared to each other after a same charge current rate. For this reason, there are three groups of discharge tests comparisons: discharges performed after charging the battery pack with 0.25C rate, discharges after charging with 0.5C and discharges tests with battery pack charged with 1.0C current rate. Each discharge group provides comparison between three different discharge current rates (0.25C, 0.5C and 1.0C).

As the manufacturer's recommendation is to charge the battery with a current rate of 0.5C, the discharge test presented in detail in this section was performed after the battery pack was charged with this rate. The results of the discharges tests performed after charges with different rate, can be observed in the appendices. Discharges after charge rate of 0.25C are available in Appendix C and after charge rate of 1.0C in Appendix D.

6.2.1 Discharge tests results with current rate of 0.25C after charging with current rate of 0.5C

In the first test, the discharge current was adjusted for 0.25C rate. The total battery pack discharge was achieved after 3h37min and the total capacity drained was 3052 mAh. The battery cell temperature increase was 3.8 °C. The main parameters of the test are summarized in Table 12.

Figure 52 shows the battery pack voltage and current during the discharge. Note that the current value remains constant, as desired, and the pack voltage drops linearly during almost all the discharge. Because of the battery chemistry behavior at low voltage stages, the curve present a different tendency at the end of the test, as expected.

Table 12 – Main parameters of discharge test with current rate of 0.25C after charging with current rate of 0.5C

Information	Value
Test	Discharge
Current	843 mA
Duration	3h37min
Controlled temperature	No
Initial cell temperature	25.5 °C
Maximum cell temperature	29.3 °C
Cell temperature variation	3.8 °C
Initial pack voltage	20.675 V
Minimum pack voltage	13.450 V
Pack voltage variation	7.225 V
Initial RSOC	100%
Final RSOC	0%
Calculated capacity	3052 mAh

Source: the author

Figure 52 – Pack voltage and current during discharge with current rate of 0.25C after charging with current rate of 0.5C

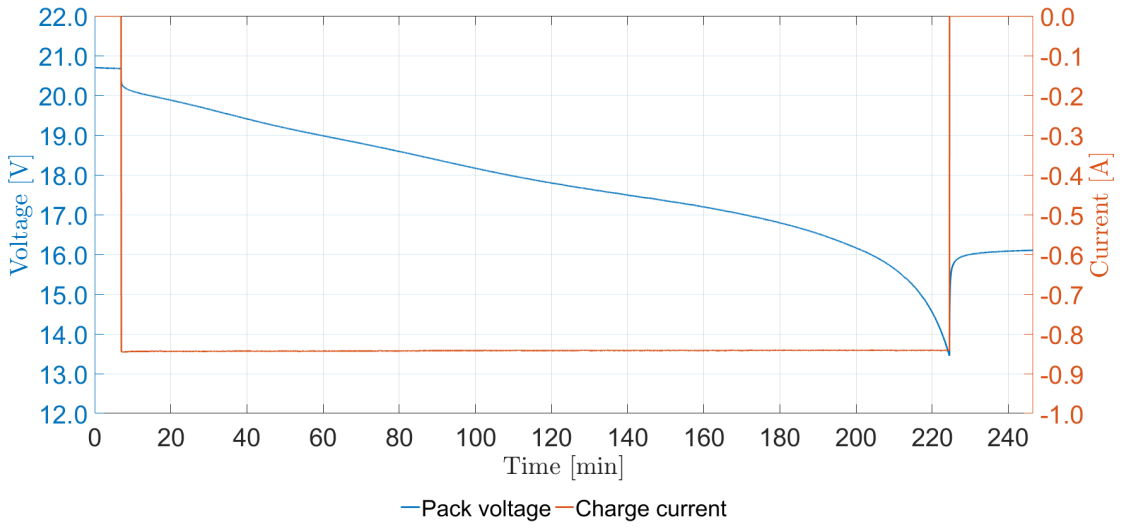

Source: the author

Each of the battery cell voltage, during the test is presented in Figure 53. Also some measurements are highlighted in Table 13. Note that the voltages are very similar during the discharge, except for the last 20 minutes. Cell 5 is responsible for activating the undervoltage protection in 2.5 V. At the end of the test, it presents a different discharge behavior, that could be caused by a increase of internal resistance and/or of temperature.

Table 13 – Cell voltages measurements during discharge with current rate of 0.25C after charging with current rate of 0.5C

Description	Cell 1	Cell 2	Cell 3	Cell 4	Cell 5
Initial open circuit cell voltage [V]	***4.130***	4.143	**4.154**	4.142	4.131
Cell voltage after 5 minutes in discharge [V]	***3.976***	3.988	**4.016**	3.978	3.986
Final discharge cell voltage [V]	2.709	2.714	**2.807**	2.727	***2.498***
Final open circuit cell voltage [V]	3.225	3.230	**3.262**	3.225	***3.162***

Source: the author

Figure 53 – Cell voltages during discharge with current rate of 0.25C after charging with current rate of 0.5C

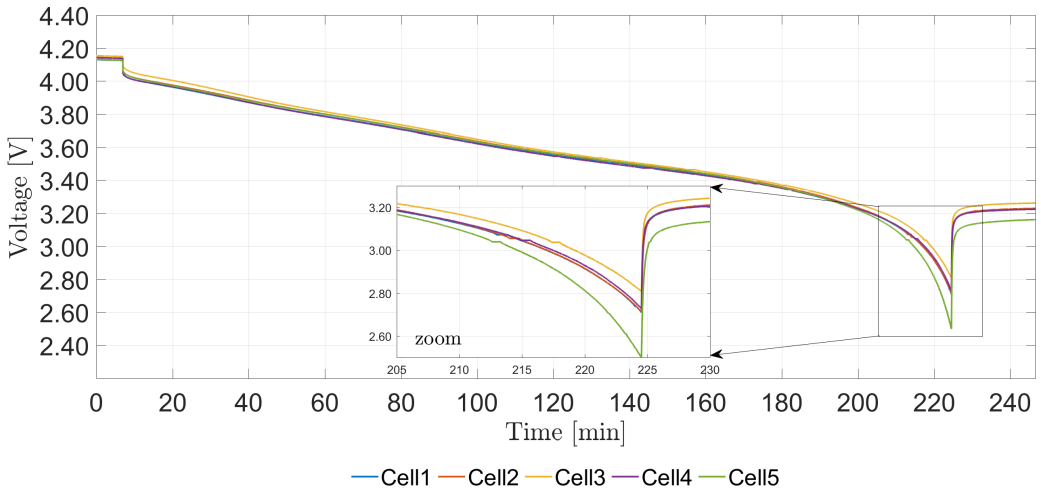

Source: the author

The remaining capacity and the relative SoC estimated by the BMS are illustrated in Figure 54. Both values start from the maximum and decrease to zero at the end of the discharge.

Figure 54 – Remaining capacity and relative SoC during discharge with current rate of 0.25C after charging with current rate of 0.5C

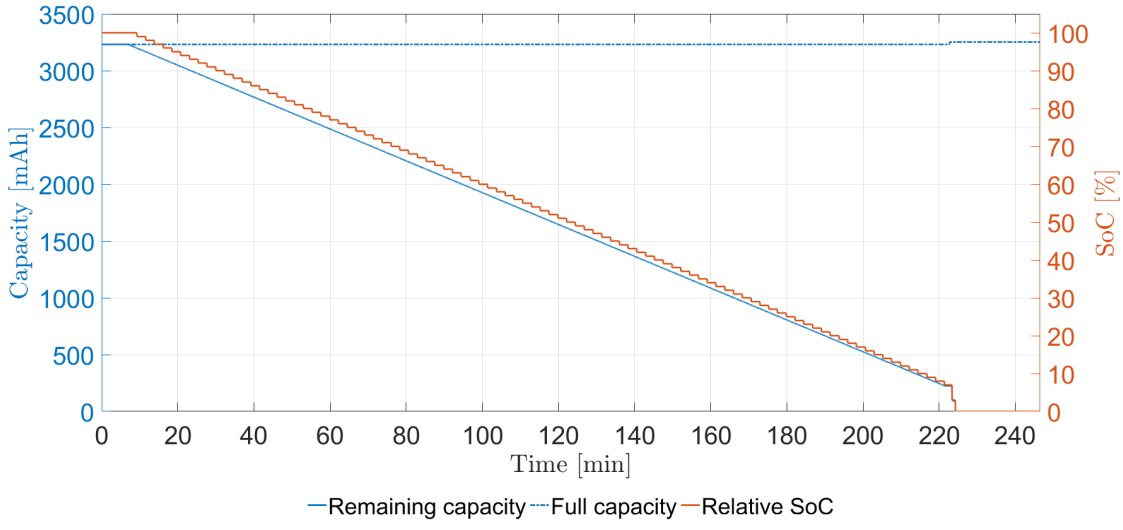

Source: the author

The battery cell temperature can be observed in Figure 55. Note that the cell temperature increases with a higher rate at the end of the test and reaches a maximum value of 29.3 °C.

Figure 55 – Battery cell temperature during discharge with current rate of 0.25C after charging with current rate of 0.5C

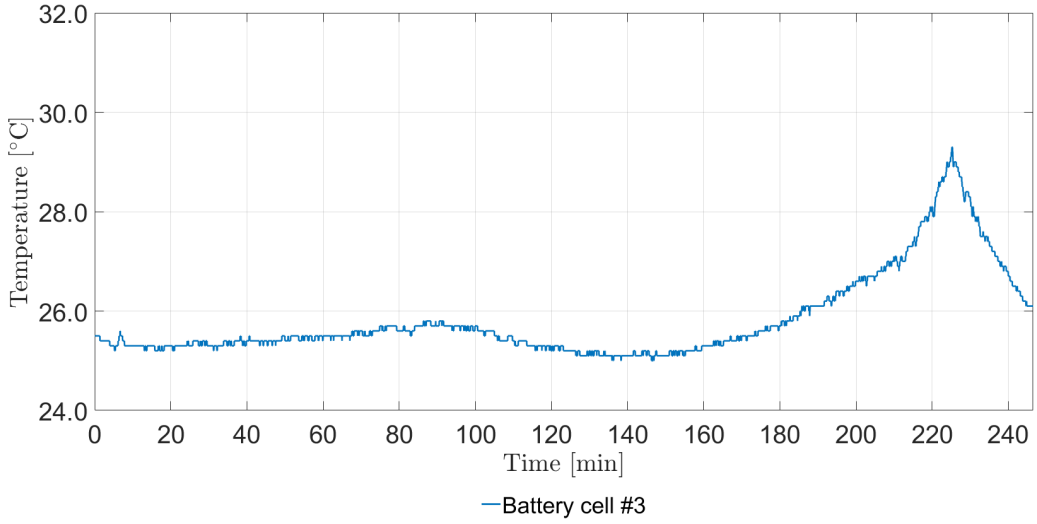

Source: the author

6.2.2 Discharge tests results with current rate of 0.5C after charging with current rate of 0.5C

A new discharging test was performed changing the current rate to 0.5C. With the battery pack completely charged, the electronic load was set to draining the current around 1650 mAh. Table 14 summarizes the main results from this discharge test. The complete discharge took 1h49min long and could deliver a calculated capacity of 3017 mAh. The battery cell temperature presents an increase of 8.9 °C during the test.

Table 14 – Main parameters of discharge test with current rate of 0.5C after charging with current rate of 0.5C

Information	Value
Test	Discharge
Current	1659 mA
Duration	1h49min
Controlled temperature	No
Initial cell temperature	24.4 °C
Maximum cell temperature	33.3 °C
Cell temperature variation	8.9 °C
Initial pack voltage	20.640 V
Minimum pack voltage	13.431 V
Pack voltage variation	7.209 V
Initial RSOC	100%
Final RSOC	0%
Calculated capacity	3017 mAh

Source: the author

The battery pack voltage and current during the discharge are illustrated in Figure 56. As in the previously test, the discharge current remains constant during the test and the battery pack voltage presents the expected behavior, decreasing until the discharge is interrupted.

Figure 56 – Pack voltage and current during discharge with current rate of 0.5C after charging with current rate of 0.5C

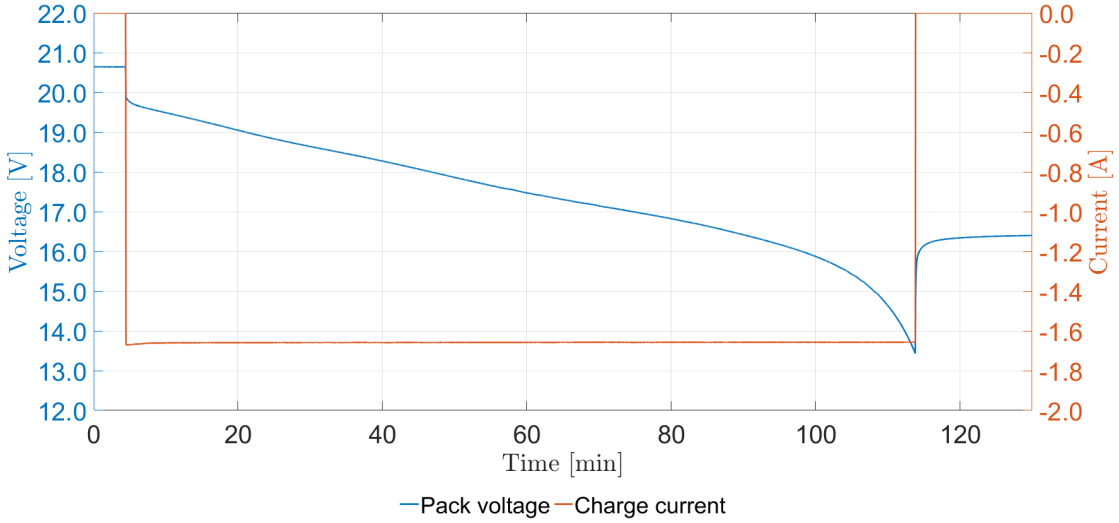

Source: the author

Figure 57 shows each cell voltage during the discharge and Table 15 summarizes some of the measurement in different times of the test. Again, the cell 5 is the first to reach the undervoltage limit and activate the protection. But in this test, the cells have a greater difference between the voltages. This difference remains constant during the discharge, with can be cause buy the internal resistance of each cell.

Table 15 – Cell voltages measurements during discharge with current rate of 0.5C after charging with current rate of 0.5C

Description	Cell 1	Cell 2	Cell 3	Cell 4	Cell 5
Initial open circuit cell voltage [V]	***4.118***	4.131	4.132	**4.143**	***4.118***
Cell voltage after 5 minutes in discharge [V]	3.846	3.854	3.889	**3.902**	***3.807***
Final discharge cell voltage [V]	2.688	2.721	2.756	**2.778**	***2.498***
Final open circuit cell voltage [V]	3.291	3.299	3.301	**3.307**	***3.254***

Source: the author

Figure 57 – Cell voltages during discharge with current rate of 0.5C after charging with current rate of 0.5C

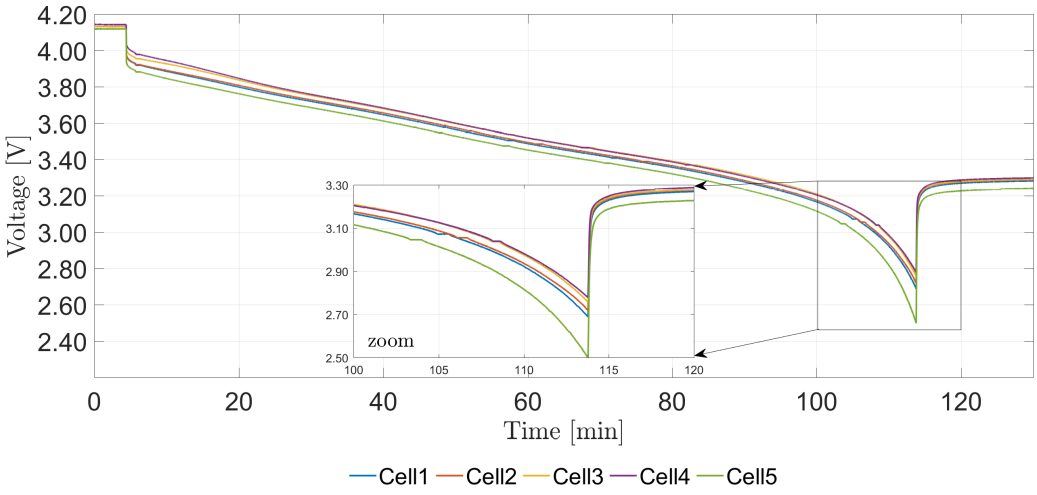

Source: the author

Figure 58 provides the estimated remaining and full capacity and the relative SoC during the discharge. The parameters values have the same behavior as the last test, the remaining capacity and relative SoC start from the maximum value and decrease until zero, at the end of the discharge.

Figure 58 – Remaining capacity and relative SoC during discharge with current rate of 0.5C after charging with current rate of 0.5C

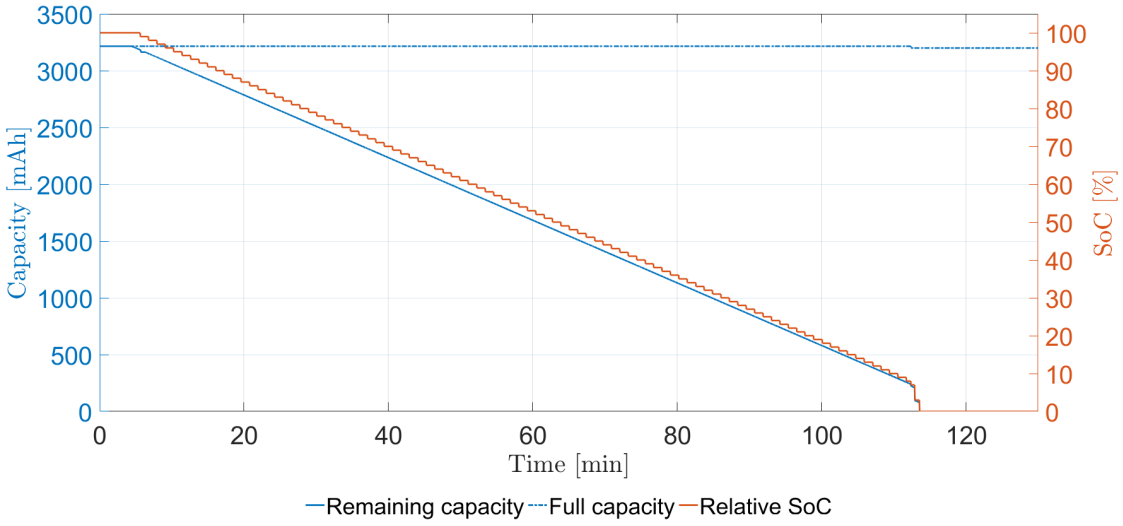

Source: the author

The battery cell temperature during the test can be seen in Figure 59. In this test, with a discharge current of 0.5C, the cell temperature increases 9.2 °C and reaches the maximum value at the end of the test. This is an expected behavior, as soon as the current drained from the batteries is higher, the cell temperature will rise.

Figure 59 – Battery cell temperature during discharge with current rate of 0.5C after charging with current rate of 0.5C

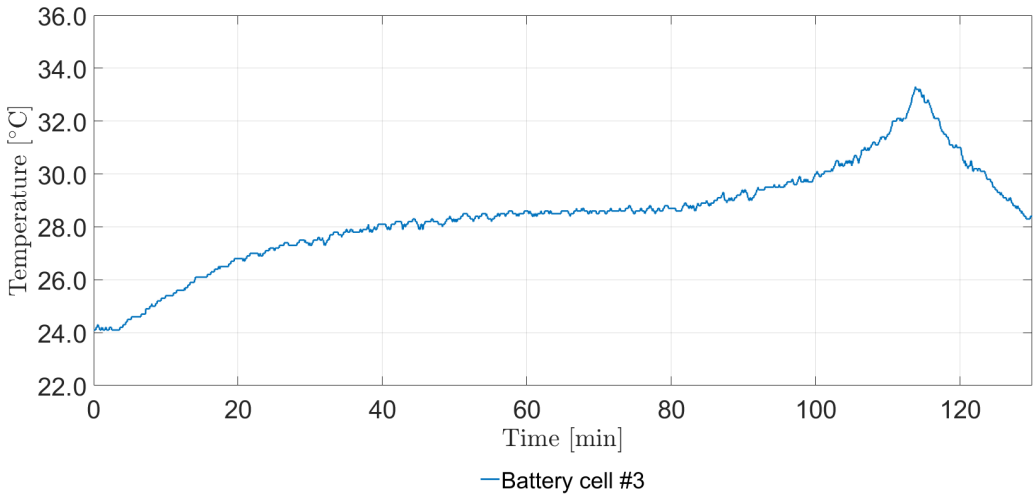

Source: the author

6.2.3 Discharge tests results with current rate of 1.0C after charging with current rate of 0.5C

To conclude, a discharge test with 1.0C rate was carried out. Table 16 summarizes the main results of this test. With a rate rate of 1.0C, the complete discharge was achieved after 55 minutes of discharge. The calculated drained capacity was 3034 mAh and the cell temperature increases 15.5 °C.

Table 16 – Main parameters of discharge test with current rate of 1.0C after charging with current rate of 0.5C

Information	Value
Test	Discharge
Current	3314 mA
Duration	0h55min
Controlled temperature	No
Initial cell temperature	21.8 °C
Maximum cell temperature	37.3 °C
Cell temperature variation	15.5 °C
Initial pack voltage	20.653 V
Minimum pack voltage	13.083 V
Pack voltage variation	7.570 V
Initial RSOC	100%
Final RSOC	0%
Calculated capacity	3034 mAh

Source: the author

The battery pack voltage and current during the discharge are shown in Figure 60. The discharge behavior is as expected, the current remains constant during the test and the pack voltage decreases until the end of the discharge. As the drained current is greater in this test, the voltage drop is also greater at the beginning of the test.

Figure 60 – Pack voltage and current during discharge with current rate of 1.0C after charging with current rate of 0.5C

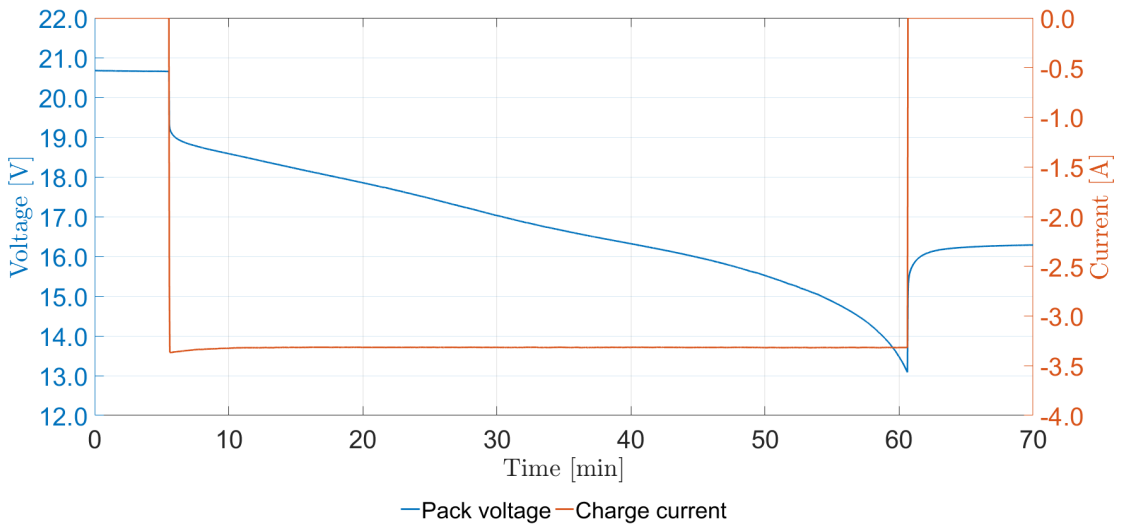

Source: the author

Table 17 presents the measurement of each cell voltage at different moments during the discharge test. Figure 61 shows the cell voltages during the entire discharge. As in the other tests, cell 5 reaches the undervoltage limit and activates the protection to interrupt the battery pack discharge. In this case, as the current level is greater than in the other tests, the difference between the voltage of the cell 5 and the others is also greater. Cell 5 presents a lower voltage during the entire discharge and the difference is constant, which is caused by the increase of the internal resistance in the cell 5.

Table 17 – Cell voltages measurements during discharge with current rate of 1.0C after charging with current rate of 0.5C

Description	Cell 1	Cell 2	Cell 3	Cell 4	Cell 5
Initial open circuit cell voltage [V]	**4.143**	**4.143**	***4.119***	4.134	4.134
Cell voltage after 5 minutes in discharge [V]	3.637	**3.665**	3.659	3.659	***3.558***
Final discharge cell voltage [V]	**2.669**	2.666	2.618	2.647	***2.497***
Final open circuit cell voltage [V]	**3.294**	3.279	***3.242***	3.267	3.253

Source: the author

Figure 61 – Cell voltages during discharge with current rate of 1.0C after charging with current rate of 0.5C

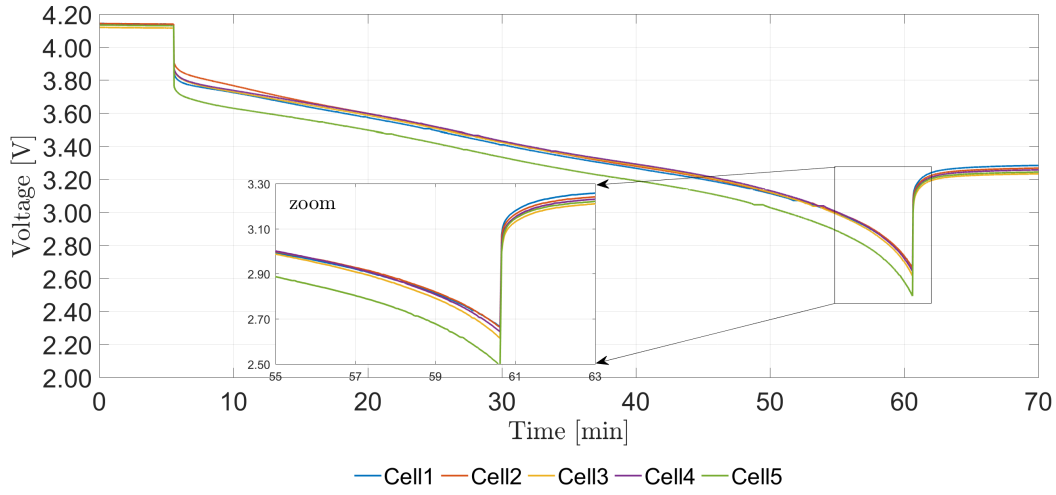

Source: the author

The estimated remaining and full capacity as well as the relative SoC are illustrated in Figure 62. Both parameters, remaining capacity and relative SoC start at the maximum values and decrease until zero during the discharge test.

Figure 62 – Remaining capacity and relative SoC during discharge with current rate of 1.0C after charging with current rate of 0.5C

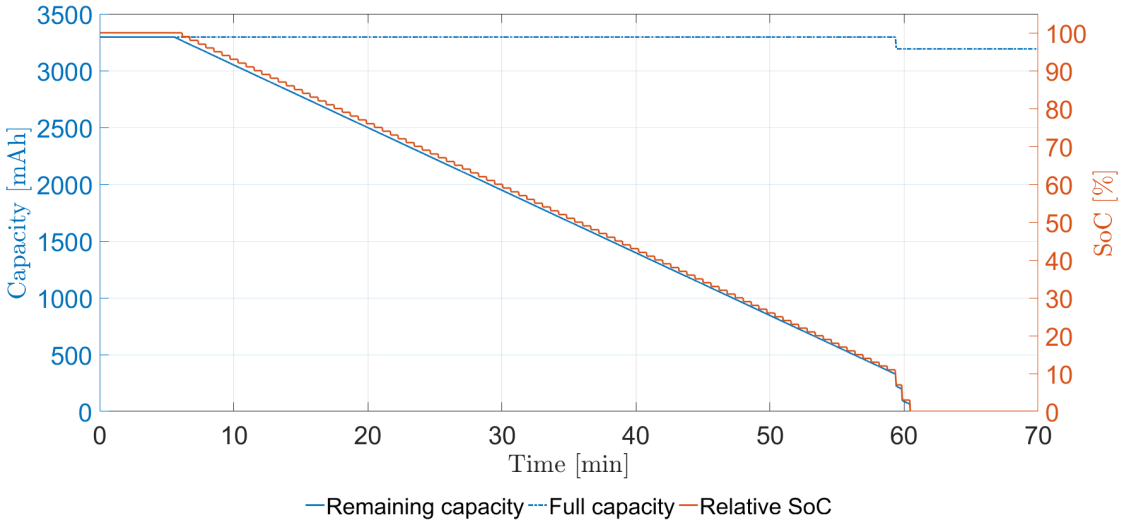

Source: the author

The battery cell temperature can be seen in Figure 63. The cell temperature behavior is as expected, increasing during the test and reaching the maximum value at the end of the discharge. In this test, as the current level is the nominal rate, the cell temperature rises 15.4 °C.

Figure 63 – Battery cell temperature during discharge with current rate of 1.0C after charging with current rate of 0.5C

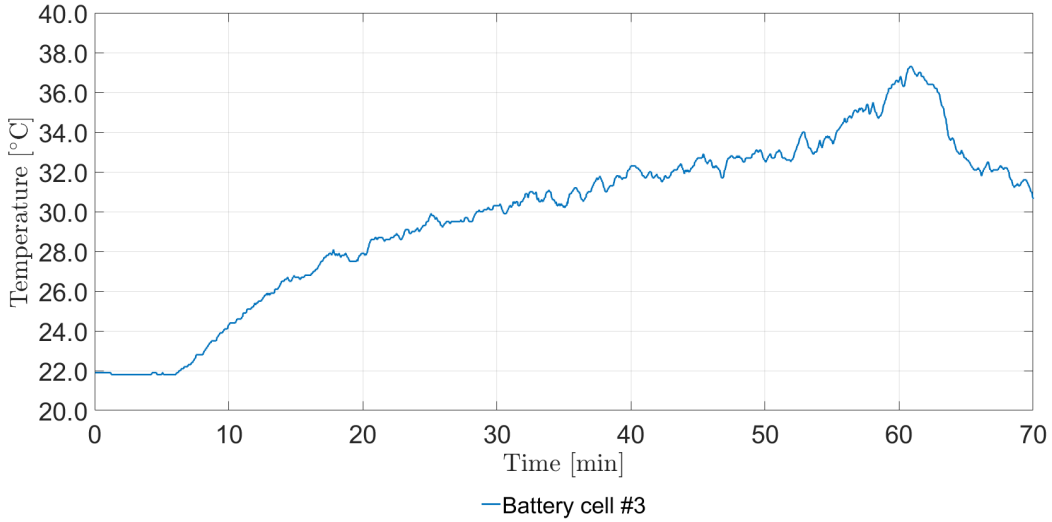

Source: the author

6.2.4 Comparison between the discharge tests under different current discharge rates after charging with current rate of 0.5C

This section presents the comparison between the discharge tests already evaluated in Section 6.2. The discharges were carried out under different rates, 0.25C (Section 6.2.1), 0.5C (Section 6.2.2) and 1.0C (Section 6.2.3), but they were all completely charged with a rate of 0.5C. Table 18 summarizes the main results for each test and present them together.

Table 18 – Comparison of the main parameters of discharge tests with current rates of 0.25C, 0.5C and 1.0C after charging with current rate of 0.5C

Information	0.25C	0.5C	1.0C
Current	843 mA	1659 mA	3314 mA
Duration	3h37min	1h49min	0h55min
Initial cell temperature	25.5 °C	24.4 °C	21.8 °C
Maximum cell temperature	29.3 °C	33.3 °C	37.3 °C
Cell temperature variation	3.8 °C	8.9 °C	15.5 °C
Initial pack voltage	20.675 V	20.640 V	20.653 V
Minimum pack voltage	13.450 V	13.431 V	13.083V
Pack voltage variation	7.225 V	7.209 V	7.570 V
Initial RSOC	100%	100%	100%
Final RSOC	0%	0%	0%
Calculated capacity	3052 mAh	3017 mAh	3034 mAh

Source: the author

The battery pack discharge rate is set by the user's application. In these tests it was observed that requiring the nominal discharge rate (1.0C) or higher involves a high cell temperature increase. If the battery pack operates in high temperature it will present an early degradation. However, using a lower discharge current involves a larger number of battery cells (parallel association), which results in additional cost and space, not desired in most of the

applications. A possible solution to keep a battery pack performance and long cycle life is the use of a thermal management system, already mentioned in this work as part of a optimal BMS (Section 3.4). With the battery pack operating in a controlled temperature range, the damage due to high current rates can be reduced.

Some applications require a high current level, in this case the lithium-ion battery needs to be chosen to satisfy this condition, according the manufacturer's recommendation.

Figure 64 illustrates the battery pack voltage during each discharge test. Note that the immediate voltage drop during the discharge with the rate of 1.0C is greater than the other test, as expected.

Figure 64 – Comparison of pack voltage in discharge test with current rates of 0.25C, 0.5C and 1.0C after charging with current rate of 0.5C

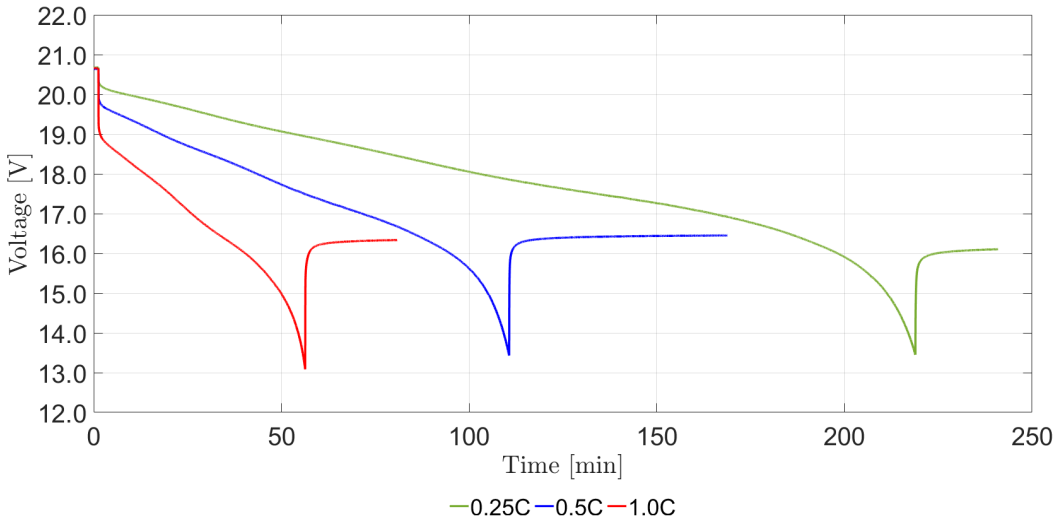

Source: the author

The calculated drained capacity for each test is presented in Figure 65(a) related to the pack voltage during the discharge and Figure 65(b) indicates the final calculated capacity. The drained capacity do not present a big difference between the tests but the results are expected, the most capacity was delivered by the discharge at the lower rate and the test with a nominal current results in more capacity than the test with 0.5C discharge rate.

Figure 65 – Comparison of drained capacity in discharge test with current rates of 0.25C, 0.5C and 1.0C after charging with current rate of 0.5C

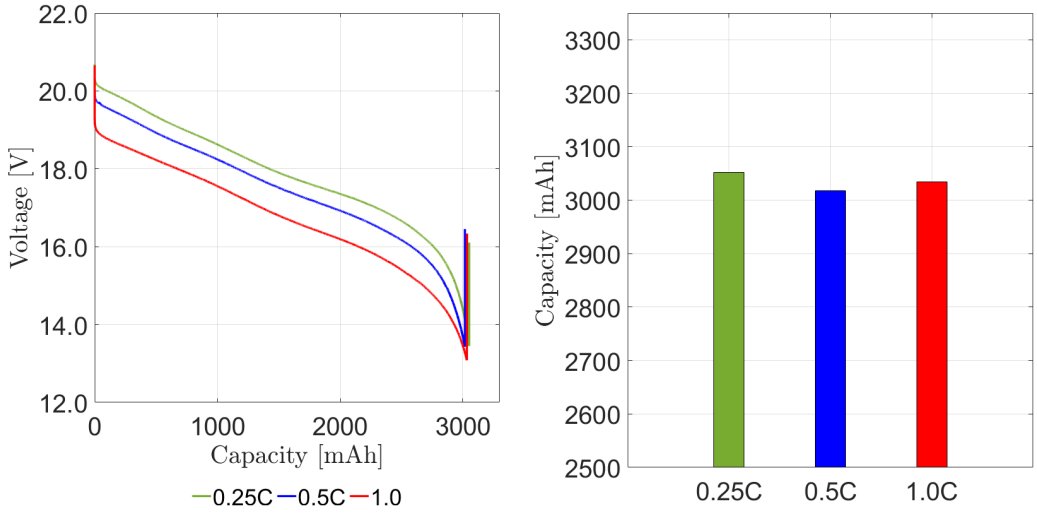

(a) (b)

Source: the author

A comparison between the battery cell temperature for each test is available in Figure 66. As already discussed, the discharge with nominal rate results in higher temperature increase and can degraded the battery pack.

Figure 66 – Comparison of cell temperature in discharge test with current rates of 0.25C, 0.5C and 1.0C after charging with current rate of 0.5C

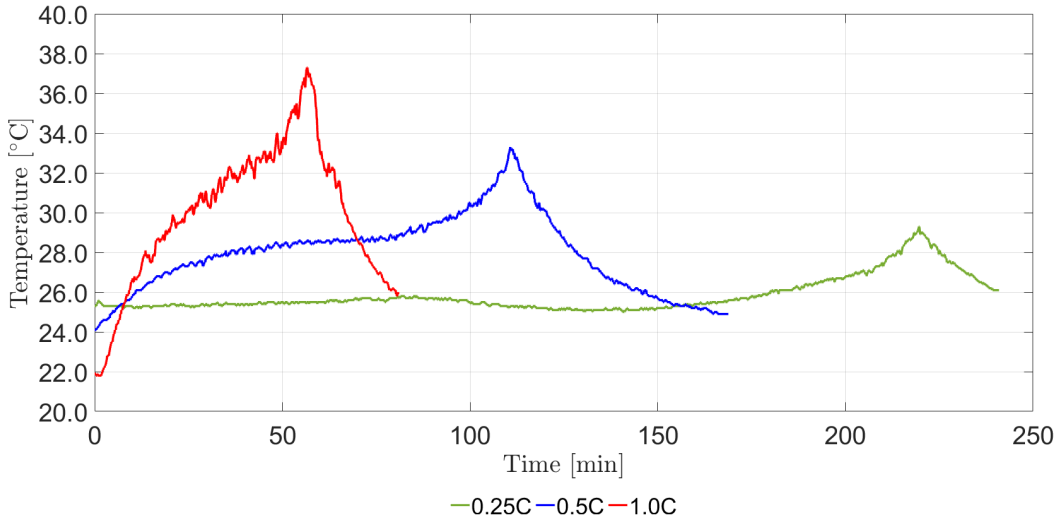

Source: the author

The next chapter presents the charge and discharge tests carried out under controlled room temperature.

7 CONTROLLED ROOM TEMPERATURE TESTS

As temperature is an important variable for battery performance and safety, some tests with controlled room temperature were realized and are presented in this chapter.

The thermal chamber Thermotron, model SE-2000-3-3 (Figure 67) provides controlled room temperatures and tests were performed in three different temperature conditions, 10 °C, 25 °C and 40 °C. Only the battery pack is inside the chamber and the same parameters of the not controlled temperature tests were observed. Tests for charge and discharge under different current rates are presented in this chapter. A picture of the experimental setup used in these tests is available in Figure 68(a), which illustrates the BMS, the laptop, DC power supply and the electronic load outside the thermal chamber and in Figure 68(b) is shown the battery pack and the NTC temperature sensor used in the BMS inside the thermal chamber.

Figure 67 – Thermal chamber model used to perform controlled room temperature tests

Source: the author

Figure 68 – Experimental setup used to perform controlled room temperature tests

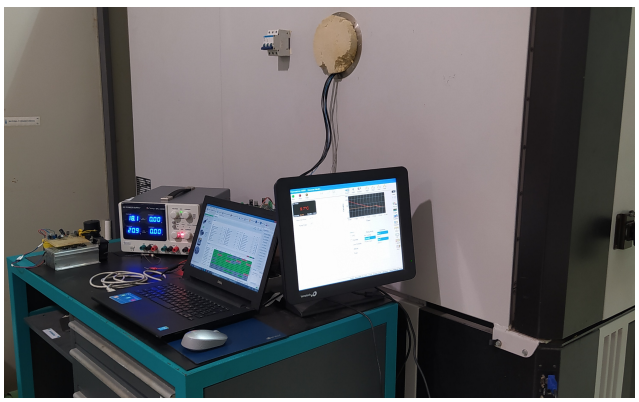

(a) Setup with the chamber control and the BMS

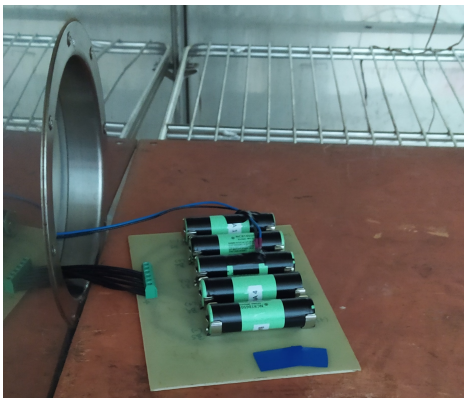

(b) Battery pack inside the thermal chamber

Source: the author

The main results of the thermal tests are summarized in Table 19. The order and the

test conditions (first tests were performed in 25 °C, considering it the standard condition for later comparison), the maximum cell temperature variation (ΔT_{cell}), the charge or discharge process duration and the calculated stored or drained capacity of the battery pack in each test are presented.

For each ambient temperature value, three charge and discharge cycles were performed. The charge rate was kept constant at 0.5C for tests at 25 °C and 40 °C and at 0.25C for tests at 10 °C, following the manufacturer's instructions. An additional test, using a new battery pack, was carried out at 10 °C with a charge rate of 0.5C and the results are also evaluated in this work. The results are presented during this chapter. A comparison between the charge tests under different temperatures is available in Section 7.1. The charge tests at 10 °C and with charge rates of 0.25C and 0.5C are compared in Section 7.2. And the discharge tests performed under different temperatures are compared in Section 7.3.

Table 19 – Main parameters of all charge and discharge tests with controlled room temperature

Order	Discharge/Charge rate	Room temp.	ΔT_{cell}	Duration	Capacity
1	Charge 0.5C	25 °C	1.7 °C	2h38min	3211 mAh
2	Discharge 0.25C	25 °C	1.4 °C	3h36min	3052 mAh
3	Charge 0.5C	25 °C	1.4 °C	2h31min	3144 mAh
4	Discharge 0.5C	25 °C	2.5 °C	1h50min	3044 mAh
5	Charge 0.5C	25 °C	1.4 °C	2h31min	3094 mAh
6	Discharge 1.0C	25 °C	5.8 °C	0h55min	3075 mAh
7	Charge 0.5C	40 °C	2.3 °C	2h35min	3109 mAh
8	Discharge 0.25C	40 °C	1.5 °C	3h41min	3151 mAh
9	Charge 0.5C	40 °C	2.9 °C	2h35min	3205 mAh
10	Discharge 0.5C	40 °C	3.4 °C	1h55min	3161 mAh
11	Charge 0.5C	40 °C	2.6 °C	2h10min	3108 mAh
12	Discharge 1.0C	40 °C	8.9 °C	0h55min	3064 mAh
13	Charge 0.25C	10 °C	0.5 °C	3h55min	3013 mAh
14	Discharge 0.25C	10 °C	1.4 °C	3h12min	2652 mAh
15	Charge 0.25C	10 °C	0.9 °C	3h17min	2708 mAh
16	Discharge 0.5C	10 °C	3.0 °C	1h26min	2366 mAh
17	Charge 0.25C	10 °C	0.6 °C	3h17min	2541 mAh
18	Discharge 1.0C	10 °C	6.6 °C	0h43min	2388 mAh
1	Charge 0.5C	10 °C	1.2 °C	1h35min	2562 mAh
2	Discharge 0.5C	10 °C	2.9 °C	1h16min	2142 mAh
3	Charge 0.5C	10 °C	1.2 °C	1h21min	2199 mAh
4	Discharge 0.25C	10 °C	1.9 °C	2h32min	2165 mAh
5	Charge 0.5C	10 °C	1.8 °C	1h18min	2147 mAh
6	Discharge 1.0C	10 °C	7.4 °C	0h34min	1909 mAh

Source: the author

7.1 CHARGE TESTS COMPARISON UNDER ROOM TEMPERATURES OF 10 °C, 25 °C AND 40 °C AND SAME CHARGE RATE OF 0.5C

To analyze the influence of temperature during the battery pack charging process, the results of the charges carried out at a rate of 0.5C and at temperatures of 10°C, 25°C and 40°C are compared in this section. The first test performed in each temperature is used in this

comparison (order 1, 7 and 13 in Table 19), but for each room temperature were performed three charge tests at the same condition, all the results are available in Appendix E.

The manufacturer's recommended temperature range during the charging process using 0.5C is 10 °C to 45 °C in the battery cell. During the tests at 40 °C, the cell temperature was monitored so as not to exceed the recommended value. For the room temperature at 10 °C, the initial indication of cell temperature is lower at 1.2 °C. The cell temperature measurement is performed using a NTC sensor and can provide a not accurate value in this temperature region. During the test, the cell temperature behavior was monitored and it remained as expected. Other charging tests were carried out at 10 °C with a charge rate at 0.25C and the both results are evaluated in the following section.

In Table 20 is possible to see the main results for each test. The order presented is related to the order in which the tests were run.

The charge tests at 25 °C and 40 °C are very similar and present the expected results. In both cases, the charge process is complete when the termination condition is achieved. As the test is performed in a controlled temperature, the cell temperature variation is lower than the charges performed in uncontrolled temperature environment. In both tests, the capacity stored during charging is close to the nominal value. In the other hand, the charge at 10 °C has a stored capacity quite low and the charging process was interrupted by an overvoltage protection. Charging the battery at low temperature causes lithium deposition, which may lead to loss of electrolyte and lithium ions inventory and the increase of the internal resistance (HAN et al., 2019). The side effects are capacity fade (battery rapid degradation) and even lead to safety issues.

Table 20 – Comparison of the main parameters of charge tests with rate of 0.5C and at 10 °C, 25 °C and 40 °C

Information	**25 °C**	**40 °C**	**10 °C**
Current	1632mA	1610 mA	1675 mA
Duration	2h38min	2h35min	1h35min
Initial cell temperature	25.5 °C	41.9 °C	8.8 °C
Maximum cell temperature	27.2 °C	44.2 °C	10.0 °C
Cell temperature variation	1.7 °C	2.3 °C	1.2 °C
Initial pack voltage	15.232 V	16.069 V	15.589 V
Maximum pack voltage	20.933 V	20.835 V	20.704 V
Pack voltage variation	5.701 V	4.766 V	5.205 V
Initial RSOC	0%	0%	0%
Final RSOC	100%	100%	78%
Calculated capacity	3211 mAh	3109 mAh	2562 mAh

Source: the author

Figure 69 presents the current behavior during the charge process. Note that even the current value is quite similar for all the tests, the duration of the charge at 10 °C is lower than the other tests.

Figure 69 – Comparison of charging current in charge tests with rate of 0.5C and at 10 °C, 25 °C and 40 °C

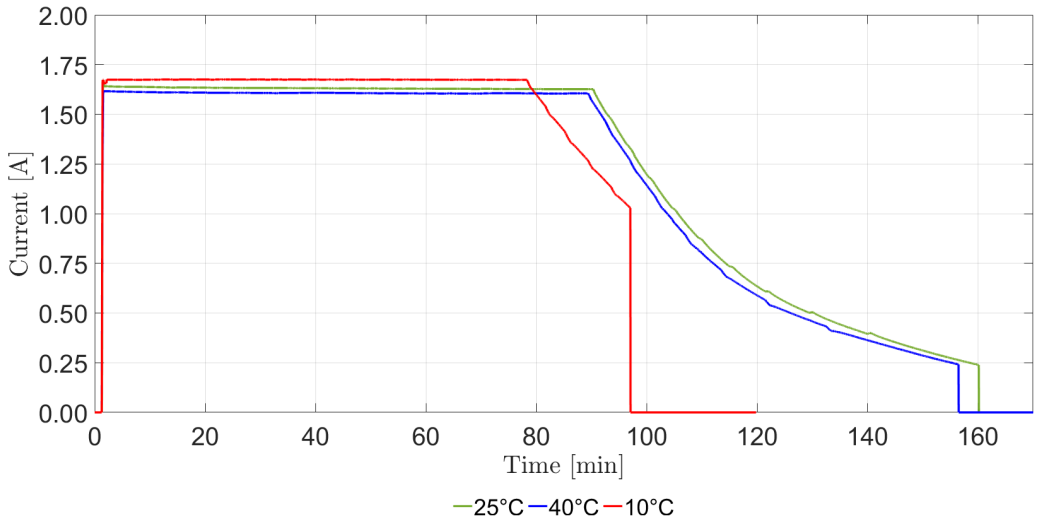

Source: the author

The battery pack voltage for each test can be observed in Figure 70. Note that after the charge current is applied, the battery pack voltage presents a different behavior for each temperature. For the room temperature at 40 °C, at the beginning of the charging, the voltage increase is lower than in the other tests, while at 10 °C it is the largest. The battery pack voltage remains higher during all the charging process and the cell overvoltage protection occurs long before the other temperatures.

Figure 70 – Comparison of pack voltage in charge tests with rate of 0.5C and at 10 °C, 25 °C and 40 °C

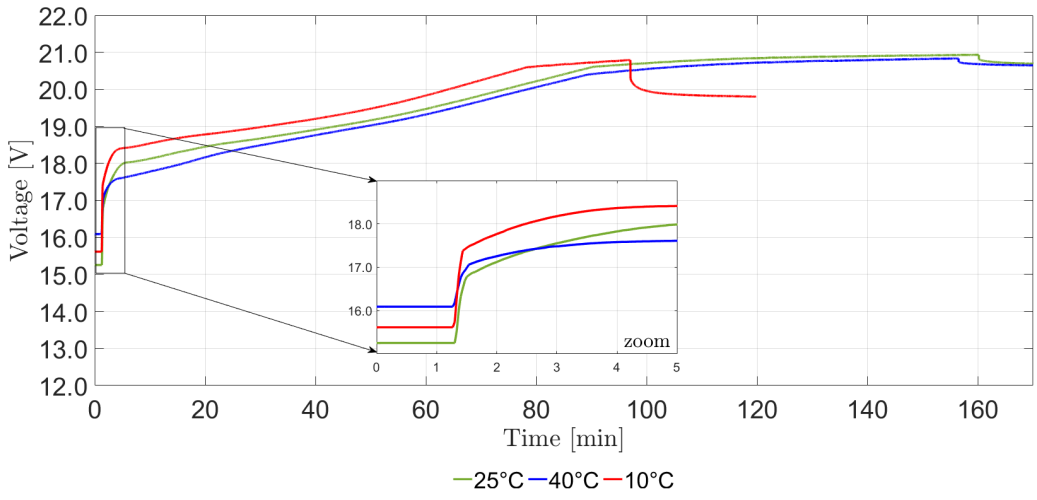

Source: the author

The cell temperature variation during the charge is presented in Figure 71. It is possible to notice that in all tests the temperature variation is low, as expected.

Figure 71 – Comparison of cell temperature in charge tests with rate of 0.5C and at 10 °C, 25 °C and 40 °C

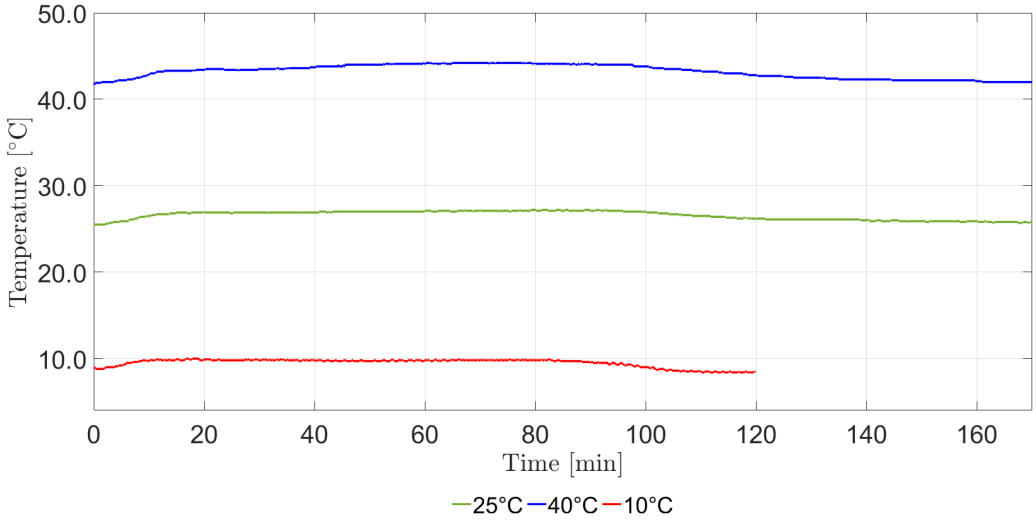

Source: the author

The stored capacity during the charge is presented in Figure 72(a) and the final value comparison can be seen in Figure 72(b). As already mentioned, for the tests at 25 °C and 40 °C the final capacity is quite near of the nominal value (95.8% and 92.8%, respectively) and the charge at 10 °C is only around 76.5% of the nominal capacity. Note, in Table 19, that the capacity value is decreasing during the following charge tests and achieve only 2147 mAh in the third charge at 10 °C, which represents 64% of nominal capacity.

As the capacity of the battery pack was greatly reduced in the charge test at 10 °C, a new test with another battery pack was carried out with a lower charge rate of 0.25C, following the manufacturer's recommendation. The test is presented in the following section with a comparison between the both charge rates, 0.25C and 0.5C.

Figure 72 – Comparison of stored capacity in charge tests with rate of 0.5C and at 10 °C, 25 °C and 40 °C

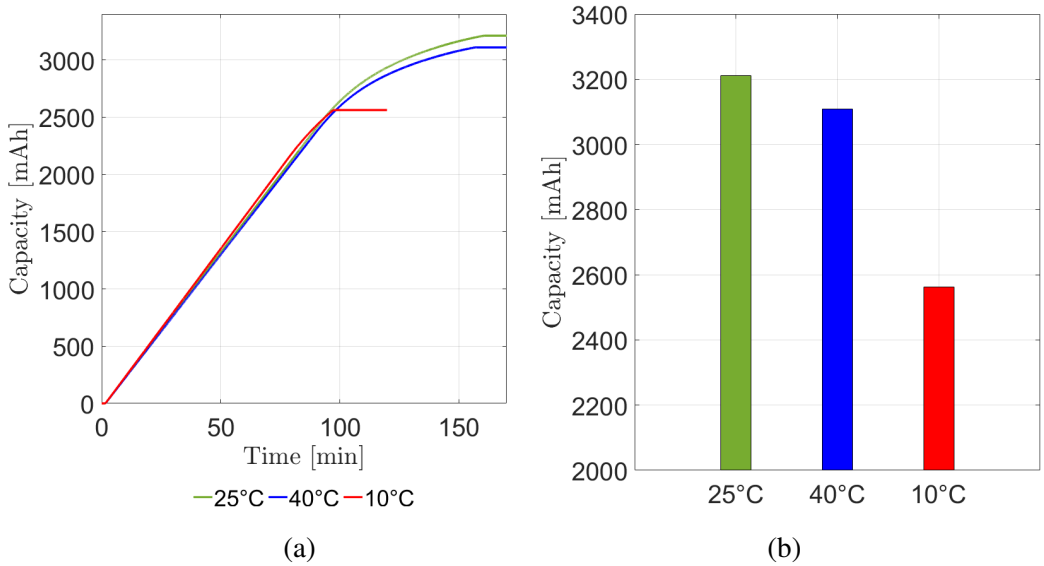

Source: the author

7.2 CHARGE TESTS COMPARISON UNDER ROOM TEMPERATURE OF 10 °C AND DIFFERENT CHARGE RATES OF 0.25C AND 0.5C

In order to understand the reduction in battery capacity during low temperature charging processes, a new test was carried out. This new test was performed with a charge rate of 0.25C and using a new battery pack without the capacity damaged. Table 21 presents the summarized results for the first charge test with 0.25C rate and also the results of the test with charge rate of 0.50C for comparison.

Table 21 – Comparison of main parameters of charge tests at 10 °C and charge rates of 0.25C and 0.5C

Data	**0.25C**	**0.5C**
Current	828 mA	1675 mA
Duration	3h55min	1h35min
Initial cell temperature	8.5 °C	8.8 °C
Maximum cell temperature	9.0 °C	10.0 °C
Cell temperature variation	0.5 °C	1.2 °C
Initial pack voltage	15.463 V	15.589 V
Maximum pack voltage	20.945 V	20.794 V
Pack voltage variation	5.482 V	5.205 V
Initial RSOC	0%	0%
Final RSOC	90%	78%
Calculated capacity	3013 mAh	2562 mAh

Source: the author

Figure 73 presents the current behavior during the charge processes using both 0.25C and 0.5C rates. For the 0.25C charge rate, the test takes a longer time to be complete, as expected. In both cases, the charge was interrupted by a cell overvoltage protection.

Figure 73 – Comparison of charging current in charge tests with rates of 0.25C and 0.5C at 10 °C

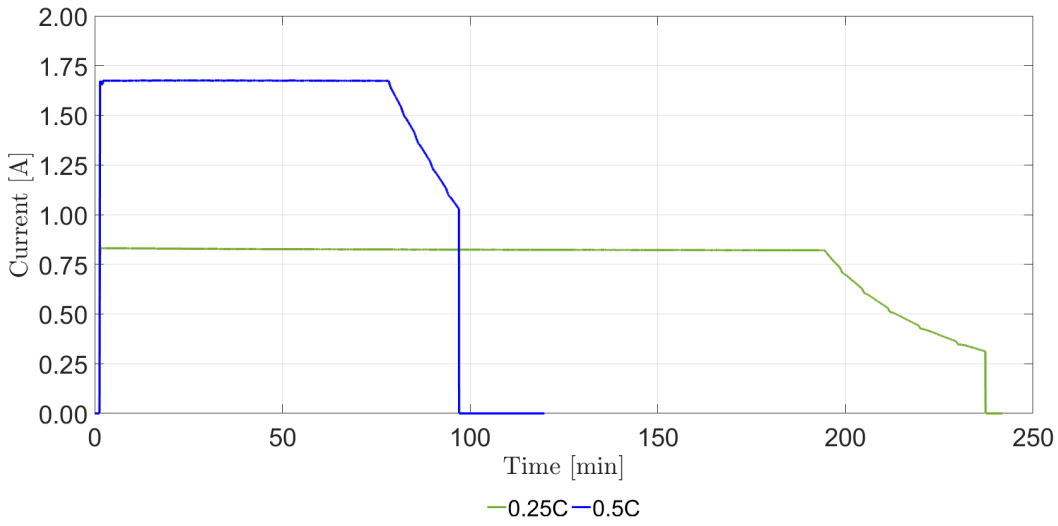

Source: the author

The battery pack voltage fore each test during the charge can be observed in Figure 74. The battery pack voltage is instantaneous increased as the current is applied. For the higher

current value, the increase is also higher. When the charge current is interrupted, the pack voltage decreased to lower value in case of 0.5C current charge rate.

Figure 74 – Comparison of pack voltage in charge tests with rates of 0.25C and 0.5C at 10 °C

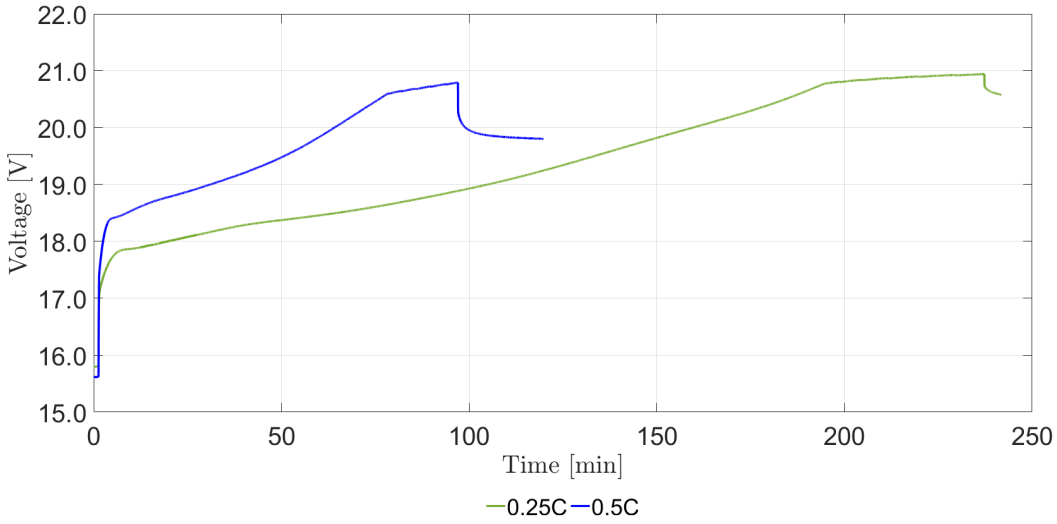

Source: the author

The cell temperatures during the charge process are presented in Figure 75. As expected, the temperature variation is lower during the charge test with rate of 0.25C.

Figure 75 – Comparison of cell temperature in charge tests with rates of 0.25C and 0.5C at 10 °C

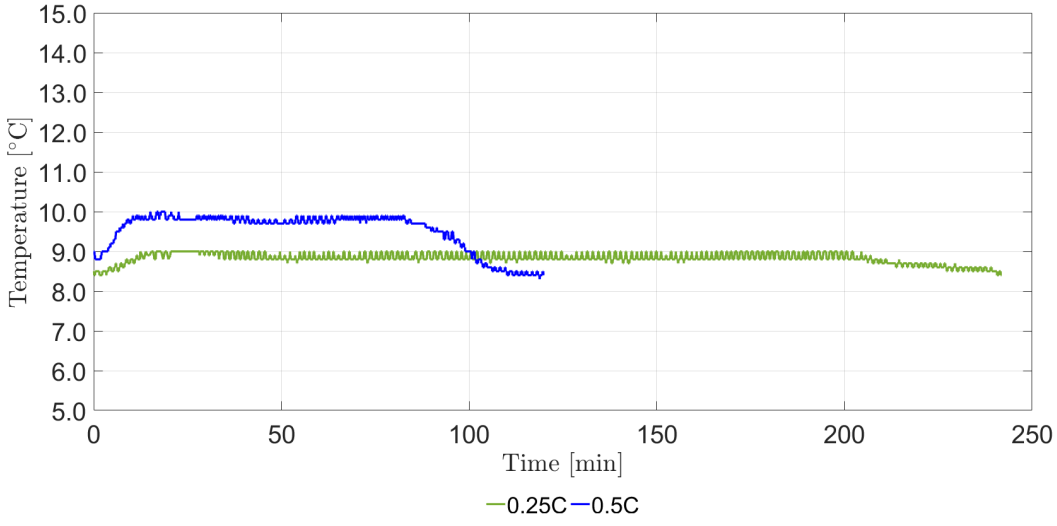

Source: the author

The stored capacities during the charge can be observed in Figure 76(a). The charge with 0.25C rate achieved a higher capacity than the charge with 0.5C rate (Figure 76(b)). As the current applied during the charge is lower, the battery is able to store more capacity. But this test was repeated three times keeping the charge conditions and the capacity decrease was observed over the tests. As already mentioned, the capacity loss is caused by the lithium plating during the charging at low temperature. The lithium plating is affected by the rate of the ion conduction and diffusion in the electrolyte, lithium diffusion in graphite particles and reaction

kinetics at graphite surface (YANG et al., 2018). In other words, the capacity loss is higher as the charging current is increased. The lithium plating at high charging currents and low temperature may cause short-circuit in the battery cell, which could result in explosion.

Figure 77 indicates the stored capacity comparison between all the charge tests performed at 10 °C and is possible to confirm the better capacity performance in the test carried out using a lower current rate, but even with this rate the capacity fade is higher than desired for most applications.

Figure 76 – Comparison of stored capacity in first charge tests with rates of 0.25C and 0.5C at 10 °C

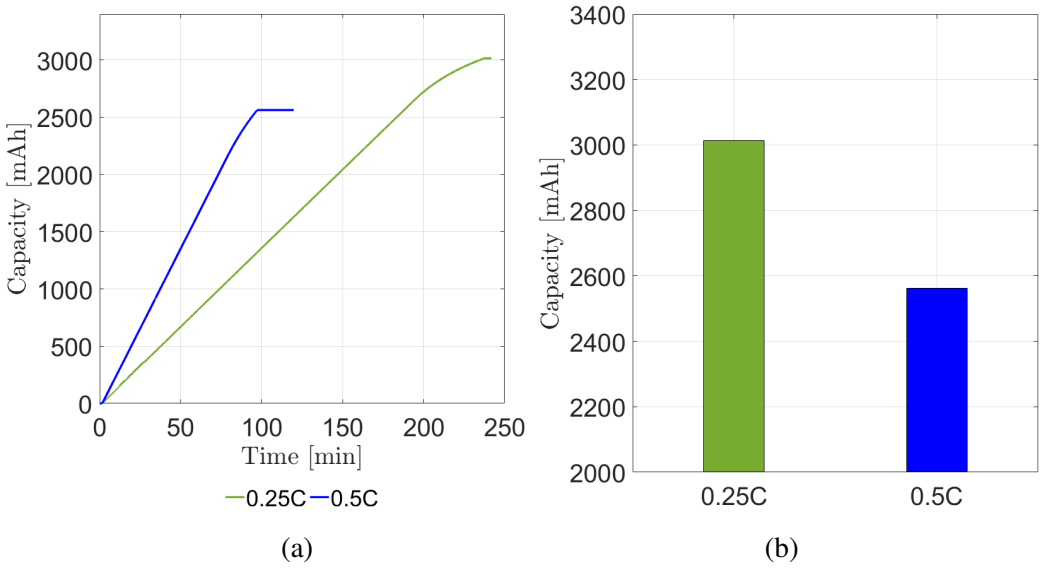

Source: the author

Figure 77 – Comparison of stored capacity in all charge tests with rates of 0.25C and 0.5C at 10 °C

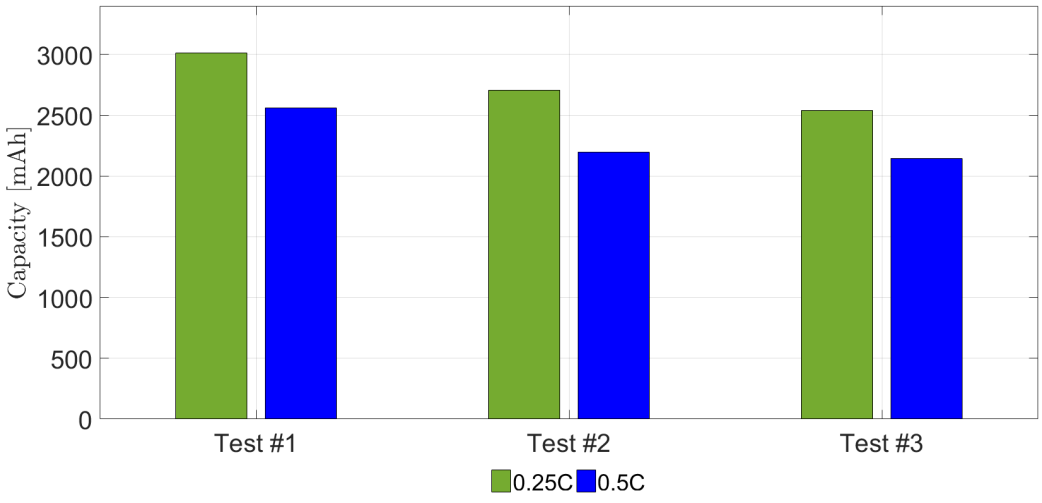

Source: the author

7.3 DISCHARGE TESTS COMPARISON UNDER ROOM TEMPERATURES OF 10 °C, 25 °C AND 40 °C

For each room temperature, three discharges tests with different rates were performed: 0.25C, 0.5C and 1.0C. To analyze the behavior of the battery pack during the discharge under different room temperatures, the results are presented keeping the same discharge rate. Note that these discharges are performed after the battery pack has been charged in the same temperature, e.g. the discharge test at 10 °C is carried out after a charge at 10 °C, which may compromise the available capacity in the battery pack.

Another point to be observed is the inclusion of the two tests at 10 °C. As already discussed (Section 7.2), there are two different tests performed at this room temperature, with 0.25C and 0.5C charge rates. The figures presented in this section include these both results where the 10 °C* indicates the results for the tests performed after a charge with 0.25C rate.

The first comparison is made for the discharge rate of 0.25C and Table 22 presents the main results of the test in each room temperature. In the tests at 25 °C and 40 °C, the battery pack is completed charged, so the discharges take about 3h30min. At 10 °C, the battery pack did not reach the nominal capacity (SoC of 67 % and 90 %), so the discharge duration was shorter, especially the test were the battery pack was previously charged at the rate of 0.5C, it takes only 2h30min. As the current drained from the battery pack is low, the temperature of the battery cell does not present a significant increase. The discharge at 40 °C resulted in the higher capacity.

Table 22 – Comparison of main parameter of discharge tests with rate of 0.25C and at 10 °C, 25 °C and 40 °C

Information	**25 °C**	**40 °C**	**10 °C**	**10 °C***
Current	846 mA	854 mA	850 mA	829 mA
Duration	3h36min	3h41min	2h32min	3h12min
Initial cell temperature	25.7 °C	42.0 °C	8.5 °C	8.4 °C
Maximum cell temperature	27.1 °C	43.5 °C	10.4 °C	9.8 °C
Cell temperature variation	1.4 °C	1.5 °C	1.9 °C	1.4 °C
Initial pack voltage	20.663 V	20.631 V	19.698 V	20.466 V
Minimum pack voltage	13.360 V	13.737 V	12.975 V	13.604 V
Pack voltage variation	7.303 V	6.894 V	6.723 V	6.862 V
Initial RSOC	100%	100%	67%	90%
Final RSOC	0%	0%	0%	0%
Calculated capacity	3052 mAh	3151 mAh	2165 mAh	2652 mAh

Source: the author

Figure 78 presents the battery pack behavior during the discharge process. After applying the discharge current, the voltage drop is greater in cases where the room temperature is 10 °C, while it is very similar during the tests at 25 °C and 40 °C. But, as the discharge is interrupted, the open circuit voltage of the battery pack is higher at 10 °C.

The battery cell temperature, for each discharge test, is illustrated in Figure 79. As already mentioned, the discharge current is low, around 850 mA, so the battery cell does not heat up during the test. The maximum increase is about 2 °C in the end of the discharge.

Figure 78 – Comparison of pack voltage in discharge tests with rate of 0.25C and at 10 °C, 25 °C and 40 °C

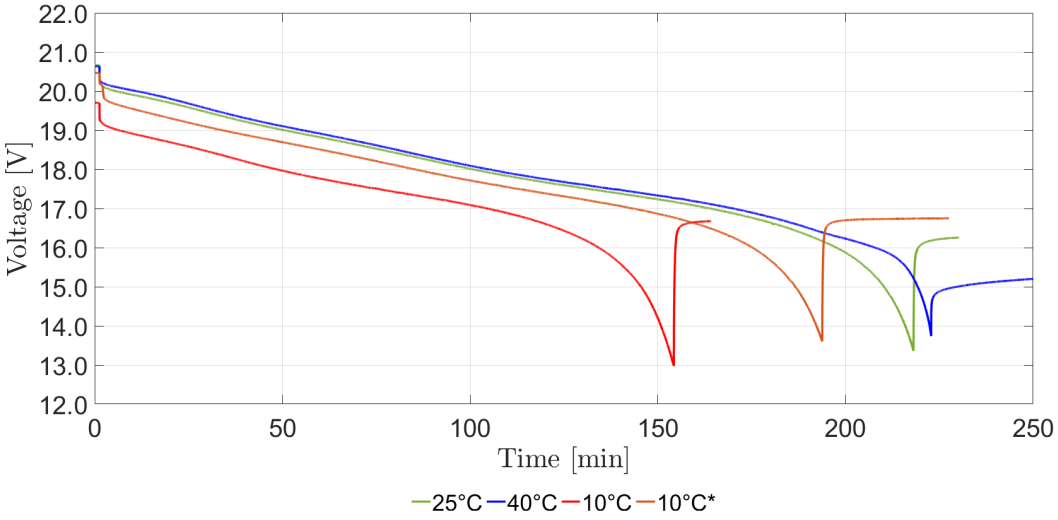

Source: the author

Figure 79 – Comparison of cell temperature in discharge tests with rate of 0.25C and at 10 °C, 25 °C and 40 °C

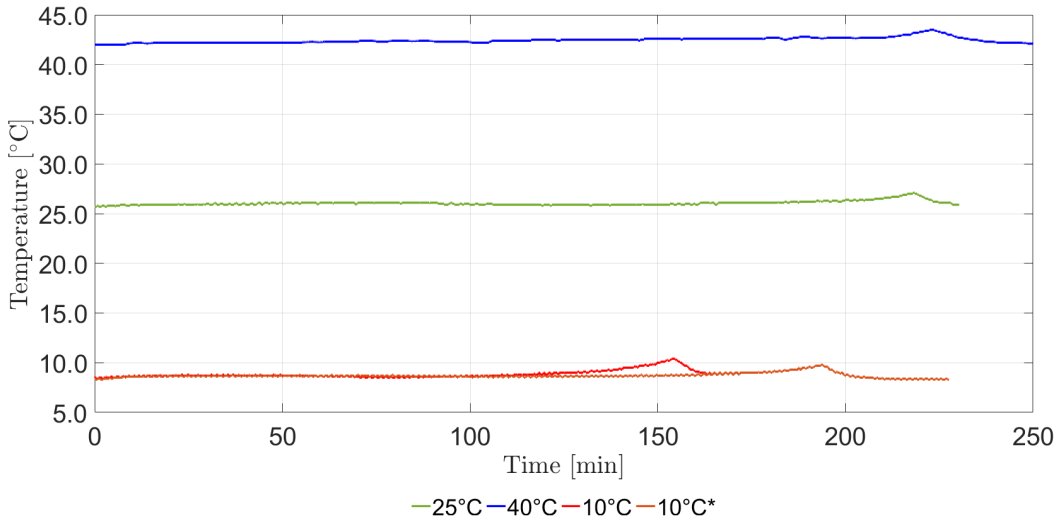

Source: the author

The calculated capacity of each discharge is presented in Figure 80. In Figure 80(a), the curves illustrate the capacity related to battery pack voltage and the Figure 80(b) indicates the absolute capacity drained of the battery pack during the discharge. Every discharge test was interrupted for a cell undervoltage protection.

Figure 80 – Comparison of drained capacity in discharge tests with rate of 0.25C and at 10 °C, 25 °C and 40 °C

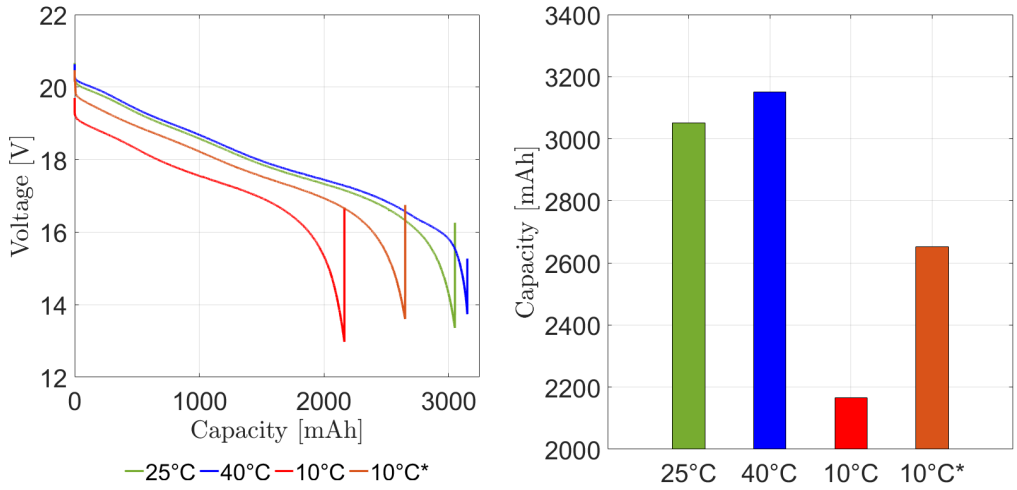

(a) (b)

Source: the author

In the same way, tests with a discharge rate of 0.5C were carried out at 10 °C, 25 °C and 40 °C. The main results of these tests are presented in Table 23. Again, the both tests in 10 °C are available and the 10 °C* indicates the discharge tests after the battery pack has been charged with charge rate of 0.25C (in all other tests, the charge was performed with a 0.5C rate). The discharges at 25 °C and 40 °C took almost 2h while those at 10 °C took less than 1h30min. The battery cell temperatures also did not present a high variation, the maximum was 3.4 °C during the discharge at 40 °C and at this room temperature was also drained the greatest capacity.

Table 23 – Comparison of main parameter of discharge tests with rate of 0.5C and at 10 °C, 25 °C and 40 °C

Information	**25 °C**	**40 °C**	**10 °C**	**10 °C***
Current	1657 mA	1650 mA	1672 mA	1642 mA
Duration	1h50min	1h55min	1h16min	1h26min
Initial cell temperature	25.8 °C	42.2 °C	8.4 °C	8.4 °C
Maximum cell temperature	28.3 °C	45.6 °C	11.4 °C	11.3 °C
Cell temperature variation	2.5 °C	3.4 °C	3.0 °C	2.9 °C
Initial pack voltage	20.681 V	20.687 V	19.795 V	20.213 V
Minimum pack voltage	13.472 V	13.521 V	12.799 V	13.528 V
Pack voltage variation	7.209 V	7.166 V	6.996 V	6.685 V
Initial RSOC	100%	100%	78%	81%
Final RSOC	0%	0%	0%	0%
Calculated capacity	3044 mAh	3161 mAh	2142 mAh	2366 mAh

Source: the author

The battery pack voltages, during the discharge, can be observed in Figure 81. As the load is connected and the discharge current is drained from the battery pack, the voltage drops and continues decreasing until the end of the discharge, when one of the cells reaches the undervoltage threshold. The tests at low temperature (10 °C and 10 °C*) presents a larger voltage drop when compared with the tests at 25 °C and 40 °C. After the discharge is interrupted, the open circuit voltage is higher at low temperature.

Figure 81 – Comparison of pack voltage in discharge tests with rate of 0.5C and at 10 °C, 25 °C and 40 °C

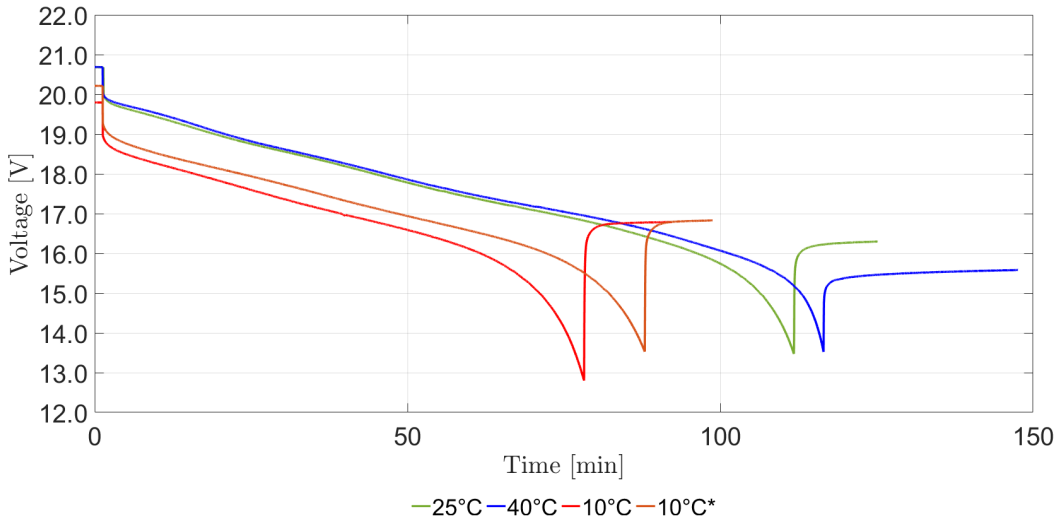

Source: the author

Figure 82 illustrates the temperature measured in the battery cell during the discharge test. The highest variation happens during the discharge at 40 °C and is still a low variation, 3.5 °C, as the room temperature is controlled.

Figure 82 – Comparison of cell temperature in discharge tests with rate of 0.5C and at 10 °C, 25 °C and 40 °C

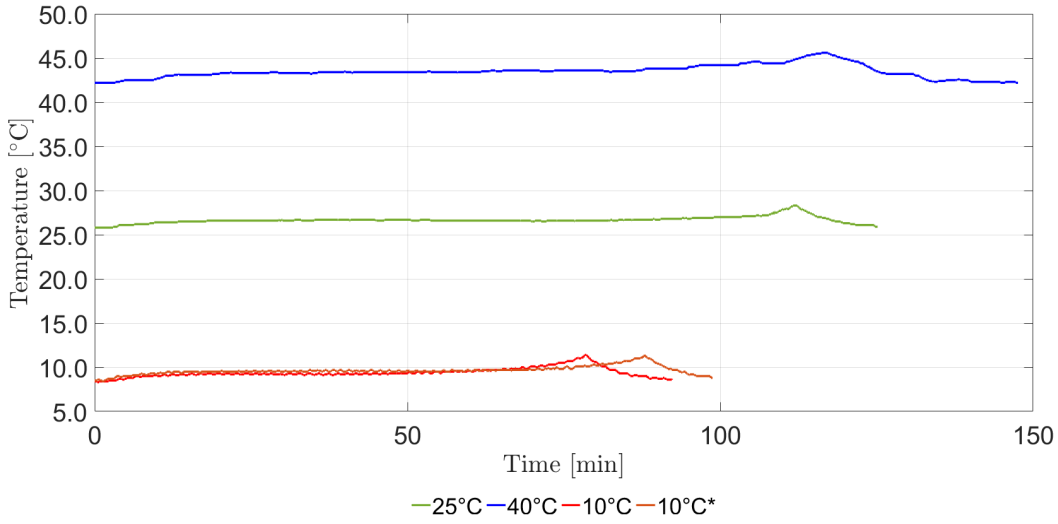

Source: the author

The calculated capacity drained in each test is presented in Figure 83. As already mentioned, the higher capacity is achieved at 40 °C. The discharges at 10 °C present a low capacity, as result of a poor stored capacity during the charge at this same temperature. The test indicated as 10 °C* was charged with a low current (0.25C) and presents the capacity with a better value.

Figure 83 – Comparison of drained capacity in discharge tests with rate of 0.5C and at 10 °C, 25 °C and 40 °C

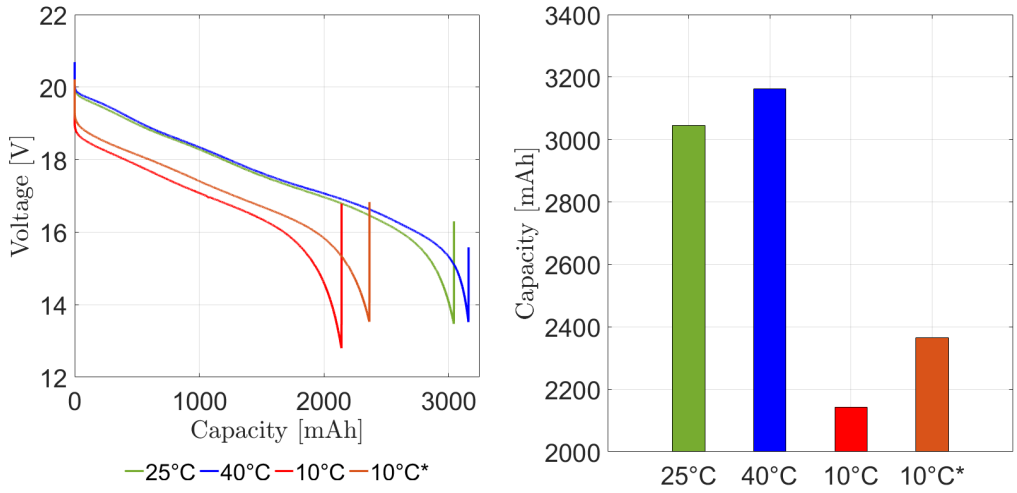

(a) (b)

Source: the author

Lastly, the same test procedure was repeated for a discharge rate of 1.0C. The battery pack performance and behavior is very similar to the previous results, as it can be observed in Table 24. The discharges performed at 25 °C and 40 °C took around 1h, while the discharges at 10 °C took less. Note that the test referred as 10 °C* (the case where the charge was carried out with a lower current) could deliver current for more time because it had more capacity stored. Unlike the other two tests, the discharge at 40 °C did no present the higher capacity, it is a similar value to the test at 25 °C, but previously, the battery pack was not fully charged due to the cell overvoltage protection interrupted the charge test (initial SoC is 93%).

Table 24 – Comparison of main parameter of discharge tests with rate of 1.0C and at 10 °C, 25 °C and 40 °C

Information	**25 °C**	**40 °C**	**10 °C**	**10°C***
Current	3320 mA	3333 mA	3360 mA	3330 mA
Duration	55min	55min	34min	43min
Initial cell temperature	25.7 °C	42.0 °C	8.5 °C	8.4 °C
Maximum cell temperature	31.5 °C	50.9 °C	15.9 °C	15.0 °C
Cell temperature variation	5.8 °C	8.9 °C	7.4 °C	6.6 °C
Initial pack voltage	20.660 V	20.592 V	19.657 V	20.468 V
Minimum pack voltage	12.987 V	13.377 V	13.085 V	13.140 V
Pack voltage variation	7.673 V	7.215 V	6.572 V	7.328 V
Initial RSOC	100%	93%	65%	76%
Final RSOC	0%	0%	0%	0%
Calculated capacity	3075 mAh	3064 mAh	1909 mAh	2388 mAh

Source: the author

The battery pack voltage behavior (Figure 84) is the same as in the others: as the discharge current is applied, the voltage drop is higher in the tests at 10 °C and as soon as the discharge is blocked, the open circuit voltage is also higher in this room temperature condition. The battery pack voltage has the same profile during the tests at 25 °C and 40 °C.

Figure 84 – Comparison of pack voltage in discharge tests with rate of 1.0C and at 10 °C, 25 °C and 40 °C

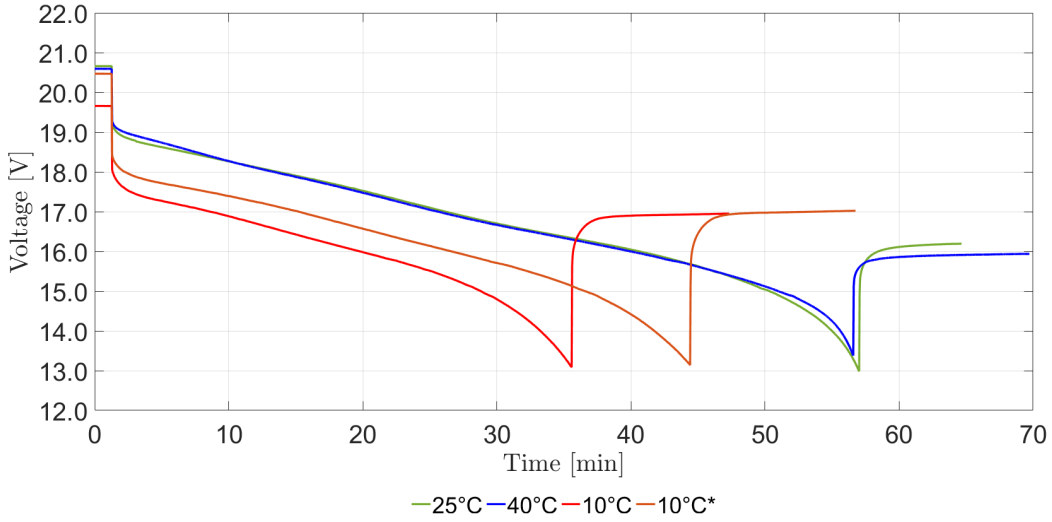

Source: the author

As the discharge current value is high in this test, the cell temperature presents also a heating. The battery cell temperature for each test is shown in Figure 85 and the test at 40 °C presented the highest temperature variation, around 9 °C, the battery cell reaches 50.9 °C in the end of the discharge.

Figure 85 – Comparison of cell temperature in discharge tests with rate of 1.0C and at 10 °C, 25 °C and 40 °C

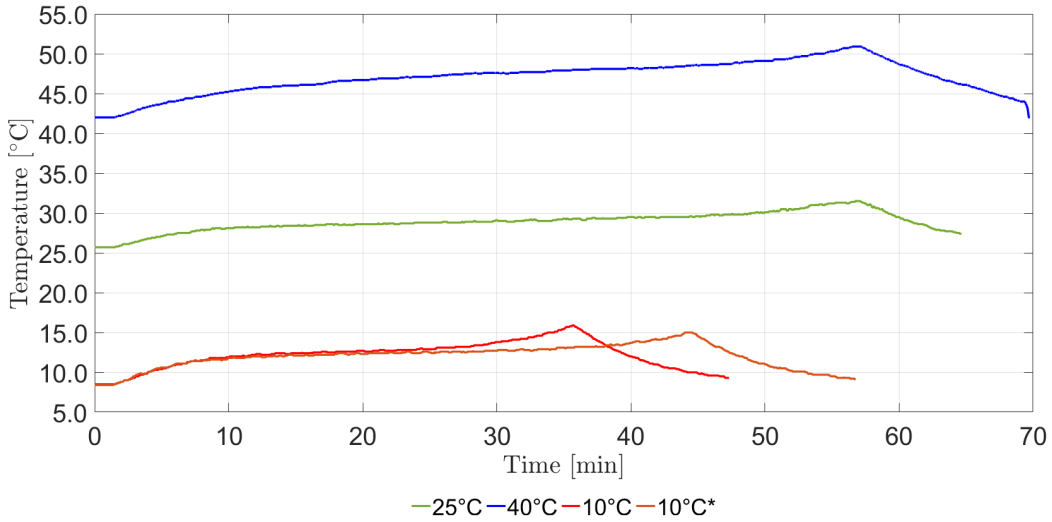

Source: the author

Figure 86 presented the capacity delivered in each test.

Figure 86 – Comparison of drained capacity in discharge tests with rate of 1.0C and at 10 °C, 25 °C and 40 °C

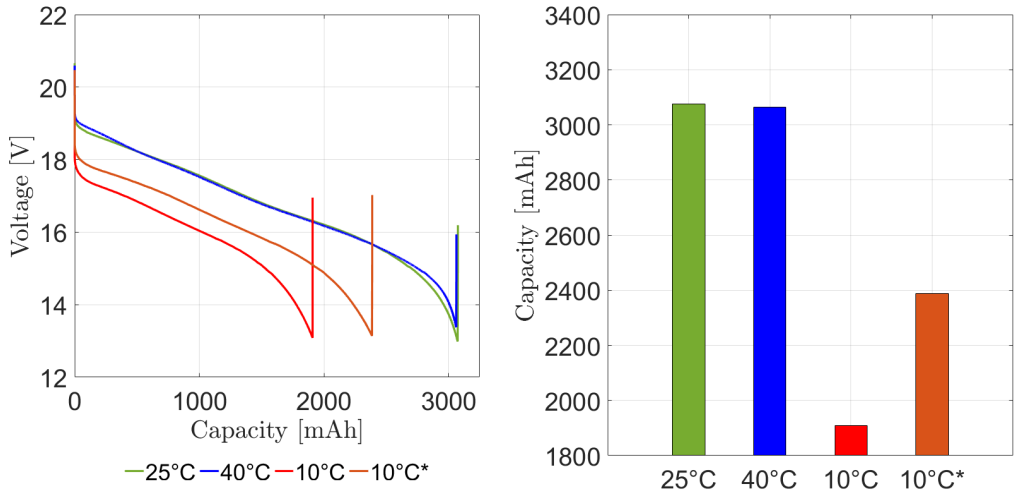

(a) (b)

Source: the author

As already mentioned, the final capacity of the tests at 25 °C and 40 °C are very similar, but is necessary to note that the battery pack discharged at 40 °C was not fully charged. The capacity for the test at 10 °C presented a really low value (only 57% of the nominal capacity), while the test at 10 °C* reaches a better value (71% of nominal capacity), a little higher than the discharge performed with a 0.5C rate.

8 CONCLUSION

This work proposed the development of a functional BMS for lithium-ion batteries. The BMS was designed using dedicated integrated circuits, bq7692000PWR and bq78350R1A, and it was used for monitoring, controlling and protecting a battery pack composed of five battery cells in series. The BMS provides the main features required by the most advanced applications: battery cell and pack voltage, current and temperature measurements, a wide variety of configurable protections, charging control, cell balancing algorithm and a capacity estimation method that provides the SoC and SoH.

Furthermore, a complete experimental setup was developed to perform tests with the battery pack. The setup is composed of the BMS evaluation board, the battery pack, the DC power supply and the electronic load. Using an interface board, EV2400, it was possible to communicate with the BMS through the *bqStudio*® software. With this software, the BMS features were configured and the battery pack parameters were monitored. This setup allowed carrying out tests of charge and discharge of the battery pack.

The BMS features were validated during this work. The measurement subsystem presented good results with low accuracy error for all the variables measured. There is a wide range of configurable protections and all the test performed in this work presented a good performance. The protection activation follows the desired threshold and delay, as well as, the recovery conditions are respected. The cell balancing feature was tested and did not present efficient results during a charge test. In this evaluation board, the internal drivers were used to perform the dissipative balancing with a limited current. The feature algorithm enables the balancing as it is configured, but there is no effect in battery cell voltage.

The variables estimated by the BMS were compared with the calculated values. The algorithm presented good results for estimating remaining capacity during charge and discharge. There is an indication error around 6% of the nominal capacity. This error is not desired but does not restrain the use of the BMS in this work. The SoC estimation is related to remaining capacity estimation and for this reason, the same behavior is presented. The remaining time estimation for the battery pack to be completely discharged is also available and the error shown during the tests was less than 10 minutes, but the estimation for the charging process presented poor results, and the information can not be used in an application. The SoH estimation is also related to the remaining capacity estimation, but it can not be properly evaluated in this work, since the tests were not performed for many cycles with the same battery pack.

After verifying the BMS functions, the battery pack behavior was evaluated under different charge and discharge conditions. Charges and discharges were carried out with three current rates: 0.25C, 0.5C and 1.0C. For the charging test, it was observed that the higher current rate (1.0C) provides the greater stored capacity and the battery pack is fully charged in the shortest time. However, at this current rate, the battery cell temperature increased more during the test. Charging with a 0.25C prevents the battery cell temperature from rising but it takes a very long time to charge the battery pack, which is normally undesired. Similarly, the discharge tests presented a good amount of capacity but also a battery cell temperature rise.

Tests with controlled room temperature were carried out to observe the battery behavior. Three different room temperatures were used, 10 °C, 25 °C and 40 °C. Charging the battery pack under low temperature presented a large decrease in the capacity, even using a low charge current. Discharging the battery pack at the higher temperature provides the greater capacity values, but it is not a recommended condition because the high temperature accelerates the aging process and lead to the battery degradation.

The results presented in this work testify the temperature-dependent performance in lithium-ion batteries. To keep the optimal operating temperature range, to ensure performance and safety, is necessary the use of a thermal management system. This system is able to cool or heat the batteries as needed.

Another important observation made during the test is about the cell voltage unbalance. Most of the discharge tests were interrupted by the same cell, which presents a higher internal resistance, based on its discharge behavior. This cell reaches the minimum voltage before the others. The use of an active balancing method during the discharge may improve the battery pack capacity.

8.1 PROPOSED FUTURE WORKS

To continue this work, the following activities are proposed:

- The automation of the test setup to perform cycle life test;
- The evaluation of the discharge performance, charge capacity retention and recovery, battery cell and pack internal resistance and endurance following the IEC 62620 standard tests recommendation.
- The development of external cell balancing circuit in bq7692000PW to improve the feature during charge;
- The implementation of an independent circuit to balance the battery cell voltages during the discharge;
- The comparison between the estimation algorithm available in bq78350R1A with a different algorithm.

BIBLIOGRAPHY

BERGVELD, H. J. *Battery Management Systems-Design by Modellin*. Enschede, Nederlands: [s.n.], 2001. Proefschrift Universiteit Twente.

BHATT, D. K.; DARIEBY, M. E. An assessment of batteries form battery electric vehicle perspectives. *IEEE International Conference on Smart Energy Grid Engineering*, p. 255–259, August 2018.

CHANG, W. The state of charge estimating methods for battery: a review. *Hindawi Publishing Corporation*, July 2013.

CHEMALI, E. et al. Electrochemical and electrostatic energy storage and management systems for electric drive vehicles: State-of-the-art review and future trends. *IEEE Journal of Emerging and Selected Topics in Power Electronics*, v. 4, n. 3, p. 1117–1134, 2016.

DUSTMANN, C. Advantages in zebra batteries. *Journal of Power Sources*, p. 85–89, 2004.

FETCENKO, M.; KOCH, J.; ZELINSKY, M. *Nickel–metal hydride and nickel–zinc batteries for hybrid electric vehicles and battery electric vehicles*. Advances in Battery Technologies for Electric Vehicles: Woodhead Publishing, 2015. 103-126 p.

GAO, Y. et al. Classification and review of the charging strategies for commercial lithium-ion batteries. *IEEE Access*, v. 7, p. 43511–43524, March 2019.

GUI, R. et al. Mechanism of the entire overdischarge process and overdischarge-induced internal short circuit in lithium-ion batteries. *Nature Scientific Reports*, July 2016.

HAN, X. et al. A review on the key issues of the lithium ion battery degradation among the whole life cycle. *eTransportation*, v. 1, July 2019.

HANNAN, M. A. et al. State-of-the-art and energy management system of lithium-ion batteries in electric vehicle applications: Issues and recommendations. *IEEE Access*, p. 19362–19378, 2018.

HUANG, C. et al. Robustness evaluation of extended and unscented kalman filter for battery state of charge estimation. *IEEE Access*, v. 6, n. 27617-27628, 2018.

HUANG, W. et al. Questions and answers relating to lithiu-ion battery safety issues. *Cell Reports Physical Science*, v. 2, n. 100285, January 2021.

INSTRUCTABLES CIRCUITS. *Tiny Load - Constant Current Load*. 2021. Retrieved from <https://www.instructables.com/Tiny-Load-Constant-Current-Load/> (2021, August 19).

KOSEOGLOU, M. et al. High effective cell equalization in a lithium-ion battery management system. *IEEE Transactions on Power Electronics*, v. 35, n. 2, p. 2088–2099, February 2020.

LELIE, M. et al. Battery management system hardware concepts: An overview. *Applied Sciences*, v. 8, n. 4, March 2018.

LI, J.; ZHU, Z. *Battery Thermal Management Systems of Electric Vehicles*. Göteborg, Sweden: [s.n.], 2014. Chalmers University of Technology.

LORENCETTI, E. J.; HEERDT, J. A. Modularized bidirectional step-up dc-dc converter with predictive battery equalization method. In: *2017 Brazilian Power Electronics Conference (COBEP)*. Juiz de Fora, Brazil: [s.n.], 2017. p. 1–6.

MENGATTO, A. *Projeto e desenvolvimento de um carregador de baterias integrado ao motor de tração de veículos elétricos*. Santa Catarina, Brasil: [s.n.], 2019. Universidade do Estado de Santa Catarina.

MOORE, S. W.; SCHNEIDER, P. J. A review of cell equalization methods for lithium ion and lithium polymer battery systems. *Society of Automotive Engineers, Inc*, 2001.

MORAES, C. G. d. S. et al. Power conversion technologies for a hybrid energy storage system in diesel-electric locomotives. *IEEE Transactions on industrial electronics*, v. 68, n. 10, p. 9081–9091, October 2021.

MORRIS, M.; TOSUNOGLU, S. *Comparison of rechargeable battery technologies*. Georgia, USA: [s.n.], 2012.

NAGUIB, M.; KOLLMEYER, P.; EMADI, A. Lithium-ion battery pack robust state of charge estimation, cell inconsistency, and balancing: Review. *IEEE Access*, v. 9, p. 50570–50582, March 2021.

NITTA, N. et al. Li-ion battery materials: present and future. *Materials Today*, v. 18, n. 5, p. 252–264, June 2015.

OMAR, N. et al. Eanalysis of nickel-based battery technologies for hybrid and electric vehicles. *Reference Module in Chemistry, Molecular Sciences and Chemical Engineering*, 2014.

PANASONIC. *Lithium Ion NCR18650B*. 2012.

POP, V. et al. State-of-the-art of battery state-of-charge determination. In: *Battery Management Systems: Accurate State-of-Charge Indication for Battery-Powered Application*. Dordrecht: Springer Netherlands, 2008, (Philips Research Book Series). cap. 2, p. 11–45.

RAHIMI-EICHI, H. et al. Battery management system - an overview of its application in the smart grid and electric vehicles. *IEEE Industrial Electronics Magazine*, p. 4–16, June 2013.

REMES, C. L. *Modelagem, simulação e estimação de carga de baterias de lítio com implementação de um carregador de baterias*. Santa Catarina, Brasil: [s.n.], 2016. Universidade do Estado de Santa Catarina.

REMES, C. L. et al. Lqg controller in cascade loop tuned by pso applied to a dc-dc converter. *Asian Journal of Control*, p. 1–10, 2020.

ROOT, M. *The TAB Battery Book: An In-Depth Guide to Construction, Design and Use.* [S.l.]: McGraw-Hill Companies, 2010. 157-182 p.

ROSOLEM, M. F. N. C.; BECK, R. F. Novas gerações de baterias de lítio para veículos elétricos e híbridos - progressos e desafios. *SAE Brazil*, 2018.

RUTHES, E. N. *Equalização ativa de banco de baterias com processamento da energia diferencial usando conversor CC-CC modular isolado*. Santa Catarina, Brasil: [s.n.], 2020. Universidade do Estado de Santa Catarina.

SENDER, R. et al. A brief overview of battery management systems for lithium ion batteries: modeling, estimation and control. *10th Seminar on Power Electronics and Control*, October 2018.

TEXAS INSTRUMENTS. *Cell Balancing in bq208x Advanced Gas-Gauge Designs*. 2004.

TEXAS INSTRUMENTS. *bq76920 Evaluation Module User's Guide*. 2018.

TEXAS INSTRUMENTS. *bq769x0 3-series to 15-series cell battery monitor family for li-ion and phosphate applications*. 2019.

TEXAS INSTRUMENTS. *BQ78350-R1A CEDV Li-Ion Gas Gauge and Battery Management Controller Companion to the BQ769x0 Battery Monitoring AFE*. 2019.

TEXAS INSTRUMENTS. *BQ78350-R1 Technical Reference*. 2020.

TIAN, H. et al. A review of the state of health for lithium-ion batteries: Research status and suggestions. *Journal of Cleaner Production*, v. 261, n. 120813, July 2020.

WEN, J.; YU, Y.; CHEN, C. A review on lithium-ion batteries safety issues: existing problems and possible solutions. *Materials Express*, n. 3, p. 197–212, 2012.

YANG, X. et al. Fast charging of lithium-ion batteries at all temperatures. *PNAS*, v. 115, n. 28, p. 7266–7271, July 2018.

YAO, L. et al. A review of lithium-ion battery state of health estimation and prediction methods. *World Electric Vehicle Journal*, v. 12, n. 113, August 2021.

ZHANG, R. et al. State of the art of lithium-ion battery soc estimation for electrical vehicles. *Energies*, v. 11, n. 7, July 2018.

ZHOU, Y.; LI, X. Overview of lithium-ion battery SOC estimation. *International Conference on Information and Automation*, p. 2454–2455, August 2015.

APPENDIX A – COMPARISON BETWEEN SOME COMMERCIAL BMS

A comparison was made between commercial BMS in order to evaluate the available functions and then select a device to use in this work. For each one, the main characteristics were verified and are presented in Table 25.

Cell number: the number of battery cells or the battery pack voltage is the first attribute to be checked and it needs to meet the application voltage;

Communication: some BMS do not allow the user to configure feature parameters, when it is allowed, it is necessary to identify the communication protocol;

Protections: the BMS needs to provide robust protection, but in some cases, an other dedicated circuit is needed to control the protections;

Scalability: some applications require a high voltage level and more than one BMS is used, the scalability should be observed during the BMS selection;

SoC and SoH: both SoC and SoH estimations can be provided by the BMS algorithm, these are not basic functions and most commercial BMS do not offer them.

Table 25 – Comparison between commercial BMS

CI - Manufacture	Cell number	Communication	Protections	Scalability	SoC	SoH
AD7280A - Analog Devices	4 - 6	SPI	√	√	X	X
ATA6870 - Atmel	6	X	√	√	X	X
ISL9208 - Renesas	5 - 7	I^2C	√	√	√	X
MC33771 - NXP Semiconductors	7 - 14	SPI	√	√	√	X
LTC6801 - Analog Devices	12	X	√	√	√	X
DS2726 - Maxim	5 - 10	X	√	X	X	X
bq34z100-G1 - Texas Instruments	3V-65V	I^2C	X	X	√	√
bq769x0 and bq78350R1A - Texas Instruments	9-15	I^2C	√	√	√	√

Source: the author

APPENDIX B – PROTOTYPE SCHEMATIC

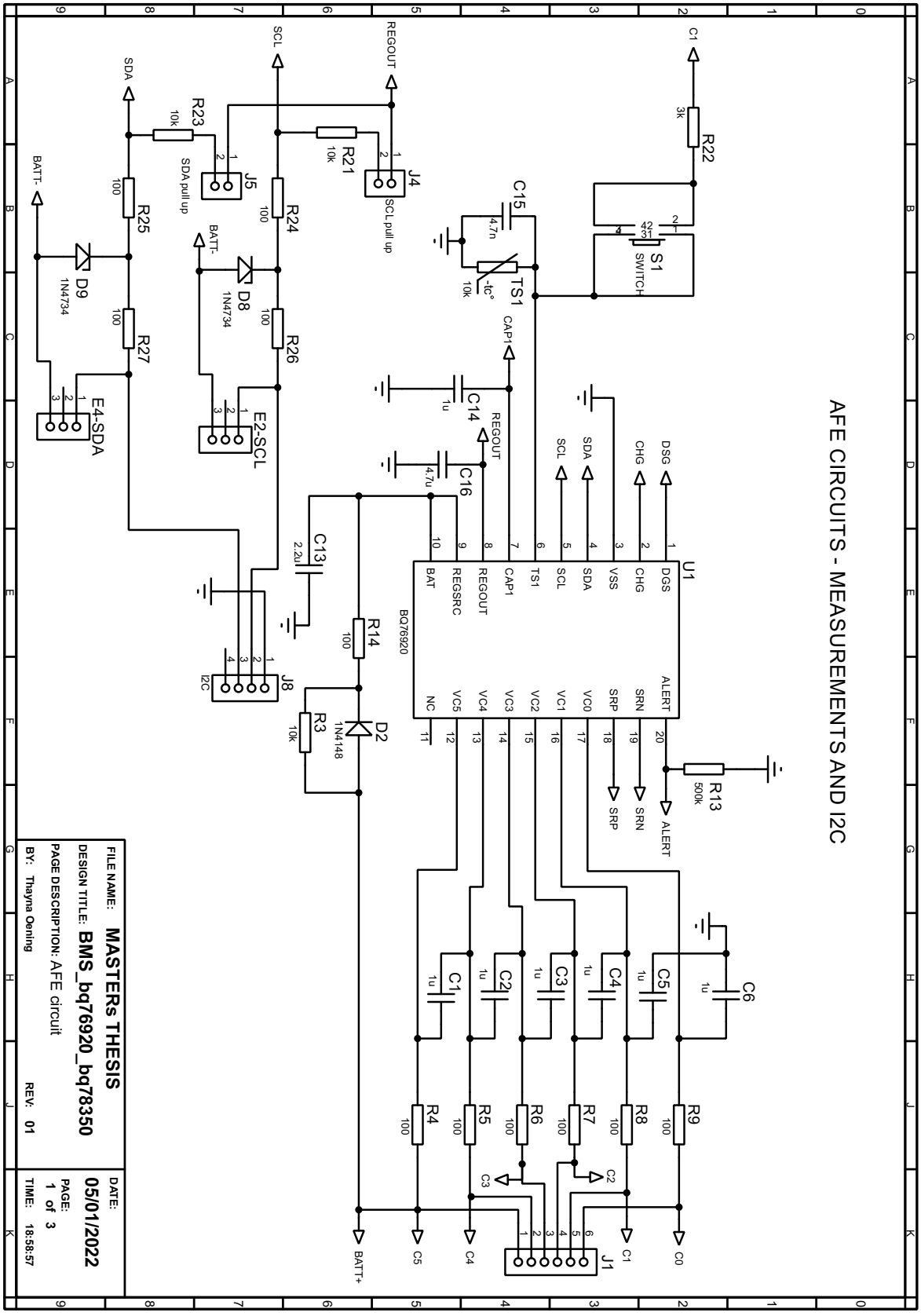

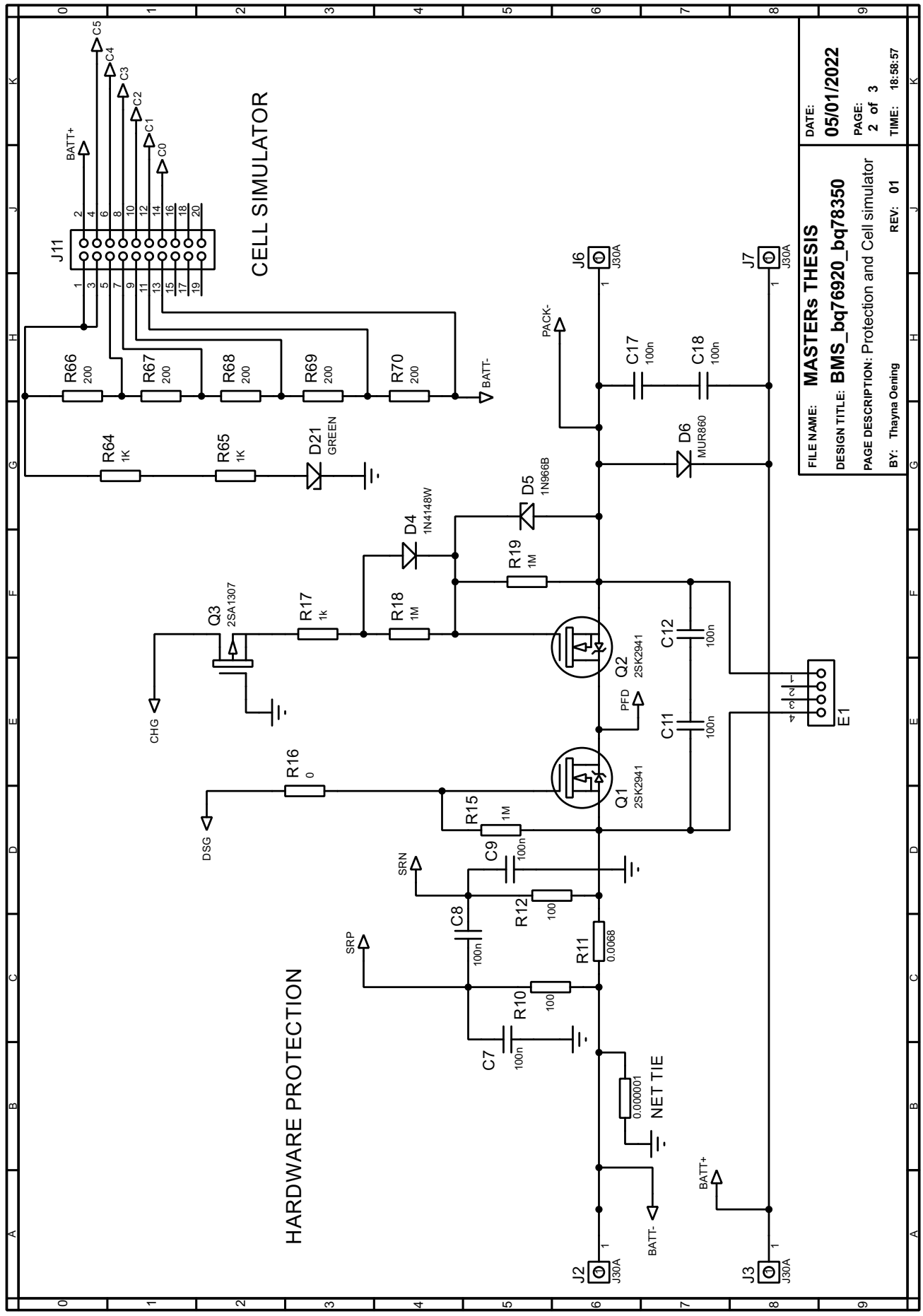
CELL SIMULATOR
HARDWARE PROTECTION
NET TIE
FILE NAME: MASTERs THESIS
DESIGN TITLE: BMS_bq76920_bq78350
PAGE DESCRIPTION: Protection and Cell simulator
BY: Thayna Oening
REV: 01
DATE: 05/01/2022
PAGE: 2 of 3
TIME: 18:58:57
J11
BATT+
C5
C4
C3
C2
C1
C0
R66 200
R67 200
R68 200
R69 200
R70 200
BATT-
R64 1K
R65 1K
D21 GREEN
J6 J30A
J7 J30A
PACK-
C17 100n
C18 100n
D6 MUR860
D5 1N966B
D4 1N4148W
R19 1M
R17 1k
R18 1M
Q3 2SA1307
Q2 2SK2941
Q1 2SK2941
C12 100n
C11 100n
CHG
PFD
R16 0
DSG
R15 1M
C9 100n
SRN
C8 100n
R12 100
SRP
R11 0.0068
R10 100
C7 100n
0.000001
E1
J2 J30A
J3 J30A
BATT-
BATT+

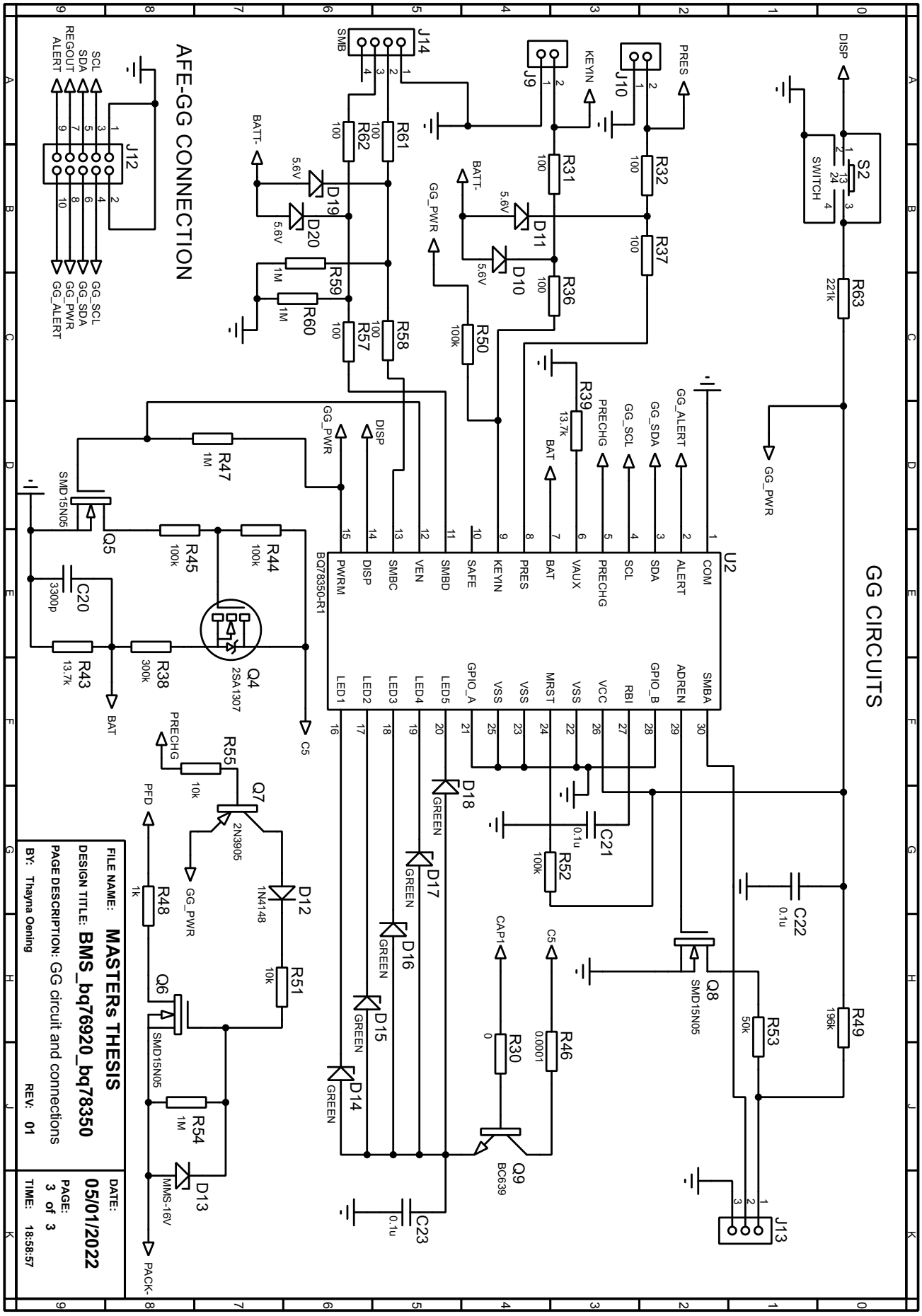
GG CIRCUITS
AFE-GG CONNECTION
U2
BQ78350-R1
S2
SWITCH
J9
J10
J12
J13
J14
Q4
2SA1307
Q5
SMD15N05
Q6
SMD15N05
Q7
2N3905
Q8
SMD15N05
Q9
BC639
D10
D11
D12
1N4148
D13
MMS-16V
D14
GREEN
D15
GREEN
D16
GREEN
D17
GREEN
D18
GREEN
D19
D20
R30
R31
R32
R36
R37
R38
R39
R43
R44
R45
R46
R47
R48
R49
R50
R51
R52
R53
R54
R55
R58
R59
R60
R61
R62
R63
R57
C20
C21
C22
C23
GG_PWR
PRECHG
BAT
DISP
PACK-
FILE NAME: MASTERs THESIS
DESIGN TITLE: BMS_bq76920_bq78350
PAGE DESCRIPTION: GG circuit and connections
BY: Thayna Oening
REV: 01
DATE: 05/01/2022
PAGE: 3 of 3
TIME: 18:58:57

APPENDIX C – COMPARISON BETWEEN THE DISCHARGE TESTS UNDER DIFFERENT CURRENT DISCHARGE RATES AFTER CHARGING WITH CURRENT RATE OF 0.25C

In this appendix is presented a comparison between discharge tests under different discharge current rates (0.25C, 0.5C and 1.0C). All the discharging test carried out for this comparison, use a battery pack previously charged with a charge rate of 0.25C.

Table 26 presents the results of each test. Discharge with a low current rate, as 0.25C, provided energy for a longer time, around 3 hours and 42 minutes in this test. In this condition, the battery cell temperature presented a low increase of 3.3 °C and the total capacity was 3117 mAh. On the other hand, discharging with a rate of 1.0C took less time, 56 minutes, and the battery cell temperatures has increased 17.8 °C. This test provided a total capacity of 3081 mAh. The test performed with a halfway discharge current (0.5C), shown a discharge time of 1 hour and 49 minutes, a cell temperature rise of 8.5 °C and a total drained capacity of 3025 mAh, the lowest value between the tests.

Table 26 – Comparison between discharges with 0.25C, 0.5C and 1.0C rates after charging with current rate of 0.25C

Information	**0.25C**	**0.5C**	**1.0C**
Current	842 mA	1657 mA	3308 mA
Duration	3h42min	1h49min	0h56min
Initial cell temperature	26.9 °C	25.6 °C	25.2 °C
Maximum cell temperature	30.2 °C	34.1 °C	43.0 °C
Cell temperature variation	3.3 °C	8.5 °C	17.8 °C
Initial pack voltage	20.745 V	20.628 V	20.663 V
Minimum pack voltage	13.470 V	13.487 V	13.161V
Pack voltage variation	7.275 V	7.141 V	7.502 V
Initial RSOC	98%	100%	100%
Final RSOC	0%	0%	0%
Calculated capacity	3117 mAh	3025 mAh	3081 mAh

Source: the author

Figure 87 illustrates the battery pack voltage during each discharge test. The battery pack voltage drops as soon as the current is requested from the battery. The greater the current, the voltage drop was greater.

Figure 87 – Comparison of pack voltage in discharge tests with current rates of 0.25C, 0.5C and 1.0C after charging with current rate of 0.25C

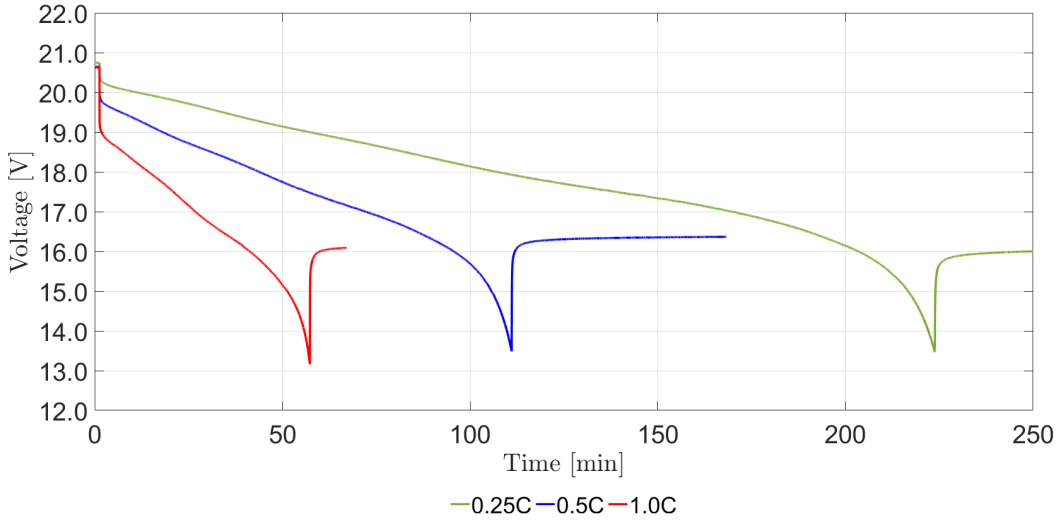

Source: the author

The calculated drained capacity for each test is presented in Figure 88. The amount of capacity drained according to the battery pack voltage is shown in Figure 88(a) and the final calculated capacity can be observed in Figure 88(b). The maximum capacity was achieved in the test of 0.25C.

Figure 88 – Comparison of drained capacity in discharge tests with current rates of 0.25C, 0.5C and 1.0C after charging with current rate of 0.25C

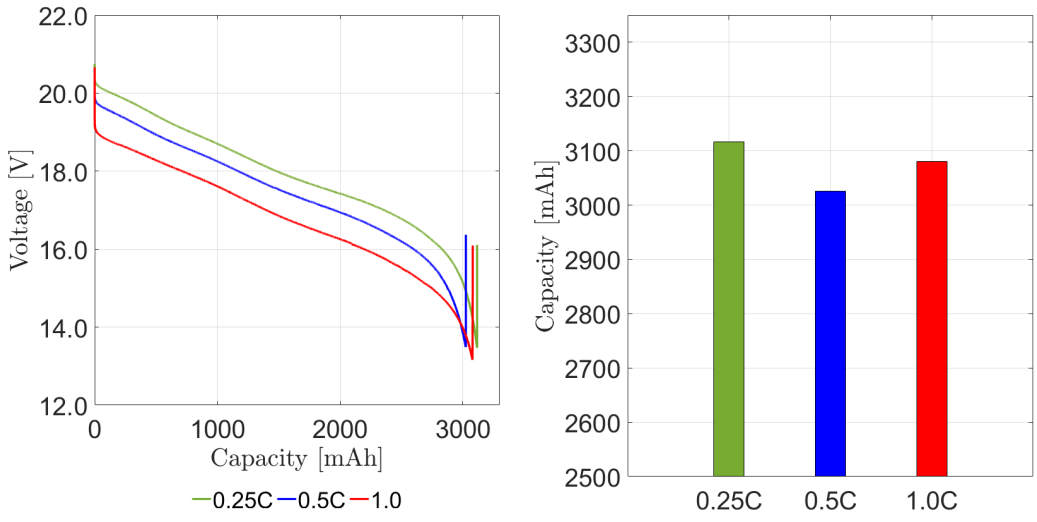

(a) (b)

Source: the author

A comparison between the battery cell temperature during each test can be seen in Figure 89. As already discussed, the discharge with 1.0C current rate presented the biggest temperature rise. In all the tests, the maximum temperature was achieved at the end of the discharge test, as soon as the discharge is stopped, the temperature decreased.

Figure 89 – Comparison of cell temperature in discharge tests with current rates of 0.25C, 0.5C and 1.0C after charging with current rate of 0.25C

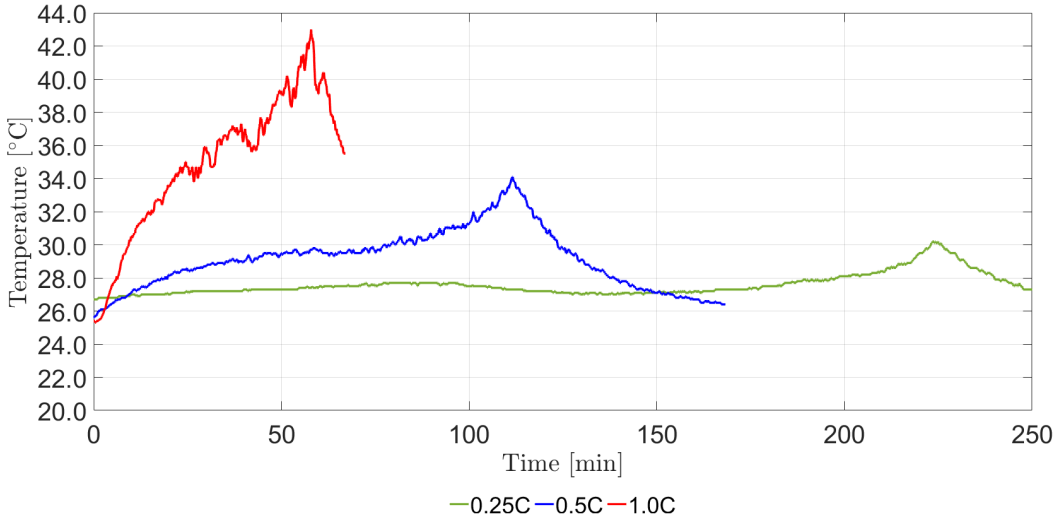

Source: the author

The next appendix presents the discharge tests performed after charging the battery pack with current rate of 1.0C.

APPENDIX D – COMPARISON BETWEEN THE DISCHARGE TESTS UNDER DIFFERENT DISCHARGE CURRENT RATES AFTER CHARGING WITH CURRENT RATE OF 1.0C

A comparison between discharge testes performed under 0.25C, 0.5C and 1.0C current rates is presented in this chapter. The battery pack was charged with a current rate of 1.0C before each discharge test. The results shown in these tests have the same behavior of the tests carried out after charges with other rates, available in Section 6.2.4 and Appendix C.

Table 27 summarizes the main results for each test. The test carried out with discharge rate of 0.25C took 3 hours and 38 minutes. During the test, the battery cell temperature increased 4.2 °C and the calculated drained capacity was 3069 mAh. For the discharge with rate of 0.5C, the complete discharge was achieved after 1 hour and 49 minutes. The cell temperature increased 9.9 °C and the capacity was 3039 mAh. Finally, the discharge test with a rate of 1.0C took 55 minutes. During the test, the maximum temperature was 46.3 °C, and increase of 20.2 °C. The calculated capacity was 3042 mAh.

Table 27 – Comparison between discharges with 0.25C, 0.5C and 1.0C rates after charging with current rate of 1.0C

Information	**0.25C**	**0.5C**	**1.0C**
Current	842 mA	1667 mA	3317 mA
Duration	3h38min	1h49min	0h55min
Initial cell temperature	26.9 °C	26.4°C	26.1 °C
Maximum cell temperature	31.1 °C	36.3 °C	46.3 °C
Cell Temperature variation	4.2 °C	9.9 °C	20.2 °C
Initial pack voltage	20.669 V	20.663 V	20.63 V
Minimum pack voltage	13.284 V	12.949 V	13.06 V
Pack voltage variation	7.385 V	7.714 V	7.570 V
Initial RSOC	100%	100%	100%
Final RSOC	0%	0%	0%
Calculated capacity	3069 mAh	3039 mAh	3042 mAh

Source: the author

Figure 90 illustrates the battery pack voltage during each discharge test. The test with the higher discharge rate, 1.0C rate, caused the greater voltage drop as soon as the discharge started.

The calculated drained capacity during each test is shown in Figure 91. The battery pack voltage-related capacity during the discharge is illustrated in Figure 91(a) and the final calculated capacity is compared in Figure 91(b). The greater capacity was achieved in the discharge rate of 0.25C, as already mentioned.

Figure 90 – Comparison of pack voltage in discharge tests with current rates of 0.25C, 0.5C and 1.0C after charging with current rate of 1.0C

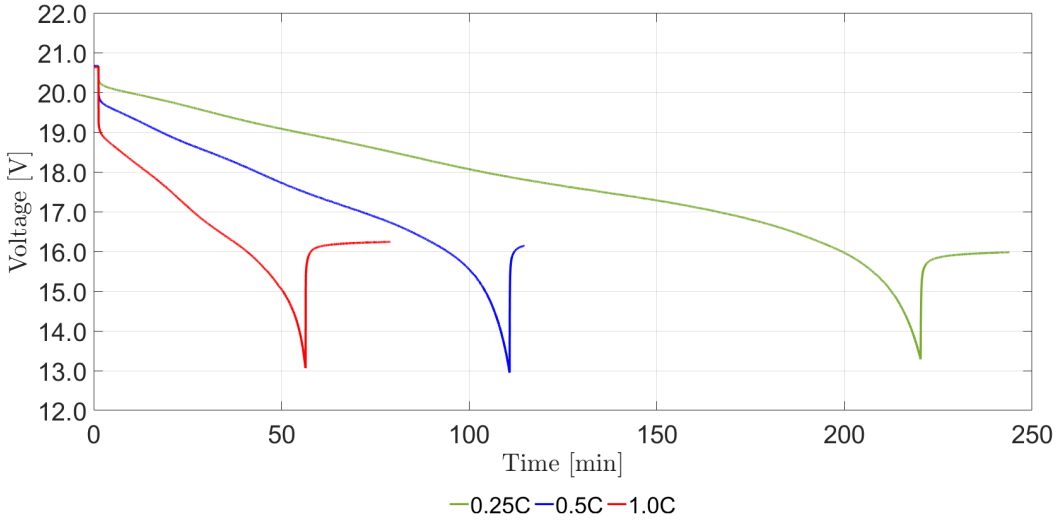

Source: the author

Figure 91 – Comparison of drained capacity in discharge tests with current rates of 0.25C, 0.5C and 1.0C after charging with current rate of 1.0C

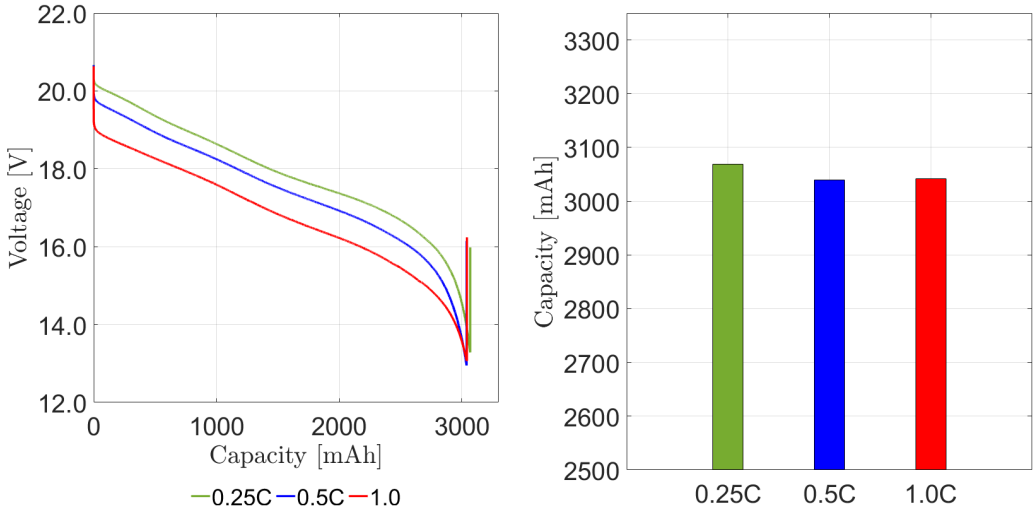

(a) (b)

Source: the author

Figure 92 presents the battery cell temperature during each test. All the tests achieved the maximum cell temperature at the end of the discharge. The maximum increase occurred during the test with rate of 1.0C.

Figure 92 – Comparison of cell temperature in discharge tests with current rates of 0.25C, 0.5C and 1.0C after charging with current rate of 1.0C

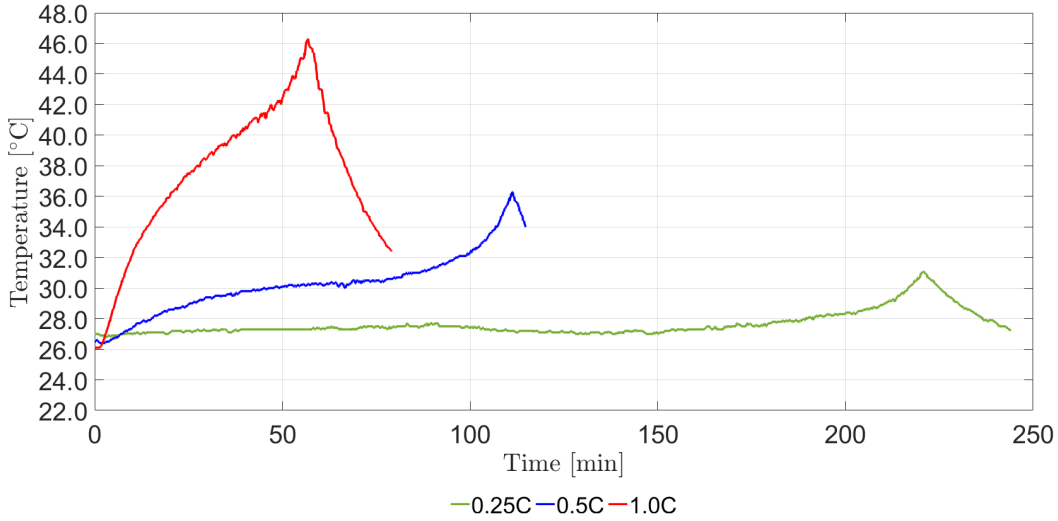

Source: the author

The next appendix presents all the results of tests performed under controlled room temperature.

APPENDIX E – COMPLETE RESULTS FOR THERMAL TESTS

The main results of each charge test at controlled room temperature are presented in this appendix, as a complement to the Chapter 7. For each controlled room temperature, three charges were perform at same current rate and three discharges were carried out with different rates (0.25C, 0.5C and 1.0C). All these tests are presented during this chapter.

The first room temperature was defined at 25 °C to provides a controlled condition with no battery degradation.

Table 28 presents the results for three charges at 25 °C and with a rate of 0.5C. The results are very similar considering the charging duration and the temperature variation. During the tests, the stored capacity was decreasing. The first test was performed with a new battery pack, which could explain the higher amount of stored capacity. All the test were completed by a termination charge conditions.

Table 28 – Charge test results with room temperature at 25°C and current rate of 0.5C

Information	Test #1	Test #2	Test #3
Current	1632 mA	1661 mA	1641 mA
Duration	2h38min	2h31min	2h31min
Initial cell temperature	25.5 °C	25.9°C	25.6 °C
Maximum cell temperature	27.2 °C	27.2 °C	27.0 °C
Cell temperature variation	1.7 °C	1.3 °C	1.4 °C
Initial pack voltage	15.233 V	15.335 V	16.268 V
Minimum pack voltage	20.860 V	20.903 V	20.931 V
Pack voltage variation	5.701 V	5.568 V	4.664 V
Initial RSOC	0%	0%	0%
Final RSOC	100%	100%	100%
Calculated capacity	3211 mAh	3144 mAh	3094 mAh

Source: the author

At the same room temperature, for each charge test was carried out a discharge changing the current rate. Table 29 summarizes the main results of each discharge test. In the first test, a current rate of around 0.25C was drained of the battery pack. The discharge took 3 hours and 36 minutes and delivers a capacity of 3052 mAh. During the discharge, a low temperature rise was observed. The second test requests a 0.5C current rate and the battery pack was completely discharged after 1 hour and 50 minutes. In this test, the final capacity was 3044 mAh and the cell temperature increased 2.4 °C. Finally, the test was performed with a 1.0C discharge rate. The duration discharge was 55 minutes and the battery pack delivers a capacity of 3075 mAh. During this test, the battery cell presents a temperature rise of almost 5.8 °C, the higher value of the tests due to the drained current.

Figure 93(a) illustrates the capacity during the discharge. The capacity value is related to the battery pack voltage during the test. A comparison between the final capacity of each test is present in Figure 93(b). The higher drained capacity was obtained during the discharge with a rate of 1.0C, but the values are very similar for all the tests.

Table 29 – Discharge tests comparison under different current rates and room temperature at 25°C

Information	0.25C	0.5C	1.0C
Current	846 mA	1657 mA	3320 mA
Duration	3h36min	1h50min	0h55min
Initial cell temperature	25.7 °C	25.9 °C	25.7 °C
Maximum cell temperature	27.1 °C	28.3 °C	31.5 °C
Cell temperature variation	1.4 °C	2.4 °C	5.8 °C
Initial pack voltage	20.687 V	20.697 V	20.661 V
Minimum pack voltage	13.360 V	13.472 V	12.987 V
Pack voltage variation	7.327 V	7.225 V	7.674 V
Initial RSOC	100%	100%	100%
Final RSOC	0%	0%	0%
Calculated capacity	3052 mAh	3044 mAh	3075 mAh

Source: the author

Figure 93 – Comparison of drained capacity in discharge tests with current rates of 0.25C, 0.5C and 1.0C and at 25 °C

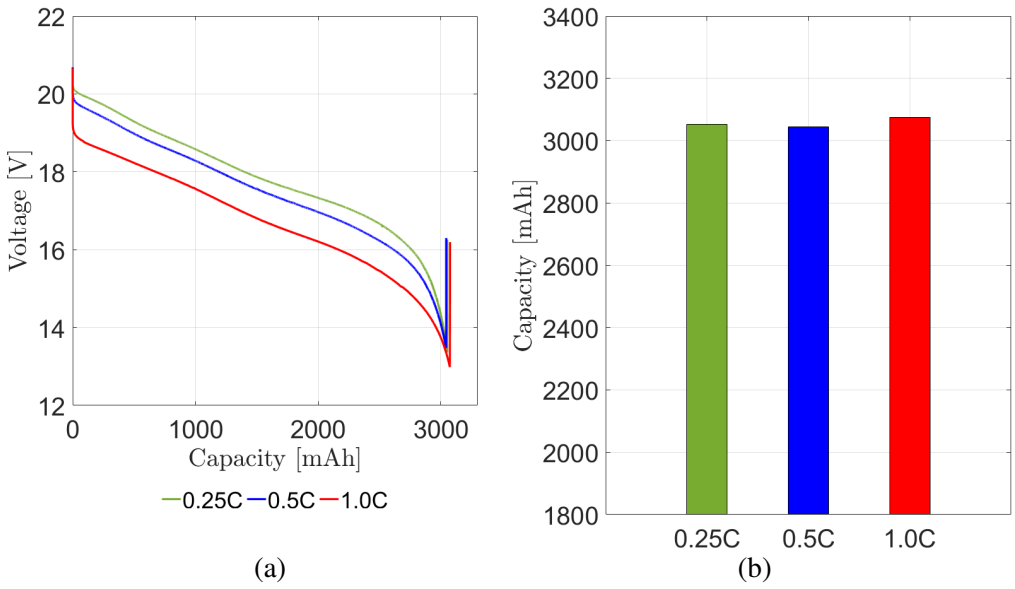

(a) (b)

Source: the author

The cell temperatures behavior during each test can be seen in Figure 94. The test with 1.0C discharge rate presents the higher temperature increase, as expected. The maximum temperature value occurs at the end of the discharge for all the tests.

Figure 94 – Comparison of cell temperature in discharge tests with current rates of 0.25C, 0.5C and 1.0C and at 25 °C

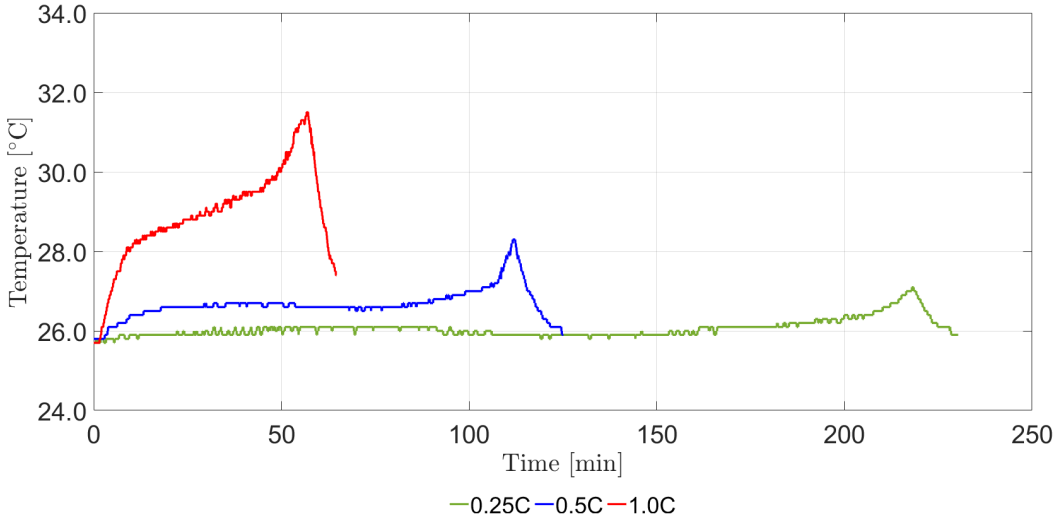

Source: the author

After that, a new room temperature of 40 °C was set in the thermal chamber. The maximum recommended cell temperature during charge and discharge are 45 °C and 60 °C, respectively. These values are defined as protections thresholds in each condition and the battery cell was monitored during the tests.

Table 30 summarizes the main results for each charge test performed at 40 °C and current rate of 0.5C. The charges presented very similar results, considering the duration, cell temperature variation and stored capacity. The higher temperature increase and stored capacity were reached in the second test, but they are still similar with the other tests. The third charge was finished by a overvoltage protection. A cell voltage reaches 4.2 V before the charge termination condition is met. For this reason, the final RSOC is only 93%. A possible reason for this behavior is the charge pack voltage was higher in this test. As the charger used in these test is a DC power supply with the voltage set with a potentiometer, a small variation may occur and provide this result.

Table 30 – Charge test result with room temperature at 40 °C and current rate of 0.5C

Information	**Test #1**	**Test #2**	**Test #3**
Current	1610 mA	1627 mA	1626 mA
Duration	2h35min	2h35min	2h10min
Initial cell temperature	41.9 °C	41.7 °C	42.1 °C
Maximum cell temperature	44.2 °C	44.6 °C	44.6 °C
Cell temperature variation	2.3 °C	2.9 °C	2.5 °C
Initial pack voltage	16.091 V	15.378 V	15.583 V
Minimum pack voltage	20.835 V	20.899 V	20.957 V
Pack voltage variation	4.744 V	5.463 V	5.338 V
Initial RSOC	0%	0%	0%
Final RSOC	100%	100%	93%
Calculated capacity	3109 mAh	3205 mAh	3108 mAh

Source: the author

For each charge test was performed a battery pack discharge and all the main results are summarized in Table 31. First, a discharge test with rate of 0.25C was carried out. With this current level, the complete discharge was achieved after 3 hours and 41 minutes. The total drained capacity was 3151 mAh and the cell temperature increase was 1.5 °C. A second discharge was performed with a current rate of 0.5C and it took 1 hour and 55 minutes. During this test, the battery pack delivered 3161 mAh of capacity and the cell battery temperature rise 3.4 °C. Finally, a new discharge test was carried out with a current rate of 1.0C and its duration was 55 minutes. In test, the cell battery temperature rise 8.9 °C and the total drained capacity was 3064 mAh.

Table 31 – Discharge tests comparison under different current rates and room temperature at 40 °C

Information	**0.25C**	**0.5C**	**1.0C**
Current	856 mA	1655 mA	3372 mA
Duration	3h41min	1h55min	0h55min
Initial cell temperature	42.0 °C	42.2 °C	42.0 °C
Maximum cell temperature	43.5 °C	45.6 °C	50.9 °C
Cell temperature variation	1.5 °C	3.4 °C	8.9 °C
Initial pack voltage	20.631 V	20.694 V	20.592 V
Minimum pack voltage	13.737 V	13.521 V	13.377 V
Pack voltage variation	6.894 V	7.166 V	7.215 V
Initial RSOC	100%	100%	93%
Final RSOC	0%	0%	0%
Calculated capacity	3151 mAh	3161 mAh	3064 mAh

Source: the author

A comparison between the capacity during the discharge tests is provided in Figure 95(a) and the final capacity values are presented in Figure 95(b). The higher value was achieved in the 0.5C discharge rate.

Figure 95 – Comparison of drained capacity in discharge tests with current rates of 0.25C, 0.5C and 1.0C and at 40 °C

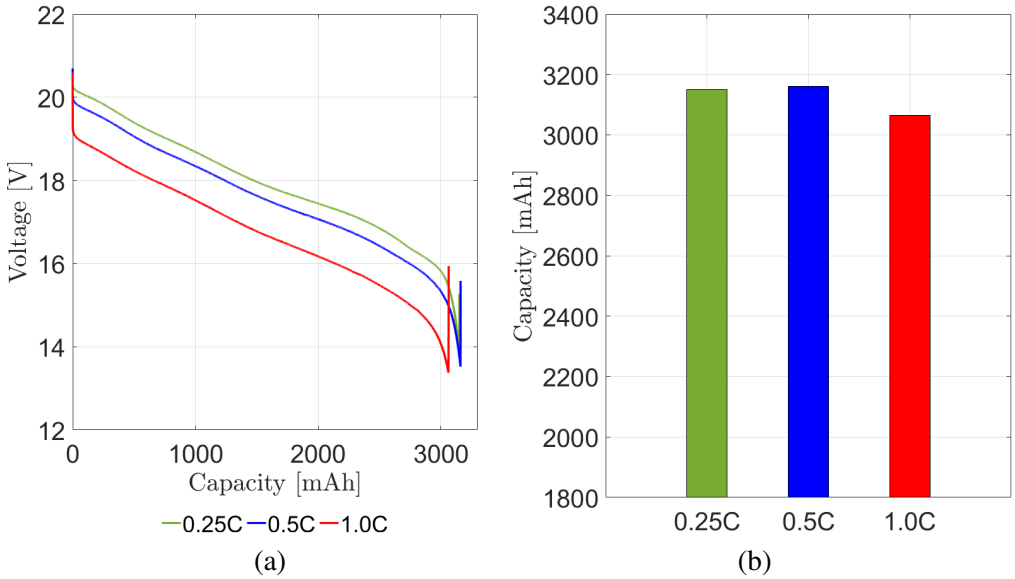

Source: the author

Also, a comparison between the cell battery temperature can be observed in Figure 96. As expected, the discharge test with current rate of 1.0C provides the higher temperature increase. The maximum temperature is achieved at the end of the test in each case. As soon as the discharge is completed and no more current is drained of the battery pack, the cell temperature decrease.

Figure 96 – Comparison of cell temperature in discharge tests with current rates of 0.25C, 0.5C and 1.0C and at 40 °C

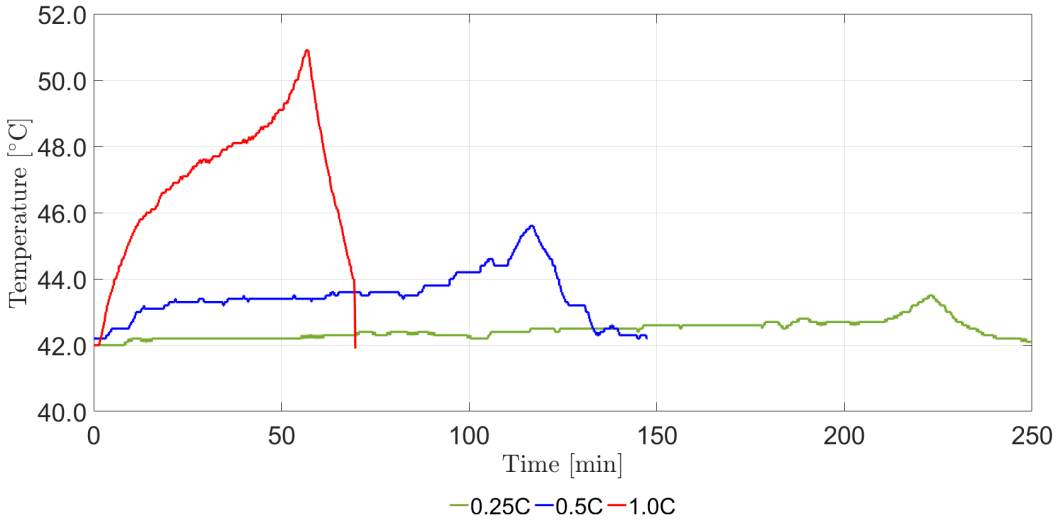

Source: the author

At last, the room temperature was set at 10 °C and the battery pack was charged with current rate of 0.5C. Table 32 summarizes the main results of each test. The charge test in low temperature results in a high capacity fade of battery pack and this fade increases as the test is repeated. All the charging process were interrupted by an overvoltage cell protection. The first charge took 1 hour and 35 minutes and the total stored capacity was 2562 mAh. The final SoC was 78%. The battery cell temperature presents a low increase of 1.2 °C. The second charge was completed after 1 hour and 21 minutes and the final capacity in only 2199 mAh, which results in a final SoC of 67%. During this charge, the battery cell temperature present the same variation of the first test. The last charge test took 1 hour and 18 minutes and the stored capacity is still lower, only 2147 mAh. The final SoC was 65% and the battery cell temperature increased 1.8 °C during the test.

Table 32 – Charge test result with room temperature at 10 °C and current rate of 0.5C

Information	Test #1	Test #2	Test #3
Current	1656mA	1670 mA	1663 mA
Duration	1h35min	1h21min	1h18min
Initial cell temperature	8.8 °C	9.1 °C	8.5 °C
Maximum cell temperature	10.0 °C	10.3 °C	10.3 °C
Cell temperature variation	1.2 °C	1.2 °C	1.8 °C
Initial pack voltage	15.616 V	16.677 V	16.691 V
Minimum pack voltage	20.794 V	20.788 V	20.781 V
Pack voltage variation	5.178 V	4.111 V	4.090 V
Initial RSOC	0%	0%	0%
Final RSOC	78%	67%	65%
Calculated capacity	2562 mAh	2199 mAh	2147 mAh

Source: the author

After each charge test, it was carried out a discharge test at 10 °C, the main results are shown in Table 33. In this case, the first discharge test was performed with a current rate of 0.5C. The complete discharge took 1 hour and 16 minutes and the total drained capacity was 2141 mAh. During this test, the battery cell temperature increased 3.0 °C. After that, a new discharge test was performed requiring a 0.25C current rate. The complete discharge was achieved after 2 hours and 32 minutes and a higher capacity was drained, 2165 mAh. Note that the battery pack started the test with less capacity (SoC=67%) compared with the first discharge (SoC=78%), which proves the improvement of the drained capacity for lower discharge rates. During this discharge, the battery cell temperature increased only 1.9 °C. Finally, a new discharge test was carried out with a discharge current rate of 1.0C. In this test, the complete discharge took only 34 minutes. The drained capacity was 1909 mAh, which represents only 57% of the nominal capacity. The cell temperature increased 7.4 °C during the test.

Table 33 – Discharge tests comparison under different current rates and room temperature at 10 °C after charging with current rate of 0.5C

Information	0.5C	0.25C	1.0C
Current	1681 mA	852 mA	3388 mA
Duration	1h16min	2h32min	0h34min
Initial cell temperature	8.4 °C	8.5 °C	8.5 °C
Maximum cell temperature	11.5 °C	10.4 °C	15.9 °C
Cell temperature variation	3.0 °C	1.9 °C	7.4 °C
Initial pack voltage	19.795 V	19.727 V	19.657 V
Minimum pack voltage	12.799 V	12.975 V	13.085 V
Pack voltage variation	6.994 V	6.723 V	6.572 V
Initial RSOC	78%	67%	65%
Final RSOC	0%	0%	0%
Calculated capacity	2142 mAh	2165 mAh	1909 mAh

Source: the author

In Figure 97(a) is illustrated the capacity behavior during each discharge test and in Figure 97(b) is compared the final capacity. The drained capacity is similar for the tests under 0.25C and 0.5C discharge rates, but it is really low for the test in 1.0C.

Figure 97 – Comparison of drained capacity in discharge tests with current rates of 0.25C, 0.5C and 1.0C and at 10 °C after charging with current rate of 0.5C

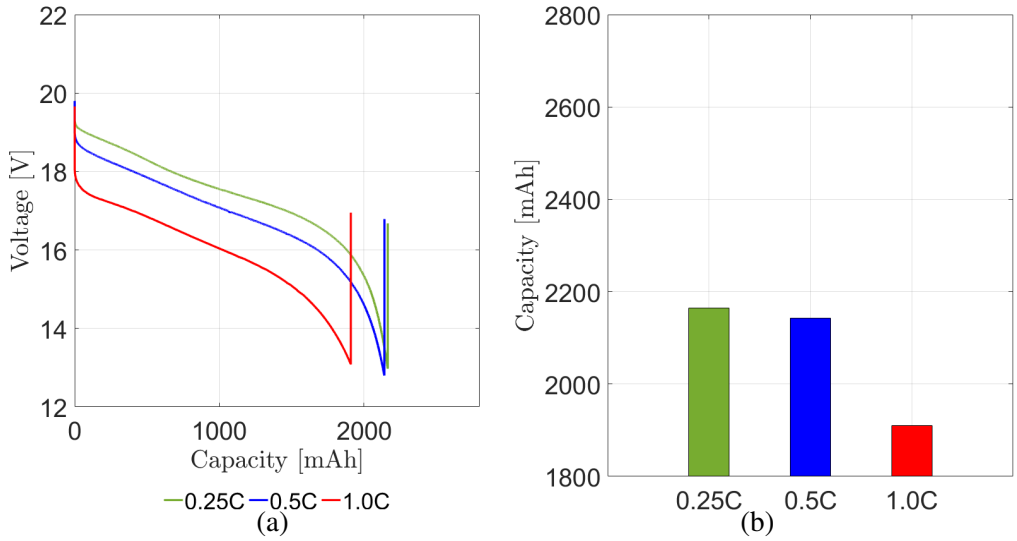

Source: the author

A comparison between the battery cell temperatures is shown in Figure 98. The discharge with the higher discharge current presents the higher increase, as expected. In all the tests, the temperature rises during the process and reaches the maximum value at the end of the discharge. As soon as there is no more current, the temperature decreases.

Figure 98 – Comparison of cell temperature in discharge tests with current rates of 0.25C, 0.5C and 1.0C and at 10 °C after charging with current rate of 0.5C

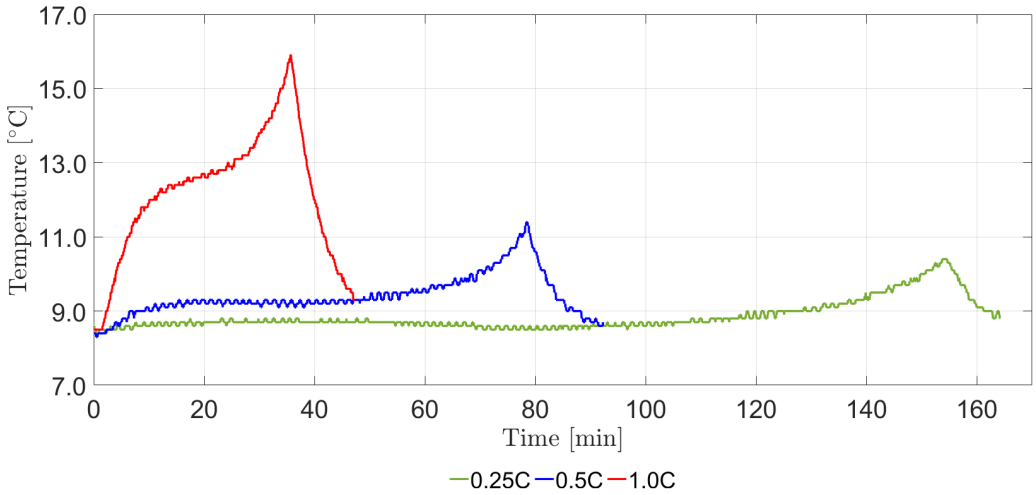

Source: the author

Due to the capacity fade presented in the tests at 10 °C, new tests were carried out using a new battery pack and with a lower charge rate of 0.25C. Table 34 presents the main results of these tests. The first charge with current rate of 0.25C took 3 hours and 55 minutes and was able to store a capacity of 3014 mAh, which indicates an improvement when compared with the charge test using a current of 0.5C. Its final SoC was 90% and the battery cell also presented a low increase of 0.5 °C. The second charge test was finished after 3h and 17 minutes and

presented a lower stored capacity of 2708 mAh. During the test, the battery cell temperature increased only 0.7 °C but the final SoC was 81%. The last charge test presented an even lower capacity. The final stored capacity was 2541 mAh (almost 76% of the nominal capacity) and the SoC was 65%. The test took also 3 hours and 17 minutes and the cell temperature increased 0.6 °C.

Table 34 – Charge test result with room temperature at 10 °C and current rate of 0.25C

Information	Test #1	Test #2	Test #3
Current	831 mA	831 mA	825 mA
Duration	3h55min	3h17min	3h17min
Initial cell temperature	8.5 °C	8.4 °C	8.4 °C
Maximum cell temperature	9.0 °C	9.1 °C	9.0 °C
Cell temperature variation	0.5 °C	0.7 °C	0.6 °C
Initial pack voltage	15.802 V	16.500 V	16.830 V
Minimum pack voltage	20.945 V	20.947 V	20.937 V
Pack voltage variation	5.143 V	4.447 V	4.070 V
Initial RSOC	0%	0%	0%
Final RSOC	90%	81%	76%
Calculated capacity	3014 mAh	2708 mAh	2541 mAh

Source: the author

To complete the tests, the discharges were carried out after each charge. The behavior is the same presented at the other tests and the main results are available in Table 35. The first test was performed with a discharging current of 0.25C and took 3 hours and 12 minutes. The total drained capacity was 2652 mAh and the battery cell temperature rise 1.4 °C. In the second discharge, the current rate was 0.5C and the complete discharge was achieved after 1 hour and 26 minutes. During this discharge, the battery pack delivered 2366 mAh and the battery cell temperature increased 2.9 °C. Finally, the last discharge test was performed with current rate of 1.0C. The discharge duration was 43 minutes and the total drained capacity was 2388 mAh.

Table 35 – Discharge tests comparison under different current rates and room temperature at 10 °C after charging with current rate of 0.25C

Information	0.25C	0.5C	1.0C
Current	829mA	1644 mA	3337 mA
Duration	3h12min	1h26min	0h43min
Initial cell temperature	8.4 °C	8.4 °C	8.4 °C
Maximum cell temperature	9.8 °C	11.3 °C	15.0 °C
Cell temperature variation	1.4 °C	2.9 °C	6.6 °C
Initial pack voltage	20.466 V	20.213 V	20.495 V
Minimum pack voltage	13.604 V	13.528 V	13.140 V
Pack voltage variation	6.862 V	6.685 V	7.328 V
Initial RSOC	90%	81%	76%
Final RSOC	0%	0%	0%
Calculated capacity	2652 mAh	2366 mAh	2388 mAh

Source: the author

The capacity behavior during each discharge test is illustrated in Figure 99(a) and in Figure 99(b) is compared the final capacity. The higher drained capacity took place in the test

under 0.25C discharge rate. The discharge test performed with 1.0C presents higher capacity than with 0.5C but also provides a higher cell temperature increase. Figure 100 illustrates the battery cell temperature during each discharge test. The greater the discharge current, the greater the temperature, as expected.

Figure 99 – Comparison of drained capacity in discharge tests with current rates of 0.25C, 0.5C and 1.0C and at 10 °C after charging with current rate of 0.25C

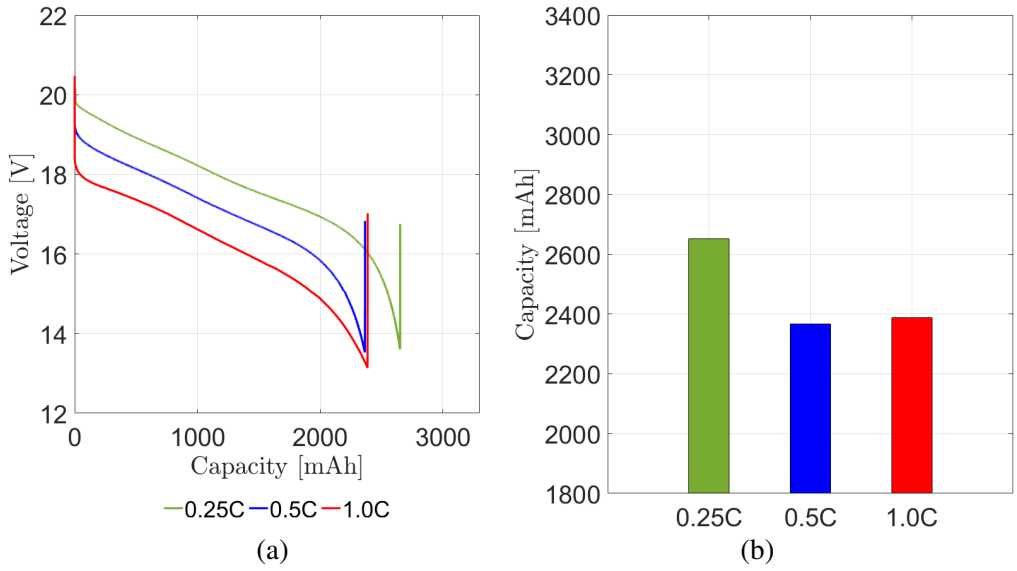

Source: the author

Figure 100 – Comparison of cell temperature in discharge tests with current rates of 0.25C, 0.5C and 1.0C and at 10 °C after charging with current rate of 0.25C

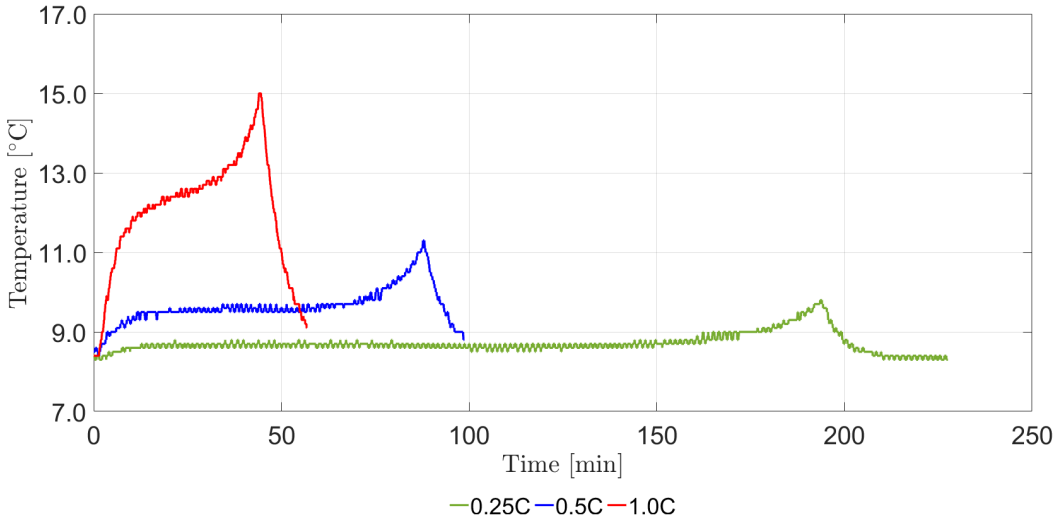

Source: the author